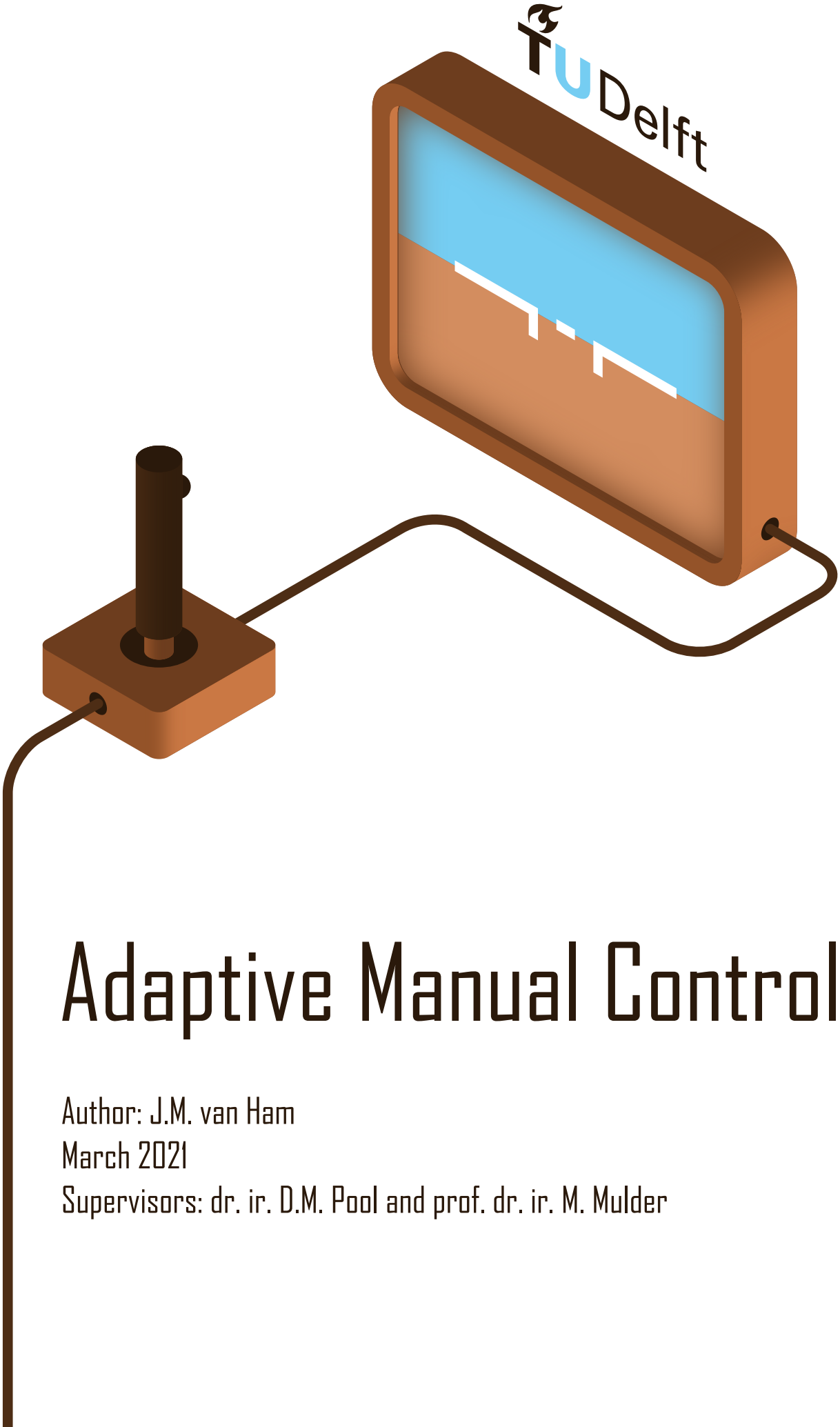

Adaptive Manual Control

Author: J.M. van Ham

March 2021

Supervisors: dr. ir. D.M. Pool and prof. dr. ir. M. Mulder

Adaptive Manual Control - The Human Response to Sudden Changes in Controlled Element Dynamics

Master of Science Thesis

For obtaining the degree of Master of Science in Aerospace Engineering
at Delft University of Technology

J.M. van Ham

8 March 2021

Faculty of Aerospace Engineering · Delft University of Technology

Delft University of Technology

Delft University Of Technology
Department Of
Control and Simulation

The undersigned hereby certify that they have read and recommend to the Faculty of Aerospace Engineering for acceptance a thesis entitled **"Adaptive Manual Control - The Human Response to Sudden Changes in Controlled Element Dynamics"** by **J.M. van Ham** in partial fulfillment of the requirements for the degree of **Master of Science**.

Dated: 8 March 2021

Readers:

dr.ir. D.M. Pool

prof.dr.ir. M. Mulder

dr.ir. M.M. van Paassen

dr. M.A. Mitici

Preface

Before you lies the thesis I have been working on for the past year. It is dedicated to a field I had little knowledge of one year ago: Adaptive Manual Control. But right now, I feel like I actually contributed in extending the knowledge and clearing the way for others to be able to continue working on this interesting topic. With this work my student time at TU Delft is concluded, a chapter at which I already look back on with great pleasure.

First of all, I would like to thank my supervisors Daan and Max. Daan, it is remarkable how much time you make available for your master students. Sometimes we would have three meetings on one day! Thanks to this and your patient way of leading me through this process, has made this thesis project a very pleasant and educational journey. Max, even though we sometimes had trouble understanding each other, I have learned a lot from you (and I hope you also learned a little bit from me). Your enthusiasm in research is contagious. You have a lot of out-of-the-box ideas, which made me excited to continue working on the topic after each of our meetings. I think I was quite lucky with this supervising duo, and I hope many future graduating students will get the chance to get the same experience.

Next, I would like to thank another big contributor to this thesis research. Jan, even though you probably would have liked to be finished earlier, I thought it was really cool to be able to work together on our studies and graduation projects. It was very useful and nice that I could always ask you to brainstorm together when I was stuck on something. I also want to thank you for the amazing graphical designs you made, one of which can be admired on the front page of this thesis.

I also want to express my gratitude to the rest of the people I studied together with during my time at the TU. They are the main factors for making sure that every day studying at either the faculty, the Fellowship, or (mainly the last year) someones home was special and a lot of fun.

Last but not least, I want to thank my parents for providing me with the tools to be able to go on this adventure.

I hope you enjoy reading my thesis!

Jacomijn van Ham
Delft, March 2021

Contents

List of Figures

List of Tables

Nomenclature

Roman Symbols	Description	Unit
A_n	Amplitude of sine wave	[-]
e	Error	[-]
$\dot{e}$ or $\frac{de}{dt}$	Error rate (with hat means expected)	[-/s]
G	Maximum rate of change	[-/s]
G_{nm}	Neuromuscular dynamics	[-]
$H(s)$	Transfer function	[-]
j	Imaginary number	[-]
K	Gain	[-]
K_p	Position gain or pilot gain	[-]
K_r	Rate gain	[-]
M	Vehicle output or time of maximum rate of change	[-]
$\dot{M}$	Vehicle output rate	[-/s]
n	index	[-]
N	Number of sines	[-]
P	Sigmoid value	[-]
P_1	Initial sigmoid value	[-]
P_2	Final sigmoid value	[-]
s	Laplace variable	[-]
t	Time	[s]
t_c	Moment of transition	[s]
t_s	Small time value	[s]
T_L	Lead time constant	[s]
u	Control input	[-]
x	Criterion signal	[-]
y	Response output	[-]
$Y(j\omega)$	Frequency response function	[-]

Greek Symbols	Description	Unit
Δ	Difference	[-]
$\Delta\epsilon$	Discrepancy	[-/s]
ζ_{nms}	Neuromuscular damping ratio	[-]
σ	Standard deviation	[-]
τ_e	Time delay	[s]
ϕ_n	Phase shift of sine wave	[rad]
ω	Frequency	[rad/s]
ω_c	Crossover frequency	[rad/s]
ω_n	Frequency of sine wave	[rad/s]
ω_{nms}	Neuromuscular frequency	[rad/s]

Abbreviations	Description
DI	Double Integrator
DR	Decision Region
SD	Standar Deviation
SI	Single Integrator
TF	Time of Failure

Part I

Scientific Article

Predicting Adaptive Human Control Behavior to Changing Controlled Element Dynamics Based on Statistical Variations in Error and Error Rate

Author: J.M. van Ham; Supervisors: D.M. Pool and M. Mulder,
Control & Simulation Section, Faculty of Aerospace Engineering
Delft University of Technology, Delft, The Netherlands

***Abstract*—This paper presents an analysis in prediction of adaptive manual control behavior to sudden changes in controlled element dynamics. A previously proposed model, the 'supervisory control algorithm', describes human adaptive behavior using binary decision moments at specific decision region limits of the error and error rate signal. This model was assessed using a compensatory pitch tracking task with sudden variations in controlled element dynamics. An experiment was conducted with six participants in a fixed-base simulator at Delft University of Technology. During the runs the participants had to perform the tracking task as accurately as possible and had to indicate detected controlled element dynamics transitions by pressing a button. The results indicate that the original decision region limits from the supervisory control algorithm do not apply to the way human operators adapt in the set-up of this experiment. From the button press data only one percent yielded a result in compliance with the algorithm, demonstrating the large discrepancy between these decision regions and the actual human detection limits in this experiment task. A final analysis is performed using a detection method based on deviations in statistical properties of pre-transitional tracking. This method demonstrated simulation results close to realistic values with a detection threshold around four times the standard deviations.**

I. Introduction

Over 50 years ago, a model was proposed, that was able to predict and simulate human control behavior in steady-state tracking [1]. This model, the crossover model, has certainly proved its use over the years [2]–[4], but has also shown its limitations [5]. For example, it cannot directly be applied for modeling time-varying systems, in which a human operator has to deal with fast changing controlled element dynamics, changing input signals, or changing environmental factors [6].

In the years following, there was a great interest in expanding the crossover model to be applicable to operators' control of systems with time-varying elements [7]–[14]. Unfortunately, a single model covering all the aspects of adaptive human control is not yet available [1]. The reason this is of such considerable interest can be found in the possible applications. Knowing the limitations of the human operator can greatly assist in the design of man-machine systems [6]. Furthermore, in an era in which we are trying to remove the human from the loop, knowledge about the human ability to perform this 'fast' type of adaptation, might advance the design of such automated adaptive control systems [15].

A key problem with the time-varying aspect of manual control with *sudden* changes in task conditions is that it cannot be investigated using traditional frequency-domain methods, as there simply are not enough data available during the transition phase, due to the fast adaptation of the human operator [1]. The first efforts into modeling adaptive manual control therefore focused on only looking at the characteristics of the time traces of tracking data during which the controlled element dynamics were suddenly changed. It was found that the full adaptation process takes place somewhere within two to five seconds, depending on the type of transition [7].

From the same research the following phases of the human adaptation process were postulated: 1) *detection*, the human operator detects the change in controlled element dynamics; 2) *identification*, the human operator identifies the correct new controlled element dynamics; 3) *modification*, the human operator modifies their dynamics to the new controlled element dynamics [7]. Further research focused on time-domain data in order to find the most suitable model describing this adaptive process using these presupposed phases. Subsequently, it was presumed that the human operator is able to store information of the system they are controlling initially, such as deviations and maximums of the error (e) and error rate ($\dot{e}$). The operator creates an internal model of the system, and will therefore notice when the characteristics of the error signal change when the controlled element dynamics are changed [9]–[13].

A promising idea for modeling the human adaptive process is the *supervisory control algorithm* [11], [15], [16]. This algorithm suggests that human operators will detect and identify the correct dynamics based on exceeding certain error and error rate limits. Accompanying experiment results in this previous research support the accuracy of this model, when well-trained in controlling the possible controlled element dynamics. Unfortunately, the model lacks an assessment of the robustness, i.e., it is unclear whether the error and error rate limits can be applied to different controlled element dynamics.

The goal of this research is to assess whether the limits from the supervisory control algorithm are also applicable to different controlled element dynamics than the ones used in the original research [11]. To achieve this goal, an experiment containing a compensatory pitch tracking task with varying controlled element dynamics was designed and conducted. The experiment was executed in a fixed-based research simulator at Delft University of Technology with six trained participants. The participants were instructed to keep the pitch error with respect to the tracking signal as low as possible, while also

paying attention to possible changes in the controlled element dynamics. When they detected the transition during a run they had to indicate this by pressing a button on the front of the side-stick. The same experiment task was applied in several earlier adaptive manual control researches [3], [17]. The results of this experiment were used to assess the performance of the supervisory control algorithm. Furthermore, an analysis was performed with the experiment data by applying different detection thresholds based on the statistical properties of the error and error rate, to find the most probable detection limits for this specific task.

This paper is structured as follows. First, the supervisory control algorithm is explained in Section II. The set-up of the experiment is elaborated upon in Section III. The results of the experiment are presented in Section IV. The last two sections, Section V and VI, contain the discussion and conclusion of this research.

II. Supervisory Control Algorithm

The model considered for the prediction of adaptive human control in this research is the supervisory control algorithm [11], [15], [16]. This algorithm is based on sequential 'yes' or 'no' decisions by following the development of the error and error rate during a run, induced by a sudden transition in the Controlled Element (CE) Dynamics. These decisions determine when and how the human operator will adapt their control strategy to maintain stable control. It assumes the following phases with respect to such a transition: *pre-failure retention (i.e, tracking post-failure dynamics, assuming pre-failure dynamics), detection of change, identification of new dynamics and post-failure steady state tracking*.

The structure of this algorithm is illustrated in Figure 1. The Supervisor and Human Operator Dynamics blocks together represent the model of the Human Operator. The 'Supervisor' is a higher-level controller capable of integrating the decision-making process of moving sequentially through the four phases of human adaptation. It does so by reorganizing the structure of the Human Operator Dynamics based on an internal model of the possible CE Dynamics. The main input of the 'Supervisor' is the error state vector (*e(t)*). The control input (*u(t)*) is also mentioned as an input of the 'Supervisor', however its exact contribution is not clarified in any of the papers. It will therefore not be treated in the rest of this explanation of the supervisory control algorithm.

The supervisory control algorithm is required to act fast enough to prevent the control loop from becoming unstable, that is, it cannot depend on having knowledge of the full process but only on past information of the system. The structure of the model cycles through different decision moments where a yes or no decision will be made, depending on the available information at that moment.

The experiment on which this algorithm was built, consists of runs with specific CE dynamics from a VTOL aircraft [18]. During a run, the attitude and/or rate feedback from this simulated aircraft would fail. In combination with the pre-failure human operator dynamics this would result in an unstable system. The four different controlled element

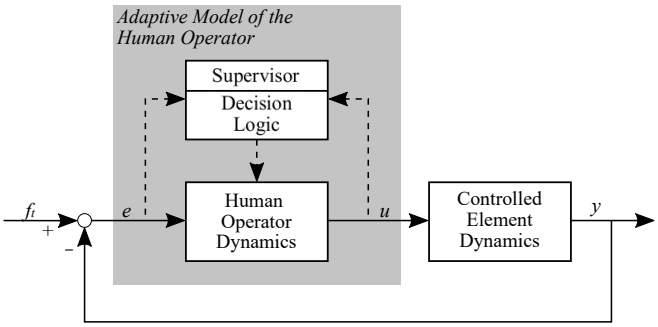

Figure 1: Hypothetical structure of the adaptive human operator model [15]

dynamics used (*A, B, C & D*) are linked to the different decision regions defined in Figure 3 and are given by the following transfer functions:

$$\begin{aligned}
&\text{A: } H_C(s) = \frac{1.72}{s^2 + 2(0.6)(5.1)s + (5.1)^2} \\
&\text{B: } H_C(s) = \frac{320}{s(s+18.6)(s^2 + 2(0.66)(10.4)s + (10.4)^2)} \\
&\text{C: } H_C(s) = \frac{0.8}{s^2} \\
&\text{D: } H_C(s) = \frac{0.7154}{s^2 - 2(0.2)(3.3)s + (3.3)^2}
\end{aligned} \tag{1}$$

The different CE options are ordered such that each subsequent set of dynamics takes more control effort from the human operator. The Bode plots of these four options are shown in Figure 2.

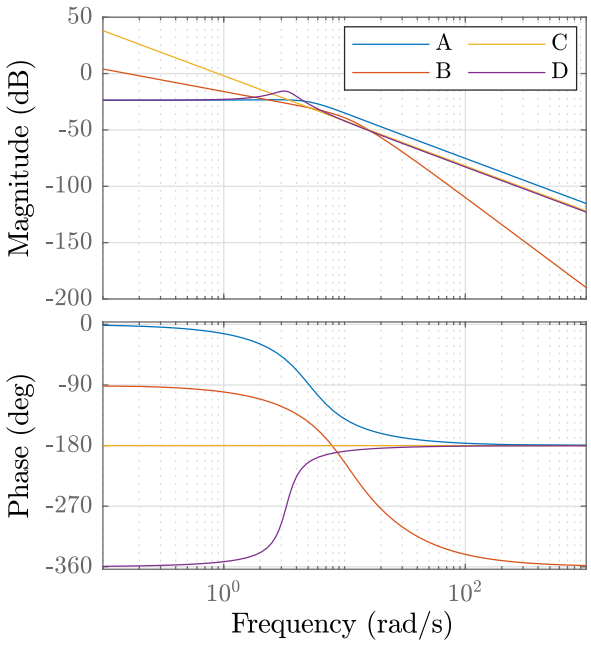

Figure 2: Frequency response of the VTOL aircraft dynamics used to validate the supervisory control algorithm [11], [18]

The procedures from the algorithm are based on the magnitudes of error (e) and error rate ($\dot{e}$) and sign changes of the error rate. Figure 3 displays a phase plane (e on x-axis and $\dot{e}$ on y-axis) with decision regions (DRs) as defined by [15]. These decision regions define the type and moment of a binary decision by the supervisory control algorithm. The moment the error or error rate passes certain decision regions, determines the response of the 'Supervisor' in the algorithm. The values for the different decision regions of this specific research were determined by analyzing data of experimentally measured transitions [11].

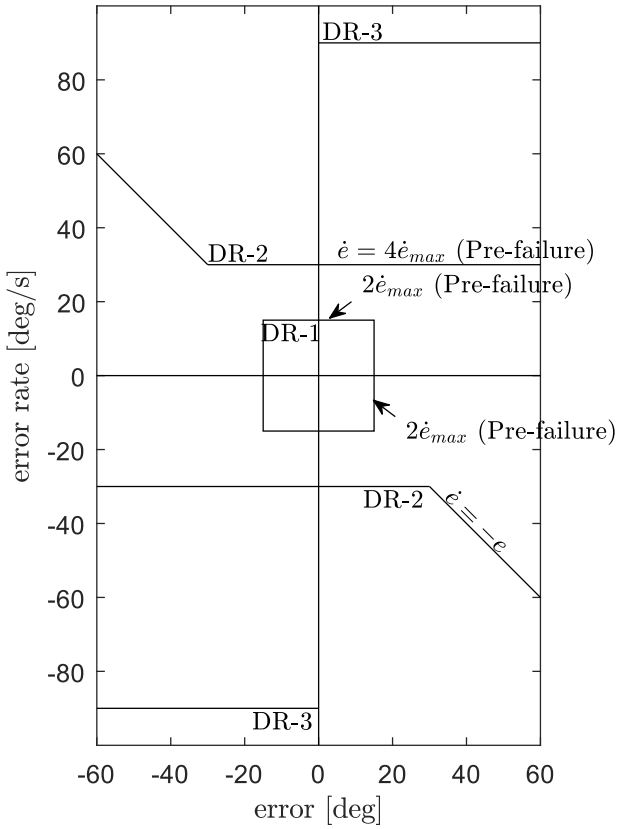

Figure 3: Original decision regions from the sequential identification model [11]

The human operator model used in this algorithm is equivalent to the simplified precision model [1]:

$$Y_p(j\omega) = K_p \frac{j\omega + Z_p}{j\omega + P_p} e^{-(j\omega)\tau_p} \tag{2}$$

where K_p is the human operator gain, Z_p and P_p are the lead and lag equalization break frequencies and τ_p is the operator time delay. These parameters are adjusted based on the decisions of the supervisor during a transition to different CE dynamics and are therefore time-varying:

$$p(t) = [K_p(t), Z_p(t), P_p(t), \tau_p(t)]^T \tag{3}$$

When the initial CE dynamics are equal to *A*, and they suddenly transition to dynamics *B*, the human operator dynamics will have to be adjusted to the new dynamics to prevent the system from becoming unstable. According to the algorithm, the human operator will detect a change when e or $\dot{e}$ passes the first decision region (DR-1 as shown in Figure 3). Upon detection, the parameters of the human operator dynamics will be corrected to the CE dynamics of this next decision region, *B*:

$$p(t) = [K_p, Z_p, P_p, \tau_p]_A^T \rightarrow p(t) = [K_p, Z_p, P_p, \tau_p]_B^T \tag{4}$$

The next steps in the algorithm depend on first awaiting the error rate to reverse sign, and then observing if the error and error rate will pass the second decision region (DR-2). If the error values stay within the limits of DR-2, the modification to CE dynamics *B* turned out to be correct. The error and error rate approach zero and the operator reaches the last phase of adaptation: *steady-state tracking*. However, if the error values do pass the next region, the previous adjustment of parameters was not sufficient, resulting in another correction to the parameters of this region, CE dynamics *C*. This process repeats until the correct CE dynamics are identified and modified to by the human operator. The flowchart of this process is shown in Figure 4.

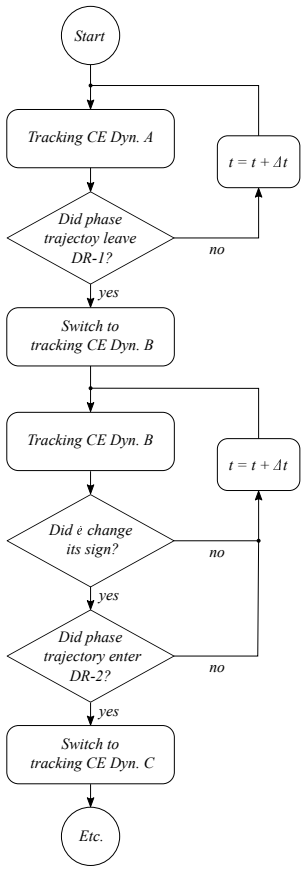

Figure 4: Flowchart of the decision logic of the supervisory control algorithm [11]

III. Method

A. Control Task

In this research, a human-in-the-loop experiment was conducted based on experiments from recent research on time-

varying human operator behavior [3], [17]. The experiment results were used to assess the supervisory control algorithm [11], [15], [16], and therefore also required an approach similar to the experiments conducted in this earlier research.

The experiment consisted of 16 runs of a compensatory pitch angle tracking task. The participants only controlled the aircraft pitch. Error e was presented using a primary flight display, as schematically visualized in Figure 5. The error is the difference between the reference input signal and the output of the system.

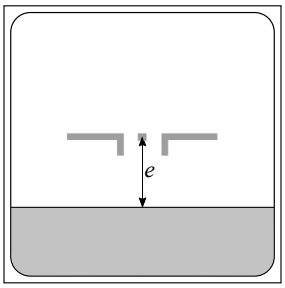

Figure 5: Pitch tracking display

The CE dynamics were defined by the following time-varying transfer function [3]:

$$H_c(s,t) = \frac{K_c(t)}{s(s+\omega_b(t))} \tag{5}$$

where K_c is the time-varying gain and ω_b the time-varying break frequency. The gain and break frequency would be switched during the run from 90 to 30 and from 6 to 0.2 rad/s, respectively. The first set of parameters approximate a single integrator (SI) the latter a double integrator (DI), in the region of the operator's crossover frequency [3].

The time-varying parameters were implemented using a sigmoid function:

$$P(t) = P_1 + \frac{P_2 - P_1}{1 + e^{-G(t-M)}} \tag{6}$$

where P_1 and P_2 are the initial and final parameter values and G and M represent the maximum rate of change and the moment of maximum rate of change, respectively. For the task considered in this paper, G was taken to be 10 s^{-1} for all the runs, as this simulates the desired instant change in parameters [3]. M was varied between 30 s and 45 s for each run to prevent predictability of the transition moment.

B. Apparatus

The experiment was performed in the Human-Machine Interaction Laboratory of the Faculty of Aerospace Engineering at TU Delft. A fixed-based aircraft simulator with a side-stick at the end of the right arm rest was used, as shown in Figure 6a. The side-stick had a movement freedom of 22 degrees in the forward and backward directions. Sideways movements of the stick were restricted since these were not required in this experiment. The forward and backward movements of the stick showed behavior similar to that of a side-stick in an aircraft, i.e., a forward movement resulted in a pitch down maneuver, a backward movement resulted in a pitch up maneuver. The distance of the rotation axis of the stick to the middle of the handle was 90 mm. Furthermore, the spring constant, inertia, damping constant and break-out moment of the side-stick were 0-35.0 Nm/rad, 0.01 kg/m^2, 0.2 Nm s/rad and 0.0 Nm, respectively. A trigger button on the front of the side-stick, as displayed in Figure 6b, was used to indicate a detection of changed controlled element dynamics. This signal was logged together with the tracking task signals. The computer logged all data at a sampling frequency of 100 Hz.

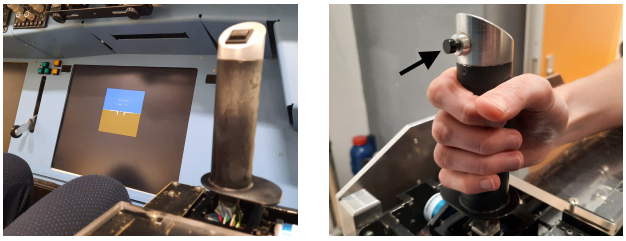

(a) Simulator set-up (b) Button on the side-stick

Figure 6: Experiment set-up with aircraft simulator

C. Independent Variables

The conditions in the experiment were defined by two variables. The first variable is the target signal realization. Eight target signals with varying phase shifts were chosen for this experiment, in order to prevent the participants from recognizing and anticipating the input. The second variable is the moment of transition to the new CE dynamics during a run, each transition moment was also selected such to prevent the participant from anticipating on the exact moment of transition. Two different moments of transition were selected for each target signal. The chosen conditions are shown in Table I together with the number of their target signal.

Table I: Experiment conditions

f_t	Condition	M [s]	Condition	M [s]
1	C1	33.5	C2	42.5
2	C3	37.5	C4	38.5
3	C5	35.5	C6	36.5
4	C7	44.0	C8	33.0
5	C9	42.0	C10	36.5
6	C11	42.5	C12	41.0
7	C13	41.0	C14	44.5
8	C15	33.5	C16	36.5

D. Forcing Functions

Eight different forcing functions were used in the experiment, each of them a sum of sinusoids as defined by:

$$f_t(t) = \sum_{n=1}^{N_t} A_t[n] \sin(\omega_t[n]t + \phi_t[n]) \tag{7}$$

where N_t is the number of sines per target signal, which was equal to 10 for each of the signals. $A_t[n]$, $\omega_t[n]$ and $\phi_t[n]$ are the amplitude, frequency and phase of the n^{th} sine,

Table II: Forcing functions parameter values

$k_t[-]$	$\omega_t[rad/s]$	$A_t[deg]$	$\phi_{t,1}[rad]$	$\phi_{t,2}[rad]$	$\phi_{t,3}[rad]$	$\phi_{t,4}[rad]$	$\phi_{t,5}[rad]$	$\phi_{t,6}[rad]$	$\phi_{t,7}[rad]$	$\phi_{t,8}[rad]$
3	0.63	0.888	3.01	3.61	4.20	3.55	1.00	0.90	2.31	0.78
7	1.47	0.481	2.33	5.06	2.26	4.29	5.21	1.51	6.05	4.73
11	2.30	0.269	3.84	0.27	1.29	0.48	4.84	2.59	0.52	0.95
17	3.56	0.138	4.29	2.83	3.83	4.31	1.33	4.67	2.98	1.37
21	4.40	0.103	5.51	2.93	0.40	3.10	4.23	3.70	5.74	1.05
29	6.07	0.063	3.71	3.06	3.33	3.56	5.52	6.14	6.08	2.30
41	8.59	0.040	0.94	3.32	0.55	5.94	2.05	0.01	4.85	1.03
53	11.10	0.034	5.77	6.04	2.09	1.18	5.43	2.23	4.17	2.95
71	14.97	0.034	4.29	0.32	0.08	1.49	4.36	6.24	6.02	2.70
87	18.22	0.023	2.31	1.62	0.43	4.70	0.71	5.40	3.66	5.89

respectively. An overview of the properties of the forcing functions is given in Table II. The values of the amplitudes were determined by a second-order low-pass filter that reduced magnitudes for higher frequencies making the target signal attainable to track for trained human operators [4]. The measurement time was 90 s. The forcing function's period, however, was 30 s, resulting in a base frequency of $\omega_m = 2\pi/T_m = 0.105$ rad/s of which the values of ω_t are integer multiples (see k_t in Table II). Each run also contained 5 s of run-in time, making the total run time 95 s.

E. Experiment Procedure

The experiment consisted of a total of 16 runs excluding training runs. Each condition was applied once in each experiment. They were tested in randomized order across the runs based on a Latin square design, such that each participant had a different order of conditions.

The forcing functions had a period of 30 s, therefore during one run the same pattern was repeated thrice. Each period represented a different phase, as shown in Figure 7. After the run-in time, the first 30 s period was always dedicated to SI tracking. Then, sometime in the first 15 seconds of the second period, the CE dynamics were changed during the Transition Region. Within this phase the participants had to detect, identify and modify to be able to continue stable tracking, and it is therefore called the Transition Phase. During the last 30 seconds, the DI Phase, the participant is assumed to be adapted and is steady-state tracking the new dynamics. The benefit of using the exact same forcing function for all three phases, is that they can be directly compared with each other, showing an equal influence of the target signal.

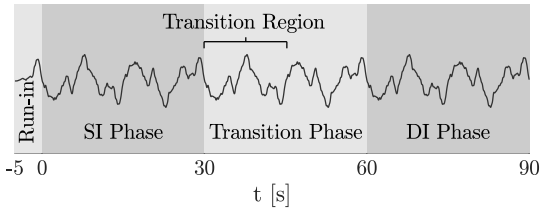

Figure 7: Example of a run with its periodic target signal, showing the different phases and transition region

The training consisted of an initial 3-5 runs with invariant CE dynamics for both SI and DI and afterwards 3-5 runs in which the dynamics *did* change. The training runs continued until the participant exhibited constant performance. The participants were asked to keep the error as low as possible, while also paying attention to the changing CE dynamics. When they detected a change, they were asked to press the trigger button on the front of the side-stick. This too was trained with three to five runs. The training runs were directly followed by the actual experiment runs. The total experiment took approximately one hour per person.

F. Participants and Instructions

In total six participants performed the experiment. At the time of the experiment all of them were master students at the Faculty of Aerospace Engineering of TU Delft, and were between 20 and 30 years old. These participants were selected based on their previous experience with similar tracking tasks, and would therefore require limited training time to get to a constant performance level.

At the start of the experiment, the participants were briefed on what they could expect. The briefing contained information about the experiment procedures and a short description about the objective of the research. After each run, the participants were presented with their score consisting of the root mean square error on the screen. However, to prevent any biases in their performance, they did not receive feedback about their performance on detecting the transition.

The project was assessed and approved by the Human Research Ethics Committee (HREC) of the TU Delft.

IV. Results

A. Detection Performance

In total 96 runs were executed across all six participants. The button pushes were recorded as a subjective indication of the detection of the transition of CE dynamics. The results of the button press per run in chronological order per participant are displayed in Figure 8. The detection lag is the time between the transition and the moment the participant pressed the button. This parameter represents the time it takes for a participant to consciously detect a transition.

The colored lines indicate the detection lag per run per participant, while boxplots show the median and the four quartiles of the data of each run. In total there were three false positives, i.e., moments where participants pressed the button before a transition, and one false negative, where the participant did not detect a transition at all.

From Figure 8 it can be observed that the participants did not improve their detection skills in later runs relative to early runs. The median of the detection lag of 6.6 s, shown by the horizontal dashed red line, lies on the higher side of the expected detection time of 2.2 s to 7.4 s [17]. Some of the participants reported that it was difficult to detect the transitions and were therefore sometimes later than expected with pressing the button.

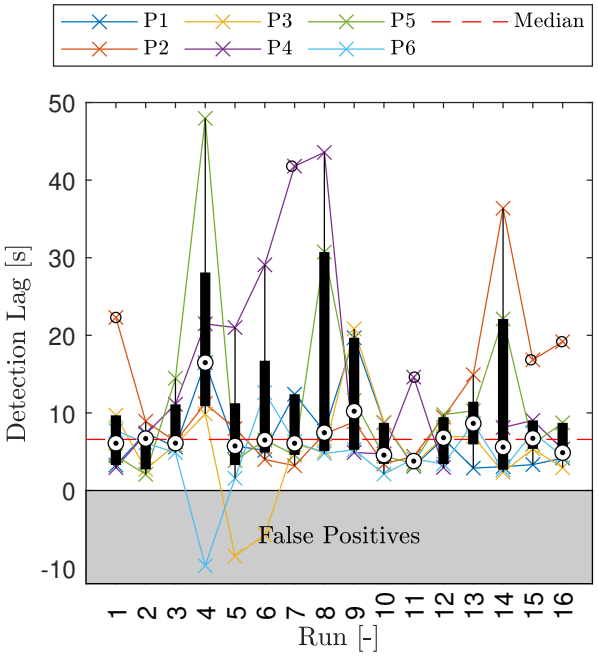

Figure 8: Detection lag per experiment run

The detection lag per condition is shown in Figure 9. The colored lines again show the detection lag for each participant, but now for each condition. The boxplots indicate the variation between participants for each individual condition. Participants tended to detect relatively quickly with specific conditions (e.g., condition 12), or relatively slow (e.g., condition 8). The forcing function realization and moment of transition, therefore, seem to have a significant influence on how long it will take for a participants to detect the transition. The exact influence was not determined in this research. This should be taken into account in future research, when designing an experiment with time-varying CE dynamics

The distribution of the detection lag per participant (excluding false positives) is shown in Figure 10. Three participants, P1, P3 and P6, show average detection lags as expected [17]. The three other participants, P2, P4 and P5, took much longer on average to detect. From Figure 10 it can also be observed that P1, P3 and P6 in general had a more constant detection performance compared to the other three, which might indicate a better feeling for the changing dynamics.

The stability characteristics of the open loop system containing both the human operator and the controlled element were analyzed to see if these were different for 'fast' and

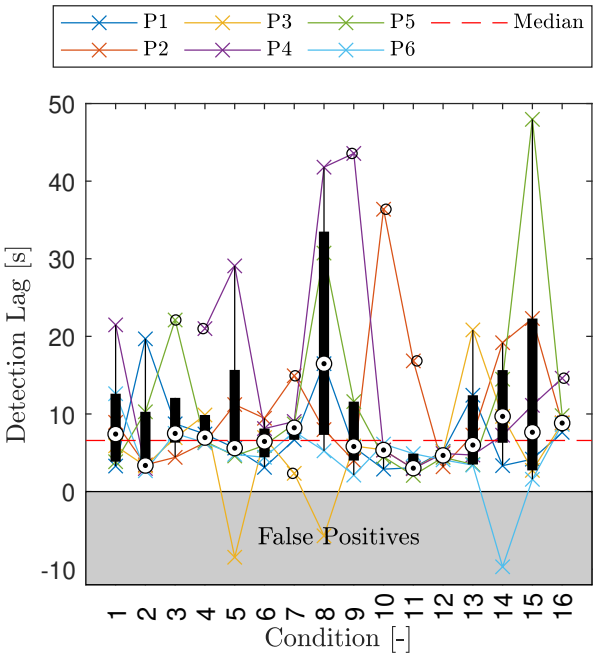

Figure 9: Detection lag per experiment condition

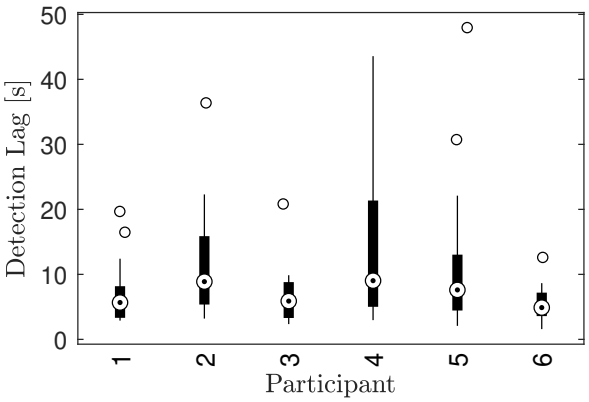

Figure 10: Boxplot of detection lag values per participant

'slow' detecting participants. No significant differences were found between these two groups. Appendix C-1 contains the determined crossover frequency, phase margin and time delay values of each participant for the SI and DI tracking phases.

B. Control Input Analysis

A first analysis was performed to assess the moment the participants pushed the button. It is remarkable that some participants took over 40 s to detect a transition, while the new dynamics require a switch from controlling velocity to acceleration and fast adaptation to prevent the system from becoming unstable [17]. The late button pushes in combination with the system not getting out of hand therefore indicate

that the participant likely unconsciously adapted to a different control strategy before they consciously noticed the change.

A simple model of the human operator obtained by linear regression was used to check the changing control strategy:

$$u(t) \approx a_1 e(t-\tau_p) + a_2 \dot{e}(t-\tau_p) \tag{8}$$

where $u(t)$ indicates the control input, $e(t-\tau_p)$ and $\dot{e}(t-\tau_p)$ the error and error rate compensated by the human operator's time delay τ_p, and a_1 and a_2 the coefficients required to fit the function. Note that this equation is a crude (and possibly biased, as obtained from closed loop data, see [19]) way to describe the pilot model given in Equation 2, from which $K_p Z_p$ and K_p are equivalent to a_1 and a_2, respectively.

The parameters a_1 and a_2 are determined by means of least mean squares regression as follows:

$$a = (X^T X)^{-1} X^T u \tag{9}$$

where $a = [a_1\ a_2]^T$ and $X = [e(t-\tau_p)\ \dot{e}(t-\tau_p)]$. The time delay, τ_p, was determined for each participant based on their pre-failure tracking data. This parameter was selected such that it would cause the coefficient magnitude for $\dot{e}$ (a_2) to be around zero for the pre-failure phase, as single integrators require no lead to be generated by the human operator, while a double integrator does. The expected $\dot{e}$ coefficients before the transition should therefore be around zero. The determined time delays per participant are given in Table III.

Table III: Determined time delays per participant

Participant	P1	P2	P3	P4	P5	P6
τ_p [s]	0.12	0.16	0.20	0.13	0.11	0.12

The magnitudes of coefficients a_1 and a_2 for a specific point in time were determined based on tracking data from a three second window around that same point in time. This method has been used to calculate the coefficient once every 0.1 s. An example of what the coefficients look like for a certain run is given in Figure 11. The vertical dashed lines indicate the moment of transition to the new CE dynamics and the moment of detection, i.e., the moment the participant pressed the button. The error coefficient a_1, is indicated by the blue line, which does not show a clear variation in magnitude before and after the transition. The error rate coefficient a_2, however, does show a trend: the coefficient clearly moves to a higher average value after the transition. It should be noted that this is a very rough representation of the human model and that it cannot be used to extract concrete numbers. In this analysis only relative changes in the coefficient values are investigated.

An overview of the error rate coefficient time trace for all the runs is shown in Figure 12. All the runs are split in two categories: those with detections (button press) faster than 7.4 s and detections slower than 7.4 s. The 7.4 s limit is based on the higher limit of the human detection time [17]. False positives and false negatives are excluded from this figure. The bright colored lines indicate the mean of the coefficients of all the runs from their category, the faded area behind the lines is the area between the minimum and maximum coefficient values across all participants. The moment at which t=0 is defined to

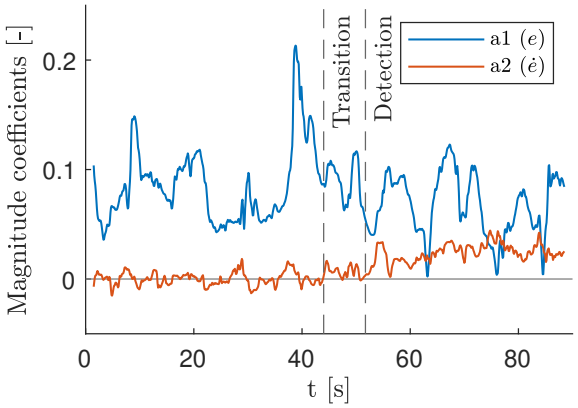

Figure 11: Error and error rate coefficients time trace obtained by linear regression

be the moment of transition, in order to be able to compare all the runs.

The post-adaption error rate coefficient for the button presses within 7.4 s has a final average value of 0.024, which is reached in 7.2 s after the transition. The error rate coefficient for the button presses later than 7.4 s has a final average value of 0.019, which is reached after 7.9 s after the transition. On average the runs in which the participant was faster than 7.4 s yield an 8.8% faster rise to the final average value of the error rate coefficient on average. Moreover, the final average value is on average 20.8% higher for the faster button press runs.

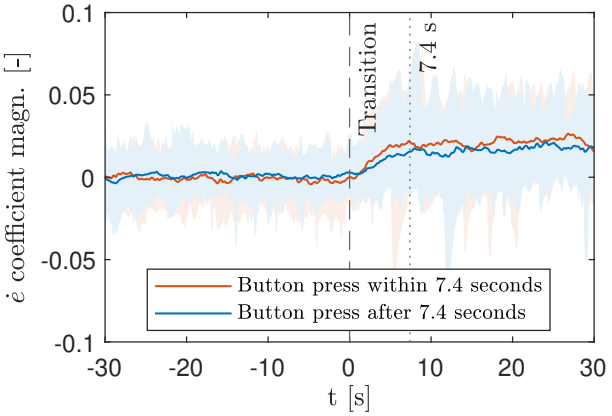

Figure 12: Error rate coefficient of all the runs (excluding false positives and false negatives) separated in detections faster or slower than 7.4 s

As a more direct comparison, the error rate coefficients of the participant with the shortest mean detection time (P6) and of the participant with the longest mean detection time (P4) are shown together in Figure 13. In this figure the difference between the average final level of the error rate coefficient is even more obvious (a_2 is 36.6% higher for P6). This difference could be explained by a different control strategy between these participants. Participants who control more 'aggressively', i.e., controlling with a lower phase margin, tend

to detect a change in CE dynamics earlier, since it will reveal higher error values sooner when tracking new CE dynamics with their pre-failure tracking strategy. They will therefore adapt quicker, causing the steeper rise. Next to that, their overall more 'aggressive' control strategy generates more lead, causing the higher final level of the error rate coefficients.

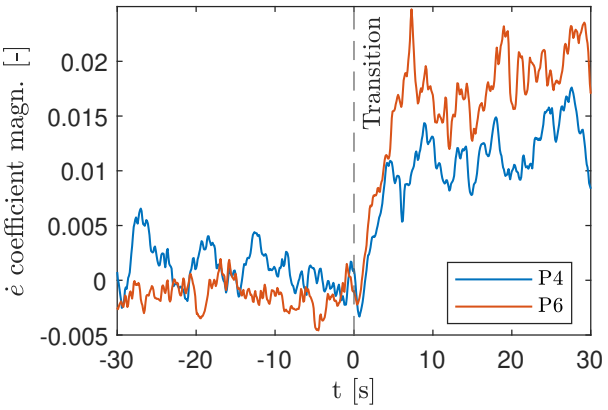

Figure 13: Mean error rate coefficients of all runs of participant 4 and 6

Figure 14, displays for each run the time it takes the error rate coefficient to rise to the adapted level after the transition versus the time it took for the participant to press the button after the transition. The rise time was determined by calculating the mean value of the coefficient of the last 30 seconds of each run (i.e., the DI tracking phase), and finding the first moment the coefficient rose above this value after the transition, as shown in Figure 15. The area containing the 'detections' within 7.4 s in Figure 14 is highlighted by the gray region.

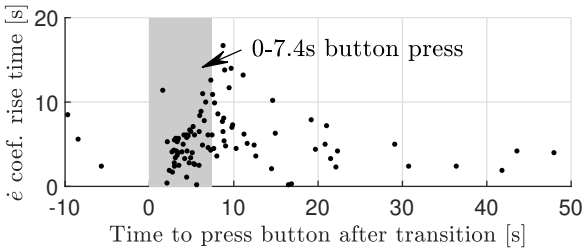

Figure 14: The time the error rate coefficient takes to rise to modified values versus the time it took to press the button to indicate detection of a change in CE dynamics

It was expected that the button press would coincide with the moment the operator model parameters are adapted to the new dynamics. The press of the button indicates that the participant detected a transition, where the next step would be to directly modify the pilot model dynamics. Many data points in Figure 14 indeed show a rather equal rise time to detection time: 1/3rd of the data points have a maximum deviation of 2 seconds between rise time to button press time. However, there is also a large portion of runs showing a rise time

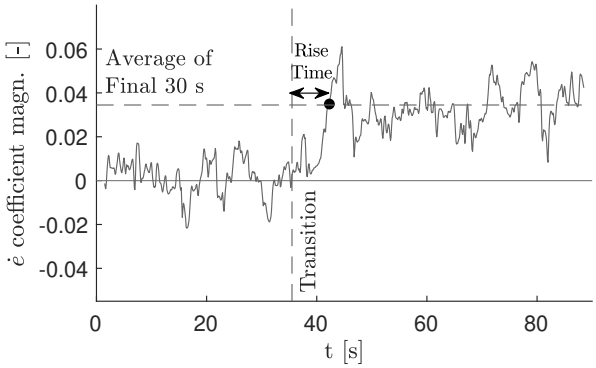

Figure 15: Determination of rise time of a_2

lower than the time the button was pressed *after* the transition. This is indeed indicative of the fact that participants already unconsciously adapted before they consciously detected the change in dynamics.

When performing analyses with subjective data, such as a button press, it should be considered that participants can have had different interpretations of the situation, as also demonstrated by Figure 14. The button press data will still be used in the following analysis, since it is expected that the principle of high error or error rate values providing the participants with the information to detect a change in CE dynamics is still valid and might give some insight in the conscious process of detection.

C. Predicted Moment of Detection

Between the moment the participant detects a change, decides to press the button and actually presses the button, some reaction time is expected. To analyze the error and error rate of the signal at the moment of detection, it was first necessary to predict the actual moment of detection based on a local maximum e or $\dot{e}$ prior to the button press. The predicted moments of detection were determined by incorporating a possible window of reaction time and finding the highest peak in either error or error rate in this window. This presumably was the trigger for human operators to detect a transition [6].

An example of how the predicted moment of detection is determined is given in Figure 16. A window before the button is pressed is considered, which is based on a minimum and maximum reaction time (RT). The values used in this analysis were 0.3 s and 0.6 s for the minimum and maximum RT, respectively. These values were extracted from earlier research in which participants had to press a button based on visual inputs with a set-up similar to this experiment [20].

In the reaction time window, indicated by the gray area in Figure 16, the maximum absolute error and error rates are identified. These values are then normalized by dividing them by their respective standard deviations, obtained from the SI tracking phase. The highest fraction indicates the largest relative magnitude of either error or error rate and is therefore selected as the most probable moment of detection. In the example of Figure 16, the predicted moment of detection for

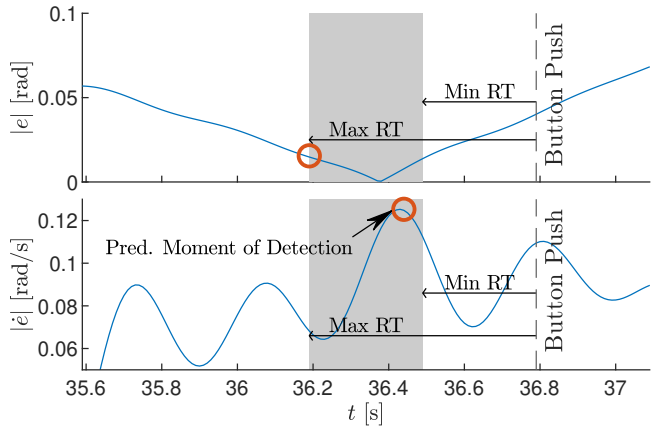

Figure 16: Predicted moment of detection determined by error rate for an example run

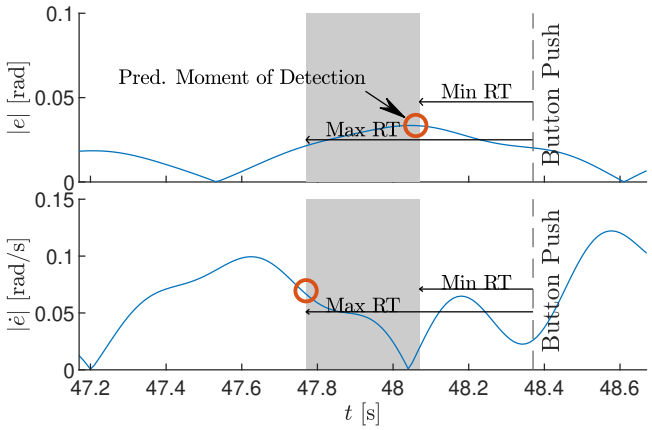

Figure 18: Predicted moment of detection determined by error for an example run

one specific run is determined by the error rate. Figure 17 shows the phase plane of the same run as was presented in Figure 16, from which the same time data are highlighted in blue. This shows that the maximum error rate in this window is indeed higher than the maximum error. Figure 18 gives an example of a predicted detection moment determined by the maximum error value. These error, error rate and time values are used as the *detection values* in further analyses.

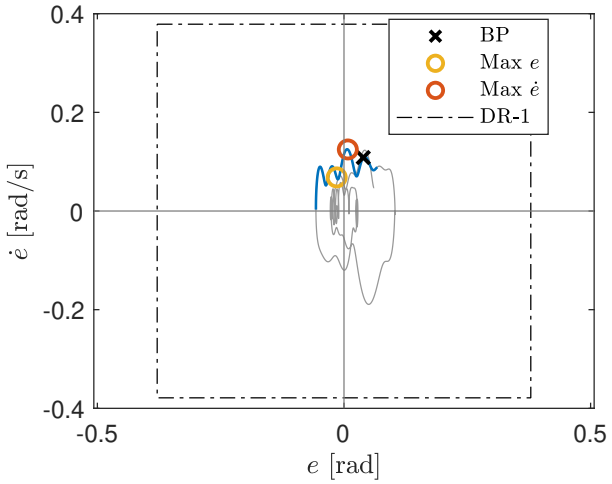

Figure 17: Phase plane of error data including first decision region showing the maximum error and error rate in the reaction time window

By applying this method to determine the predicted moment of detection, it was discovered that the highest error value regularly occurs at the boundary of the time window. The consequence is that the size of the window has a significant influence on the identification of the maximum absolute error value. This is mainly a problem when a larger value is located left of the reaction time window, since an earlier higher value based on the current cost function would theoretically also result in an earlier predicted detection. In 31.2% of the runs the 'true' local maximum was located left of the reaction time window. Since the participants were asked to perform two tasks simultaneously (tracking and pressing the button when detecting the change), it can be presumed that these tasks influenced each other, possibly yielding an increased reaction time for pressing the button when the participant was mainly focusing on their tracking performance. A sensitivity analysis of the reaction time window in Appendix C-4, shows that a higher maximum reaction time (1.6 s) results in similar magnitudes of e and $\dot{e}$ compared to the magnitudes when using the maximum reaction time of 0.6 s. In the end, it was decided to prioritize the use of a realistic window size, since these are the only values supported by literature [20].

D. Error and Error Rate Analysis

The Decision Regions from [11] are based on the difference in magnitude of error and error rate in pre-failure and post-failure tracking. The pre-failure tracking in this paper was always performed with the same CE dynamics, which closely resemble a single integrator in the crossover region, as can be observed from the bode plot in Figure 2. In Figure 19 histograms of all error and error rate values of the pre-failure tracking phase for all runs are displayed. The curves around the histograms are the normal representations of the histograms based on their mean and standard deviation values. The curves and the histograms do not have a perfect fit. The null hypothesis is rejected for both data sets with the one-sample Kolmogorov-Smirnov test, due to the lack of data points in the peaks in combination with the large amount of total data points [21]. Since the two data sets are, however, close to being normally distributed, it was decided to continue working with the normal distribution conventions.

The spread of error and error rate SI tracking values is plotted in a top view in blue in Figure 20. The predicted detections are plotted with red cross symbols, while the false positives are indicated by yellow crosses. The dashed line shows the region of two standard deviations from the mean of the SI tracking data; assuming a normal distribution this encloses about 95% of the data. 8.4% of the detections based on the predicted detection moments lie within this region, as

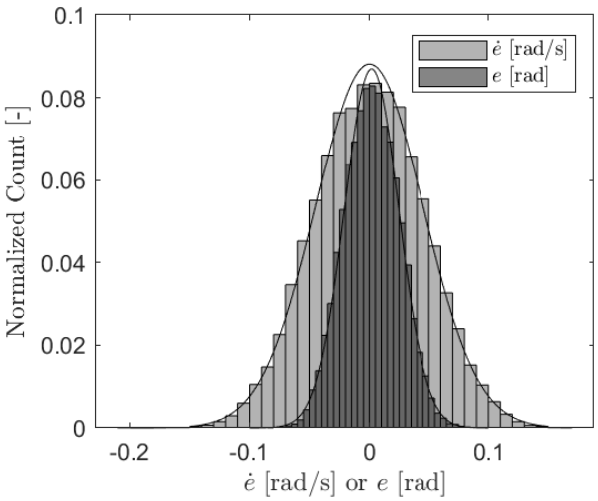

Figure 19: Distribution of pre-failure error and error rate values for all runs

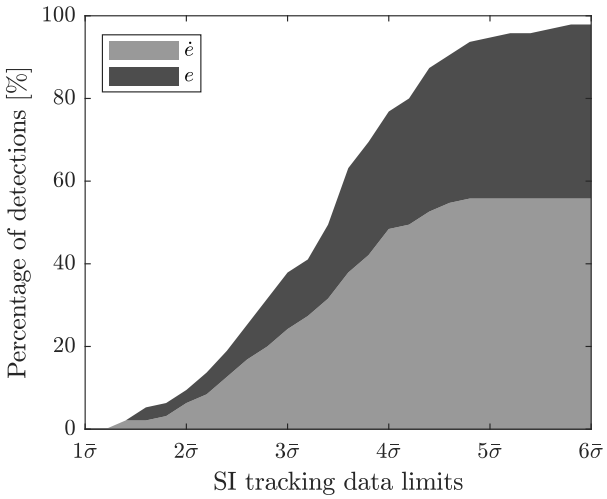

Figure 21: Distribution of error and error rate detections outside the SI tracking standard deviations limits

well as one of the three false positives. The dash-dot line indicates the limits of the first decision region (DR-1) from [11], this is the average maximum $\dot{e}$ over all runs multiplied by two. Only one of the predicted detection moments lies outside this region, i.e., 95.8% lie within the region. The detections are located in a more stretched out fashion around the center of the plot, which are in contrast to what the square shape of DR-1 would suggest.

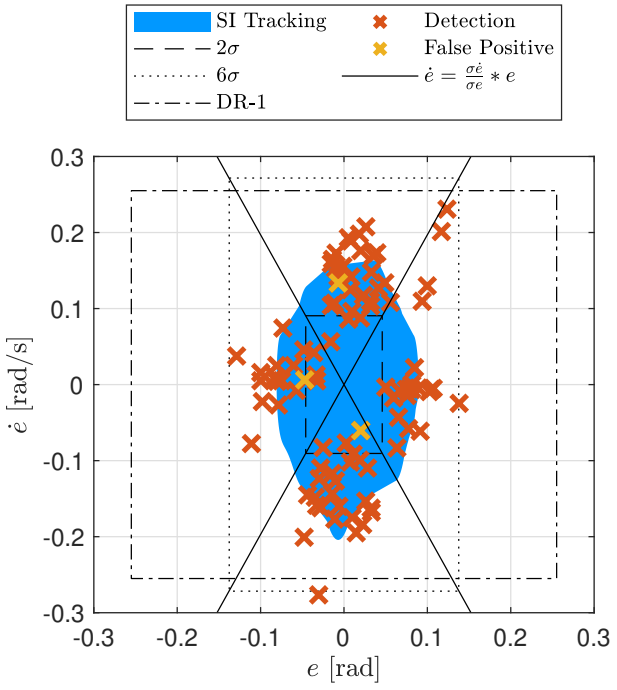

Figure 20: Spread of detections on the pre-failure tracking area

The diagonal lines in Figure 20 indicate the division of error and error rate detections based on the calculation of the predicted moments of detection. The detections left and right are *error detections*, the detections up and down are *error rate detections*. In total there are 41 error detections and 54 error rate detections (not significant according to the sign test).

Figure 21 shows the percentage of error and error rate detections outside certain limits. The limits are multiples of the standard deviation for the SI tracking phase. The 2σ limit (dashed) and 6σ limit (dotted) limits are also illustrated in Figure 20. The majority of detections, 67.4%, lies between 2σ and 4σ.

In Table IV, the pre-failure tracking standard deviation values for error and error rate for each participant are shown. It also contains the DR-1 limit values, $2\dot{e}_{max}$, for each participant. The last column contains the mean values of each parameter. The values indicate the large average gap ($2\dot{e}_{max} \approx 12\sigma e$ and $2\dot{e}_{max} \approx 6\sigma\dot{e}$) between normal tracking of pre-failure dynamics and the expected error values for post-failure tracking according to [11].

Table IV: Individual and average pre-failure tracking standard deviation and DR-1 limit values

	P1	P2	P3	P4	P5	P6	Mean
σe [-]	.023	.022	.023	.023	.024	.022	.023
$\sigma\dot{e}$ [-/s]	.047	.043	.046	.042	.046	.043	.045
$2\lvert\dot{e}_{max}\rvert$ [-/s]	.312	.291	.276	.255	.299	.253	.281

E. Proposed Detection Limits

The size of the original first decision region from [11] is solely determined by $2|\dot{e}_{max}|$ in all directions. From Figure 20 it can quickly be observed that most of the predicted detections do not even come near these limits of DR-1. To link the theory of the decision regions to the results up until now, it is interesting to investigate what kind of limits would result in more realistic detection moments.

The proposed limits used in this analysis are multiples of the standard deviation values of the error and error rate of pre-

failure tracking. Since the detections in Figure 20 are presented relative to the blue distribution on either axis, a rectangular detection boundary based on both the standard deviations of the error and error rate signal for the limits is more appropriate. The standard deviation limits were calculated for each participant separately. These *new limits* were then applied on the experiment run data of each participant to determine the *first moment* at which the error or error rate would pass them, i.e., the predicted detection according to the new detection method. An example of how these new detection points were determined is shown in a phase plane in Figure 22. The classification of the predicted detections based on the error limit, i.e., left or right border, is demonstrated in Figure 23. This contains three of the detections of Figure 22.

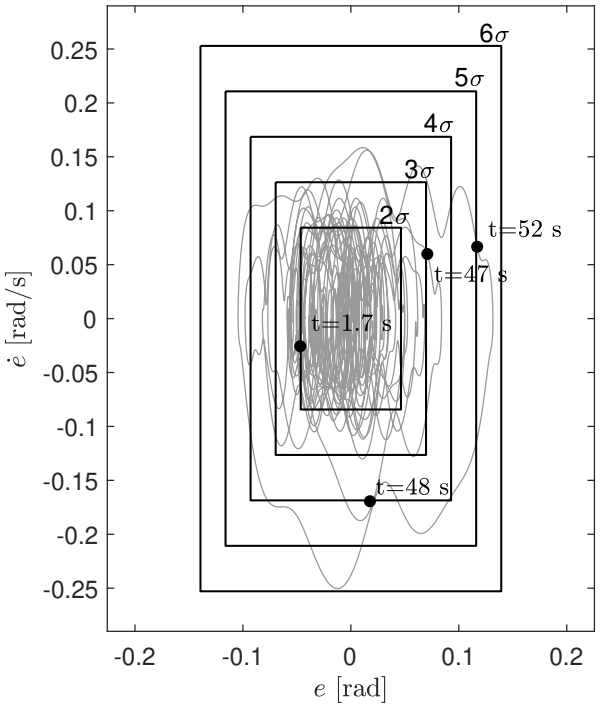

Figure 22: Phase plane of an example run showing the determined detection moments per detection limit

Expected detections are detections that fall in the range of the expected human detection time, which is 2.2-7.4 s [17]. Simulated detections that occur earlier than this 2.2 s are considered (too) early detections, i.e., false positives. When detections occur sometime later than 7.4 s but before the end of the run, they are classified as late detections. The last category consists of all the combinations of detection limits and runs that did not deliver a detection at all, i.e., false negatives. The detection limit of 6σ in Figure 22 yields a 'no detection' in this run. All together, these four categories cover all the possible detection options and therefore always add up to 100%. The overview of the distributions of classified simulated detections per limit based on each participant's individual standard deviation (σ_p) is shown in Figure 24.

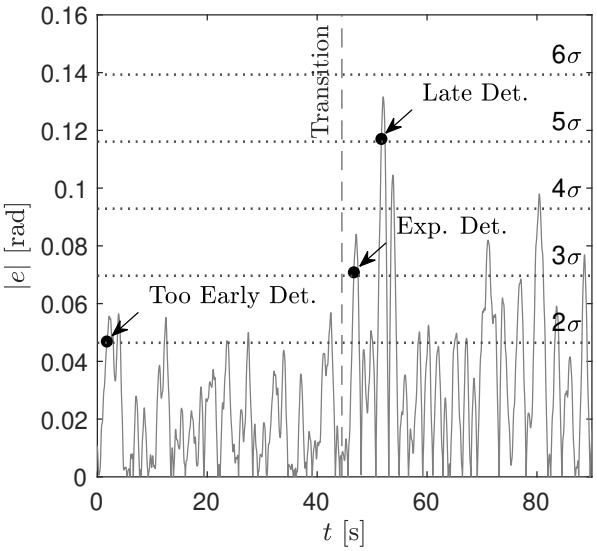

Figure 23: Absolute error signal of an example run showing the determined detection moments per detection limit together with their classification

Figure 25 shows the classification of simulated detections for the limits retrieved from the average standard deviations ($\bar{\sigma}$) of error and error rate for all participants together, which is 0.023 for error and 0.045 s^{-1} for error rate. The difference between Figure 24 and Figure 25 is mainly visible in the smoother shape of Figure 24, caused by the use of individual standard deviations. However, the data from the two figures only differ 1.0% per detection limit and classified detection on average. This implies that the average standard deviation can be used to model individual results, similar to using individual standard deviations.

The number of too early detections only starts to decrease after about 2.5σ in Figure 24. This makes sense considering that a deviation of 2σ from the mean during the pre-failure phase is very plausible, see also Figures 22 and 23. Around 4σ the expected and late detection parts become proportional, yielding a more realistic model regarding the experiment results. After that, the limit becomes too large resulting in many runs without detections.

When DR-1 [11] is applied, which for this experiment corresponds to a detection boundaries of 18σ for the error signal and to 9σ for the error rate signal for pre-failure tracking data, there are no early detections and no expected detections, 7.29% late detections and 92.7% no detections. The limit of $2\dot{e}_{max}$, thus, does not approximate to how the participants detected in this experiment.

The detection limit with the lowest proportion of early and no detections is 3.9σ, where in 9.38% of the runs there would be too early detections and in 11.5% of the runs would result in no detections. The portion of expected detections would in that case be 46.9% and the rest, 32.3%, would contain late detections. This detection limit yields results closer to what has been found with the button press data than when using DR-1: 6.25% too early detections, 50.0% expected detections,

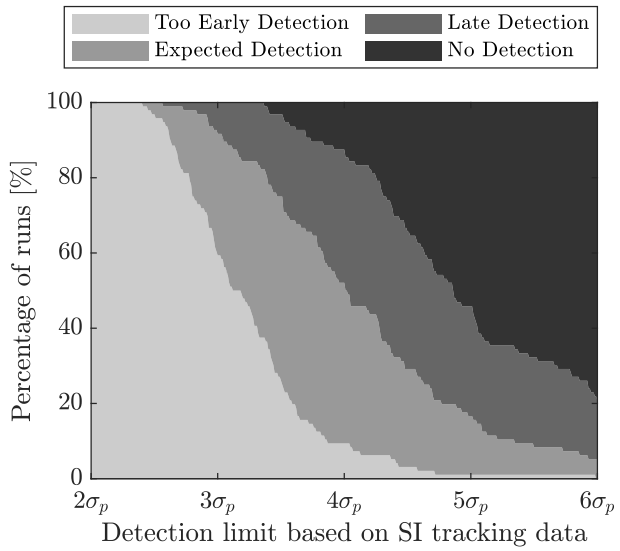

Figure 24: Classification of simulated detections from experiment data obtained by applying new detection limits with individually determined detection boundaries

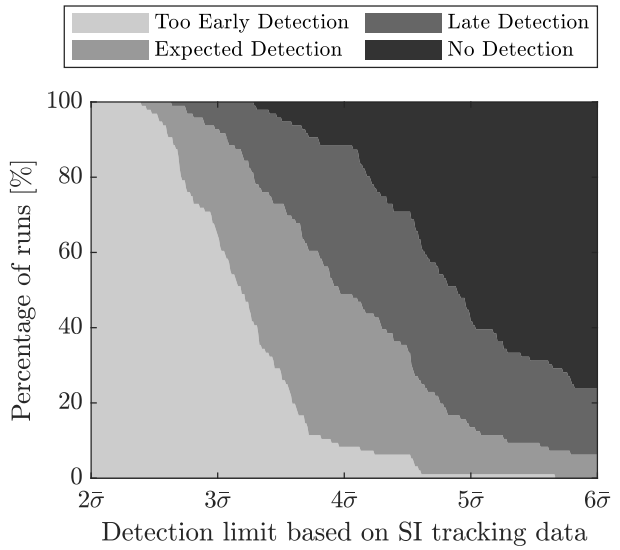

Figure 25: Classification of simulated detections from experiment data obtained by applying new detection limits with overall determined detection boundaries

42.7% late detections and 1.05% no detections. It is expected that the true detection limit of human operators is located in the vicinity of this value of 3.9 times the standard deviations of error and error rate, in contrast to what was proposed in [11] with the first decision region.

V. Discussion

The goal of this research was to gain a better understanding of adaptive manual control by assessing the supervisory control algorithm [11]. An experiment was executed in which participants were asked to perform a pitch tracking task. During the experiment the controlled element dynamics would change from single integrator to double integrator dynamics. The participants had to indicate, by pressing a trigger button on the side-stick, when they detected this transition. In total 6 participants performed 16 of these runs each with different moments of transition and different forcing function realizations. The data were analyzed to assess the supervisory control algorithm and come up with recommendations for more accurate and robust modeling of the adaptation process of human operators.

The supervisory control algorithm [11], [15], [16] tries to explain the way human operators adapt to changing controlled element dynamics. The first decision region (DR-1) from this algorithm was assessed in this research. Based on experiment results the general applicability of this decision region cannot be confirmed. First of all, the detections recorded by pushing the button yielded only one detection outside DR-1, apparently the participants detected the transitions at much lower error and error rate levels. Second, when applying the decision region on the experiment data to investigate if the error or error rate signals passed these limits, it was found that this occurs in only 8.4% of the runs. It was expected that there would be higher peaks in error and error rate signals immediately after the transition [11].

At least a more tailored detection limit is required for specific sets of dynamics. This might be solved by looking at relative error changes between the controlling of different controlled element dynamics [9]. Furthermore, DR-1 is square-shaped, i.e., the error and error rate have the same magnitude for their detection limit, while from the button press data a more stretched out shape arises. This suggests that there should be two limits defined: one for the error values and another one for the error rate values [12]. An initial analysis was performed on finding new detection limits based on standard deviations of the error and error rate of the pre-failure tracking data. A limit around 4σ appears to give realistic results.

As regards to the newly proposed limit, it was determined that using either individual standard deviations or average standard deviations yielded highly similar detection results with only a 1% difference on average per detection limit and detection classification. It might therefore be possible to determine a generally applicable value for the detection limit, instead of individual detection boundaries based on each participant's pre-failure tracking behavior.

Although the experiment results showed that DR-1 was not applicable for this specific set of dynamics (only one of the detections lay outside this region), and a more thorough investigation in which the dynamics of the original research [15] are implemented, is essential. It is striking that the observed results are so far off from what was expected. Repeating parts of the initial research could shed some light on the issue in future research. Furthermore, a closer look should be taken at the remaining decision regions. In this paper only the first decision region was considered, while the supervisory control algorithm is more extensive than that.

Since participants were selected who had earlier experience with similar tracking tasks, it was assumed that they would require little training to get to a constant performance. From

the greatly varying moments of detection in combination with the findings in control input adaptation, it becomes clear that the experience the participants had in 'normal' tracking tasks was not sufficient for this experiment. Most of the participants indicated they found it difficult to detect the transition. Training participants better in recognizing each dynamics option separately would presumably have produced less noisy results. In several occasions it also occurred that a participant confused the direction when the error would build up causing an even higher error, which also could have been prevented with better training. Therefore, in experiments with time-varying controlled element dynamics, participants should be well-trained in not only separate dynamics options, but also specifically in tracking with time-varying dynamics. They should be trained up until a point where not only their performance in tracking, but also detecting with the button press is more or less constant.

Another reason the button press data yielded such varying moments of detection is the fact that it is a subjective measurement. The participants had to press the button when they were certain that the dynamics were changed, but different participants have varying thresholds for detecting this change. Furthermore, they had to focus on both tracking performance and detecting the transition with the same side-stick. When either of these would have their priority, the performance in the other would probably decrease. The situation in which a participant gives a higher priority to tracking performance might increase their reaction time for pressing the button, since they have to switch their attention from moving the stick to pressing the button on the same stick. A possible way of avoiding this last issue is to separate tracking and pressing the button from each other, for example by using two different sticks: a stick on the right arm rest for tracking and a stick on the left arm rest for indicating detection. This might make it possible for the participants to give equal priority to both tasks.

For the control input analysis, a simplified model acquired with linear regression was used. Even though this gave some impression of the relative changes in control behavior, it is certainly not a realistic representation of the adaptive pilot model. To be able to compare absolute numbers, a more realistic pilot model should be applied [1], [17], [22], [23]. In this way a more accurate calculation of the pilot model parameters can be performed in the stable parts of a run (i.e., before the transition and at the end). Other current research is modeling the pilot model of the full process using time-domain data [3], [4], [17], [22]. A combination of binary decision models and this type of continuous modeling of the human operator might give a more complete idea of the human adaptation process [17].

A final discussion point concerns the choice of controlled element dynamics in the experiment. Only transitions between two specific controlled element dynamics were investigated, the choice of which was based on recent research using the same dynamics [4], [17] to be able to compare results. However, in the end this comparison was not performed, due to time constraints, and more simple controlled element dynamics could have been used (e.g., pure single and double integrator dynamics). Additionally, besides varying forcing functions and moments of transition, there was little variation between runs. The transition was always in the same direction (SI to DI) and every run would contain this change in controlled element dynamics. To prevent the participants from expecting (the same types of) transitions every run, which was not checked in this experiment, a more diverse experiment set-up could have resulted in more generally applicable results.

VI. Conclusions

In this paper, an attempt was made to validate an existing model of the human adaptive control process. The framework that was applied in this research was the *supervisory control algorithm*. In this algorithm the applied human operator dynamics move through different decision regions, using binary decision logic, when a transition in CE dynamics occurs. When the correct CE dynamics are identified and modified to the human operator finally assumes steady-state tracking. An experiment was conducted in which participants were asked to perform a single-axis pitch tracking task during which, after a varying amount of time, the dynamics would suddenly change from single integrator to double integrator dynamics. Besides keeping the error as low as possible, the participants were also asked to indicate when they detected this transition by means of pressing a button. The button press data are essential to have a concrete indication of when conscious detection would occur.

A first analysis was performed on the control input, from which it was observed that the participants adapted almost immediately when the dynamics changed, despite late indicated detections of sometimes even 40-50 s. Afterwards, a more indepth analysis on the detection process was performed. Results show that the originally reported first decision region of the supervisory control algorithm, which is responsible for the initial detection based on exceeding $2|\dot{e}_{max}|$, does not apply to the set-up of the experiment performed in this research. Based on the button press data, the participants detected on e and $\dot{e}$ values between 2 and 5 times the pre-failure standard deviation values, while the first decision region would lie in the vicinity of 18 and 9 times the standard deviation for e and $\dot{e}$, respectively. When new detection limits based on the standard deviation values of e and $\dot{e}$ were applied to the experiment run data, it was shown that the first decision region would result in almost 93% false negatives, since this level of e or $\dot{e}$ was never reached. A region yielding more promising results was located around four times the standard deviation of e and $\dot{e}$ of the pre-failure tracking data.

References

[1] D. T. McRuer and H. R. Jex, "A review of quasi-linear pilot models," *IEEE Transactions on Human Factors in Electronics*, vol. HFE-8, no. 3, pp. 231–249, 1967. [Online]. Available: https://dx.doi.org/10.1109/THFE.1967.234304

[2] D. M. Pool and P. M. T. Zaal, "A cybernetic approach to assess the training of manual control skills," *IFAC-PapersOnLine*, vol. 49, no. 19, pp. 343–348, 2016. [Online]. Available: https://dx.doi.org/10.1016/j.ifacol.2016.10.588

[3] P. M. T. Zaal, "Manual control adaptation to changing vehicle dynamics in roll–pitch control tasks," *Journal of Guidance, Control, and Dynamics*, vol. 39, no. 5, pp. 1046–1058, 2016. [Online]. Available: https://doi.org/10.2514/1.G001592

[4] P. M. T. Zaal and D. M. Pool, "Multimodal pilot behavior in multi-axis tracking tasks with time-varying motion cueing gains," Proceedings of AIAA Modeling and Simulation Technologies Conference, National Harbor, MD. [Online]. Available: https://dx.doi.org/10.2514/6.2014-0810

[5] M. Mulder, D. M. Pool, D. A. Abbink, E. R. Boer, P. M. T. Zaal, F. M. Drop, K. van der El, and M. M. van Paassen, "Manual control cybernetics: State-of-the-art and current trends," *IEEE Transactions on Human-Machine Systems*, vol. 48, no. 5, pp. 468–485, 2018. [Online]. Available: https://dx.doi.org/10.1109/THMS.2017.2761342

[6] L. R. Young, "On adaptive manual control," *Ergonomics*, vol. 10, no. 4, pp. 292–331, 1969. [Online]. Available: https://dx.doi.org/10.1109/TMMS.1969.299931

[7] L. R. Young, D. M. Green, J. I. Elkind, and J. A. Kelly, "Adaptive dynamic response characteristics of the human operator in simple manual control," *IEEE Transactions on Human Factors in Electronics*, vol. HFE-5, no. 1, 1964. [Online]. Available: https://dx.doi.org/10.1109/THFE.1964.231648

[8] J. D. McDonnell, "A preliminary study of human operator behavior following a step change in the controlled element," *IEEE Transactions on Human Factors in Electronics*, vol. HFE-7, no. 3, pp. 125–128, 1966. [Online]. Available: https://dx.doi.org/10.1109/THFE.1966.232651

[9] D. C. Miller and J. I. Elkind, "The adaptive response of the human controller to sudden changes in controlled process dynamics," *IEEE Transactions on Human Factors in Electronics*, vol. HFE-8, no. 3, pp. 218–223, 1967. [Online]. Available: https://dx.doi.org/10.1109/THFE.1967.233971

[10] D. H. Weir and A. V. Phatak, *Model of human operator response to step transitions in controlled element dynamics*. NASA, 1967. [Online]. Available: https://dx.doi.org/10.1037/e506122009-007

[11] A. V. Phatak and G. A. Bekey, "Model of the adaptive behavior of the human operator in response to a sudden change in the control situation," *IEEE Transactions on Man-Machine Systems*, vol. 10, no. 3, pp. 72–80, 1969. [Online]. Available: https://dx.doi.org/10.1109/TMMS.1969.299886

[12] R. J. Niemela and E. S. Krendel, "Detection of a change in plant dynamics in a man-machine system," *IEEE Transactions on Systems, Man, and Cybernetics*, vol. SMC-5, no. 6, pp. 615–617, 1975. [Online]. Available: https://dx.doi.org/10.1109/TSMC.1975.4309403

[13] R. A. Hess, "Modeling pilot control behavior with sudden changes in vehicle dynamics," *Journal of Aircraft*, vol. 46, no. 5, pp. 1584–1592, 2009. [Online]. Available: https://dx.doi.org/10.2514/1.41215

[14] ——, "Modeling the pilot detection of time-varying aircraft dynamics," *Journal of Aircraft*, vol. 49, 2012. [Online]. Available: https://doi.org/10.2514/1.C031805

[15] A. V. Phatak, "On the adaptive behavior of the human operator in response to a sudden change in the control situation," Ph.D. dissertation, University of Southern California, 1969.

[16] A. V. Phatak and G. A. Bekey, "Decision processes in the adaptive behavior of human controllers," *IEEE Transactions on Systems Science and Cybernetics*, vol. 5, no. 4, pp. 339–351, 1969. [Online]. Available: https://dx.doi.org/10.1109/TSSC.1969.300227

[17] W. Plaetinck, D. M. Pool, M. M. van Paassen, and M. Mulder, "Online identification of pilot adaptation to sudden degradations in vehicle stability," *IFAC-PapersOnLine*, vol. 51, no. 34, pp. 347–352, 2019. [Online]. Available: https://dx.doi.org/10.1016/j.ifacol.2019.01.020

[18] D. H. Weir and W. A. Johnson, *Pilot dynamic response to sudden flight control system failures and implications for design*. National Aeronautics and Space Administration, 1968, vol. 1087.

[19] M. M. van Paassen and M. Mulder, "Identification of human operator control behaviour in multiple-loop tracking tasks," *IFAC Proceedings Volumes*, vol. 31, no. 26, pp. 455–460, 1998. [Online]. Available: https://dx.doi.org/10.1016/s1474-6670(17)40135-2

[20] S. Thorpe, D. Fize, and C. Marlot, "Speed of processing in the human visual system," *Nature*, vol. 381, no. 6582, pp. 520–522, 1996. [Online]. Available: https://dx.doi.org/10.1038/381520a0

[21] V. W. Berger and Y. Zhou, *Kolmogorov–Smirnov Test: Overview*. American Cancer Society, 2014. [Online]. Available: https://onlinelibrary.wiley.com/doi/abs/10.1002/9781118445112.stat06558

[22] A. van Grootheest, D. M. Pool, M. van Paassen, and M. Mulder, "Identification of time-varying manual control adaptations with recursive ARX models," Proceedings of AIAA Modeling and Simulation Technologies Conference, Kissimmee, FL. [Online]. Available: https://dx.doi.org/10.2514/6.2018-0118

[23] R. Costello, "The surge model of the well-trained human operator in simple manual control," vol. 9, no. 1, pp. 2–9, 1968. [Online]. Available: https://dx.doi.org/10.1109/TMMS.1968.300028

Part II

Preliminary Thesis Report

NB: This part has been graded under AE4020 Literature Study

Chapter 1

Introduction

McRuer and Jex [12] provided a basis for understanding pilot control with the crossover model. This model is based on tasks where the task variables are constant and of a repeated nature, such that the circumstances are ideal to draw conclusions on the pilot response characteristics. However, still little is known about human behavior in response to tasks with varying task variables, like following a change in controlled element dynamics [13]. Due to the ability of human controllers to very rapidly adapt when being faced with a sudden failure, only a short time frame of data is available. This makes the popular and well-known strategies, which depend on average responses over a longer time span, for analyzing human behavior less useful [1].

In general, human controllers are very capable in the instantaneous detection of and adaptation to new dynamics. This is why most vehicles today are still being controlled or supervised by human operators. However, we are evolving into a world where more vehicles are getting more autonomous and require less human input [1]. It is necessary to assure that human operators will be able to at all time safely and securely control vehicles, especially considering that the 'simple' tasks will be the first ones being taken over by machines, requiring the 'harder' tasks still to be performed by human operators. For this reason, it is important to have a better understanding of how an operator is able to control machines and is able to adapt to new control situations. This information can be used to map the limitations of human controllers and to implement this in the designs of new evolving vehicles. The main research question of this research is:

How do human operators adapt instantaneously to a sudden change in controlled element dynamics?

To answer this question there will be a focus on understanding the different phases of the adaptive process: detection, identification and modification [2]. Furthermore, it is interesting to investigate if there is a difference in strategy adapting to different transitions in controlled element dynamics (i.e. stabilizing or destabilizing transitions) [1, 2, 3].

Several researchers already investigated this adaptive process [1, 3, 4, 5, 7, 14, 15, 16, 17, 18, 19, 20], but a general model or framework applicable to all cases is still lacking. The first part of this preliminary research therefore consists of an elaborate literature review in which

the most interesting models are mapped. Subsequently, a trade-off will be performed to show which models are most promising to extend on. The second part of this preliminary research consists of an initial simulation-based analysis of human adaptive behavior. This same part is used to elaborate on methods that can be used to analyze the simulation data and to identify a (time-varying) pilot model from measured data.

This report gives an overview of the preliminary work done on this topic and it is divided in different parts. In Chapter 2 a literature review on adaptive manual control is presented. It contains a background on the type adaptation that will be considered in this research and an overview of previous researches. Furthermore, it contains a part about a suitable analysis method. The next chapter, Chapter 3, is dedicated to computer simulations. It shows how the time-varying pilot model will be implemented and will present some resulting simulations. Finally, some initial simulations with step input and continuous input will shown. Chapter 4 contains the conclusions on this preliminary research, these will be used as a basis for the final part of this research. The final chapter, Chapter 5, is used to present the next steps of this research.

Chapter 2

Adaptive Manual Control

About 60 years ago, adaptive behavior of a human operator to changes in controlled element dynamics was of great interest in many investigations [1, 3, 4, 5, 14, 15, 16, 17, 18], which was primarily caused by the immense research budget of NASA due to the first moon missions at the time. However, the amount of interest decreased in the following years and only more recently this topic has had a revival in number of investigations [7, 19, 20]. Still, there is a lack of a general idea of what exactly happens during the adaptive process.

In this chapter an overview of the most interesting research on adaptive control behavior will be presented. Section 2-1 will give an overview of which factors can be responsible for inducing adaptive behavior. The next section, Section 2-2, consists of an overview of different models and ideas on the adaptive process. The section after that is used to show an analysis method that is often used in this research area: phase plane analysis. The last section, Section 2-4, contains the conclusions and summary of this chapter, where there is elaborated on which models might be most interesting to extend or to continue researching.

2-1 Adaptive Control Factors

Young [1] presents four adaptive functions that are responsible for fast adaptation in manual control. These functions are shown in a block diagram in Figure 2-1. *Input adaptation and prediction* concerns the ability of humans to recognize patterns in input signals. Depending on how predictable the signal is, the human operator can more or less control in an open loop fashion. Furthermore, it is also found that human operators use different control strategies when different bandwidths are used in input signals [21], which is quantitatively described in the crossover model by McRuer and Jex [12]. *Controlled element adaptation* indicates the ability of a human operator to adapt to changing system dynamics. In real life this may be caused by a sudden failure, or environmental factors causing the system dynamics to behave differently. *Task adaptation* refers to the strategy the human adopts depending on which factors of a task are considered more important. The objective of a certain task might be to minimize total error, which requires a different control strategy than when the operator has to minimize control effort. Last, *Programmed adaptation* is best described by open loop adaptive control, which is determined by knowledge of the environment. A human operator can apply certain control strategies based on memory of and experience with certain situations.

During this review there will be a main focus on the adaptation which occurs due to sudden changes in the controlled element dynamics. This type of transitions will induce so-called "fast" adaptations, the operator has only limited time to adjust their controlling behavior. There also exist "slow" adaptations, which could be induced by fatigue of the operator [1]. This type of adaptation is of less interest for this specific research.

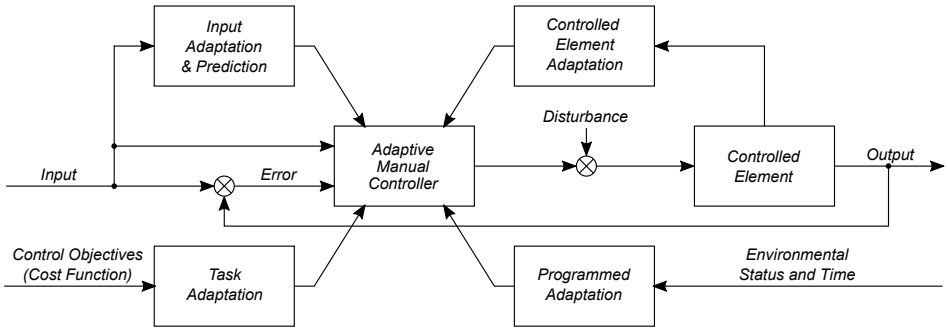

Figure 2-1: Four functions responsible for adaptation in manual control [1]

2-2 Previous Research

The next sections give an overview of previous research on adaptive manual control, which is presented in chronological order. Section 2-2-1 consists of one of the most early researches, in which was mainly focused on analyzing experimental data on adaptive behavior. In Section 2-2-2 a mode-switching model is presented, in which the human acts as an optimal controller as a first reaction to a change in dynamics. The next section (Section 2-2-3) contains a model based on the idea that a human operator has an internal model of the controlled element dynamics, that they can use to make predictions. Then, in Section 2-2-4, the sequential identification model is explained. Section 2-2-5 contains a description on how the human detection time can be accurately determined. The last section, Section 2-2-6, contains a mathematical model that can be used to describe the adaptive process for pursuit and multi-axis tracking tasks.

2-2-1 Early research on adaptive manual control by Young et al.

In 1964 Young et al. [2] performed one of the first reported experiments on human adaptive control. They then merely focused on the human adaptive behavior following sudden changes in gain and polarity of the controlled element dynamics being *a simple gain*. With this research they were trying to find an answer to two questions. They wanted to know how fast human adaptation takes place and which factors influence his speed. Furthermore, they wanted to find out what the process was of adaptation within the human operator, i.e., what information do they use to adjust to the new environmental dynamics.

The experiment was conducted with an analogue computer. It was able to give two parallel channels of control modes, which could be switched during the experiment. Each channel consisted of 10 options for different controlled element dynamics. It was possible to set one option on a channel per time. The channel was only switched when the conditions were such

that no discontinuities would occur during the transition. After the channel was switched the 'free' channel could be set to a different controlled element dynamics for the next transition. The experiment was performed with both compensatory and pursuit tracking. Participants were well-trained in the different gain cases and were aware that gain changes would suddenly occur during the runs. They got the instruction to act as quickly as possible in adapting to the new system and at all time keep the error as low as possible. In Table 2-1 the set-up of the experiment performed by Young et al. [2] in this research is summarized.

Table 2-1: Experiment overview Young et al. [2]

Experiment description	Each subject performs two runs with 24 transitions for each controlled element dynamics mode. The instantaneous transition were restricted to switching between only two control modes each run.
Apparatus	Spring restrained control stick connected to an Electronic Associates Incorporated TR-48 analog computer
Display	Compensatory & Pursuit (single-axis, horizontal tracking task)
CE dynamics	Unity gain (+1, +2, +4, +8, -1, -2, -4, -8)
Forcing Function(s)	Step input: random series of discontinuous jumps. Continuous input: sum of sinusoids, rectangular spectrum of high frequency cutoff at 0.24cps and RMS amplitude of 1.5 inch on display
Participants	Only results of *two* participants were presented

Firstly, Young et al. [2] investigated the adaptive process in response to a step input with a couple of informal experiments. The response to a step input is fairly well-known and therefore it would give a clear view of the difference between a desired output and the output after a transition of controlled element. From the test it became clear that humans have a reaction time of 0.2-0.4s after which a fast movement was initiated to directly compensate the error, reaching the stable amplitude after 0.3-0.5s. When the gain was increased, the output would contain a couple of overshoots around the desired amplitude which would be reduced to zero error within 2 seconds. In successive runs with the same gain, the human operator showed quick adaptation where less overshoots occurred and even some undershoots, indicating that he had lowered his own gain to compensate the higher controlled element gain. When the gain was decreased, the initial response consisted of an undershoot followed by some corrective movements to reach the desired amplitude. Similar to the increase of the gain, the participant was within few runs able to adapt to the new system showing a cleaner response to the step input, indicating that he now had increased his own gain. From the tests with the step input, it was concluded that almost the full adaptation process took place within the first run. Due to this rapid process, they argued that using a step as input to analyze this process is less interesting than looking at the response of a continuous input.

Then, Young et al. [2] performed some tests with a continuous input. The experiments consisted of gain increases, gain decreases, polarity reversals and combinations of those. The difficulty with using a continuous input for analyzing adaptation is that the input also contributes inconsistently to the error. Therefore, the data of the response after transition were

analyzed using average error waveforms. The average error waveform filters the errors which are not common in response to a transition, while it does show the error shapes which occur regularly after a transition. Furthermore, in all their analyses they subtracted the average waveform without transition from the average waveform with transition, which diminished the influence of the input signal on the analysis even more. An example of such an average error waveform after a polarity reversal and increase in gain is given in Figure 2-2.

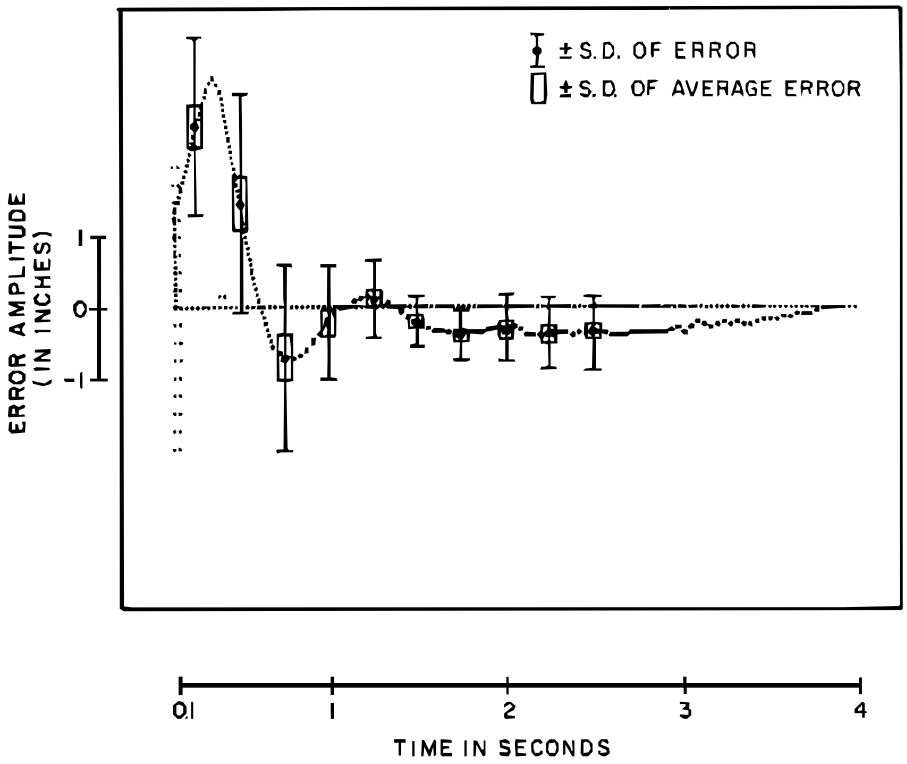

Figure 2-2: Average error waveform following a reversal increase with a compensatory display [2]

Immediately after a polarity reversal the system has an unstable positive feedback loop. The human operator needs to act fast in reversing his own polarity to stabilize the system again. From the experiments it was shown that the initial response after the transition contains a sharp rise until after 0.5s the error drops again as rapidly. After the operator reverses his control, the error is quickly brought within bounds. When only a gain increase is applied a similar effect as with the step input is found. There immediately is a large error increase, but within 0.3s the error is corrected resulting in a smaller overshoot on the other side. This means the operator was able to already stabilize the system before the second peak. After that the error is brought back to the desired bounds in 1-2s. For a gain decrease the consequences are smaller. The error only increases slowly, i.e., there is no question of an unstable system. Within 1-2s the operators were able to adapt to the new system. Then, for a combination of gain increase and polarity reversal the initial response gives the highest peak error. Lastly, the system becomes sluggish when a reversal decrease is applied. It takes some time for the error to build up, after which it also takes a long time for the error to reach its asymptotic value again. From the combined transitions it was also found that human operators first change their polarity and only afterwards adapt to the new gain. However, more thorough

research has to be performed for a better and more general understanding of this process.

Young et al. [2] suggested in conclusion that the adaptation process consists of three phases: detection, identification and modification. Furthermore, they stated that the main information on human adaptation can be found by analyzing the error signal. Since, the discussion in this research solely focused on the outcome of the compensatory tracking task experiment, it remains unclear what the specific influence of a pursuit display would be on the adaptive behavior of a human operator.

2-2-2 Optimal human controller by Weir and Phatak

Weir and Phatak [3] came up with a mode-switching model with a main focus on the phase just after detection of a change in controlled element by the human operator, which they believe is of an optimal control nature under certain conditions. Their model consists of three modes/phases.

The first phase is the phase before a change in controlled element dynamics is detected. In this *pretransition retention* phase the operator continues to control the controlled element as if it contains the pretransition dynamics.

After detection the operator starts behaving like a *time-optimal controller*, to immediately decrease the (too) large error and error rate to acceptable levels. Plotting such time-optimal or bang-bang control behavior in a phase plane gives a distinct shape. In Figure 2-3 such a trajectory is plotted. At t_1 a control reversal occurs, this continues until t_2, which is the first bang. At t_2 the second reversal is initiated to move the error and error rate back to the threshold values. The second bang is generally shorter than the first bang. Depending on the dynamics of the posttransition system and the maximum stick deflection, this trajectory will look different. In earlier work [22, 23] it was found that human operators tend to control as a time-optimal controller when control tasks become harder or when sudden increases in error occur (e.g., due to discontinuous input signals), which is consistent with this hypothesis for specific transition cases where the system briefly is unstable and therefore 'hard' to control.

The last phase of their switching-mode model is the *posttransition steady state* phase. When the error and error rate are within bounds again after the time-optimal control response, the human operator switches back to the steady-state quasi-linear control form that fits the new system dynamics. Weir and Phatak [3] did not focus on this part of the adaptation process and do not present a model by what method identification takes place. They merely assume the human operator is able to identify and adjust to the correct dynamic system for steady-state tracking.

To verify their model they used data of earlier research and experiments. In these experiments the controlled element dynamics were varied by means of an instantaneous change in order, gain and/or polarity. These changes occurred randomly during a run, but were restricted by a moment where the input rate was large enough not to result in a large deficiency in display error. The only information that was given to the human operator was the value of the error (compensatory tracking task). The input was a low frequency random-appearing forcing function, where the operator only had to control in one direction. A more detailed overview of this experiment is given in Table 2-2.

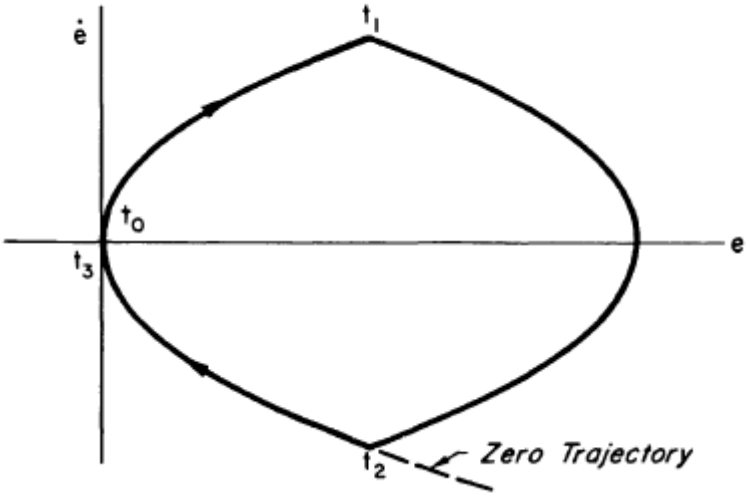

Figure 2-3: Bang-bang response in a simple single-order system ($\frac{K}{s}$) [3]

Table 2-2: Experiment overview Weir and Phatak [3]

Experiment description	Data from older experiments was used. Experiment runs consisted of randomly picked, instantaneous transitions to different controlled element dynamics, the operator was not aware of when the transition would occur and what the type of transition would be.
Apparatus	Spring restrained control stick
Display	Single-axis compensatory
CE dynamics	K, K/s, K/s^2 (transitions consisted of (a combination of) changes in order, gain magnitude, or polarity)
Forcing Function(s)	Sum of sinusoids, rectangular spectrum with cutoff frequency at 1.5rad/s
Participants	NA

For their analysis Weir and Phatak [3] mainly focused on transitions which would yield an unstable system during the pretransition retention. These situations gave the most time-optimal control type of trajectories, as the participant had to react quickly to retain control. In most of these cases the data is consistent with the mode-switching model following the bang-bang trajectory in the phase plane quite nicely. However, there were some unexpected results were the human operator reversed control, while there was no polarity reversal in the controlled element dynamics. It is discussed that this is caused by the high penalty imposed for not reacting in time to a polarity reversal and letting the error get too large. The human operator is therefore too careful by immediately mitigating the chance of a high error due to a polarity reversal by reversing the control beforehand. Furthermore, there was

no direct knowledge on how well the participants were trained. And, since, there also was a clear distinction between the levels of performance of the participants, the data might not be comparable.

2-2-3 Miller and Elkind's model of the human decision process following a transition in controlled element dynamics

Miller and Elkind [4] continued the research on the adaptive response of the human controller in 1967. They presented one of the first practical models for adaptive manual control. In their model they considered a well-trained human operator performing a compensatory tracking task using a single integrator controller with a continuous input. The adaptive behavior of the operator would be triggered by step changes in the controlled element dynamics. They described the processes for each separate phase of adaptation: detection, identification and modification, and optimization [2, 18].

Model

They state that in the *detection phase* the recognition of a change in controlled element dynamics by a human operator is based on the difference between actual and expected change in error rate (see Equation 2-2, where $\widehat{\Delta\frac{de}{dt}}$ is the expected change in error rate). As an example, the calculation of the expected change in error rate for single integrator controlled element dynamics, assuming the operator's internal model approaches the true model well, is given by the following equation:

$$\widehat{\Delta\frac{de}{dt}} = -K_m\Delta c \tag{2-1}$$

K_m is the gain of the operator's internal model of the dynamics and Δc is the change in control input. Due to the fact that only well-trained human operators were considered, it could be assumed that the operator has an internal model of the controlled element dynamics that approaches the actual dynamics fairly well. Therefore, it can be deduced that the operator also has a good idea of the expected change in error rate for the current dynamics.

$$\Delta\epsilon = \Delta\frac{de}{dt} - \widehat{\Delta\frac{de}{dt}} \tag{2-2}$$

Due to the unpredictability of the input signal and prediction errors due to memory limitations in the internal model, the human operator is not able to completely accurately predict the error signal, however, they will know what the standard deviation ($\sigma_{\Delta\epsilon}$) is of $\Delta\epsilon$ during tracking of the time-invariant controller dynamics. When the ratio between these values ($\frac{\Delta\epsilon}{\sigma_{\Delta\epsilon}}$) exceeds a certain limit, the controller will detect that a change in dynamics has occurred. This limit Miller and Elkind [4] called the "acceptability limit". This way of modeling directly accounts for the differences in the moment of detection which were found in other researches [14, 18]. It is now clear that this highly depends on the input signal and current dynamics of the controlled element.

After detection the operator enters the *identification phase*, where he needs to identify which system he has to adjust to to recover within the acceptability limits. Again, the operators considered for this model are well-trained in all possible systems, therefore they have a good internal model of all of them, i.e., single integrator systems with varying gains. To identify the system that fits the new change in error rate, the operator internally calculates the $\Delta\epsilon_i$ for every system and tries to find the one(s) that generates a $\Delta\epsilon$ below the acceptability limits. When he finds that none of the systems yield a low enough $\Delta\epsilon$, it can be the case that the detection occurred during the transition, which means that $\Delta\epsilon$ will be too large for any system to give a fit. In this case the transition itself should also be accounted for in identifying the correct new system. This is done by considering the change in system gain during the interval and including this change in calculating $\Delta\epsilon_i$. When this still not yields a suitable system, the operator will move on to the next time interval and go through the whole decision process again until the new system is identified. This identification process is visualized by means of a decision tree in Figure 2-4.

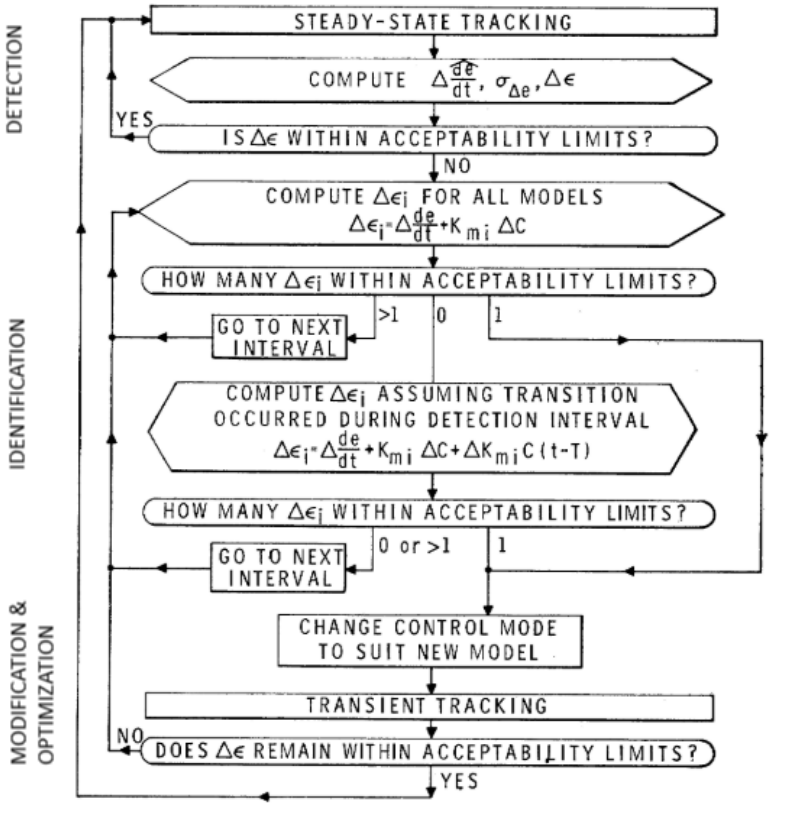

Figure 2-4: Identification process decision tree [4]

The last phases, *modification and optimization*, consist of the operator adjusting his own parameters to the new found system and getting the error within thresholds again. Miller and Elkind [4] based this on previous research from [2, 3].

Experiment

Miller and Elkind [4] had three participants in their experiment, who were well-trained in the different dynamic systems (10/s, -10/s, 2/s, -2/s) and could recognise transitions between those systems. The set-up consisted of a compensatory tracking display which showed a dot which could be controlled by a joystick (only left and right) to keep it on the target circle in the center. On the joystick was also a button, which the participants were instructed to release when they detected a change in system dynamics. They researched if adding this action to the tracking task had a significant influence on the performance and it did not [24]. The overview of the experiment performed by Miller and Elkind [4] is given in Table 2-3.

Table 2-3: Experiment overview Miller and Elkind [4]

Experiment description	Participants were trained in controlling with each CE dynamics separately and in controlling with all transitions between CE dynamics. Next to normal tracking (keeping error as low as possible), they were also instructed to release a signaling button once they detected a change in CE dynamics.
Apparatus	11-inch-long nylon stick attached to a Measurement Systems Inc. Model 435 force-sensitive hand control. Stick could move left-right and up-down. Only left-right movement used in experiment.
Display	Single-axis compensatory
CE dynamics	10/s, -10/s, 2/s, -2/s (transitions consisted of an instantaneous gain increase, gain decrease or polarity reversal)
Forcing Function(s)	Quasi-Gaussian distribution of amplitude with a 0.24 Hz cutoff frequency. Signal caused a 2.1 cm RMS movement of $\dot{e}$ in presence of no stick-input.
Participants	3 participants (all 21-year-old males)

Firstly, they investigated the process during the *detection phase*. The reaction time of a human operator is approximately 200 [4], so it was assumed that the operator detected the transition 200 ms before the button on the joystick was released. By plotting the expected change in error rate ($\widehat{\Delta \frac{de}{dt}}$) against the difference between the expected and actual change in error rate $\Delta\epsilon$ at the moment of detection, the acceptability limits could be determined. From this it was found that there was a large variation in detection times for the transitions where the system became unstable (gain increases and polarity reversals), due to the change in error rate going up too fast. However, the gain decrease transitions did give more stable results as the error had a slower build-up. From the latter the acceptability limits were deduced, which afterwards were used to predict the detection times and compare them to the measured detection times. There was an average discrepancy of about 400 ms where the model indicated that detection would take place earlier then the measured data, which can be seen in Figure 2-5. This could be explained by the reaction time and calculation time of a human operator, which are combined about that same duration.

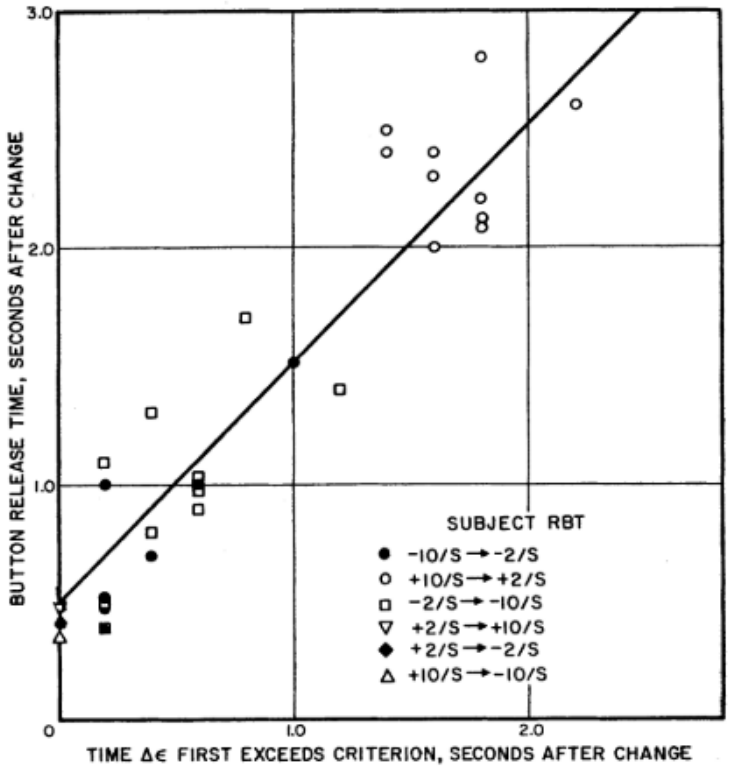

Figure 2-5: Predicted versus actual detection data from [4]

The next step was to check if the model could also predict the correct system after transition and if, when a participant made a mistake, the model could clarify why this happened. The participants always correctly identified the right system when the transition was a gain increase or a polarity reversal. The model was not far off too comparing it with the experiment data. Except for some corner cases, where the participant possibly made a decision for one system based on probability calculations, while for that interval there were more possible options giving a $\Delta\epsilon$ inside the acceptability limits. When the transition was a gain decrease, the participants had more trouble identifying the right system, identifying it almost half of the time as a polarity reversal. The model in this case also identified most of those runs as a polar reversal, showing that the model can even predict when a human is not able to identify the right system.

2-2-4 Sequential identification of control situations by Phatak and Bekey

Phatak and Bekey [5, 10] expanded on the earlier models [3, 4] by trying to make the decision-control logic complete for the response of a human operator to a change in controlled element dynamics. The model they proposed is based on the idea that the identification process happens in a sequential order of possible modes using pattern recognition of the error and error rate. The error and error rate pass so-called "decision regions" when a failure occurs, depending on when these values pass these decision regions certain system dynamics can be deduced by the human operator.

Model

It is hypothesized that a human operator is able to store the normal error values for the prefailure system dynamics, when these values pass certain limits, defined by the decision regions, the operator will detect a failure. In Figure 2-6 a phase plane with error and error rate on the axes and containing the decision regions is shown. During a change in controlled element dynamics the error and error rate will increase. When these values pass the first decision region, the supervisory control algorithm will move to the next step in the decision tree. The human operator model is adjusted based on the mental model of that specific level in the decision tree. Consequentially, the error rate will change sign and move to the other side of the phase plane. The next step is determined by whether the error values enter the second decision region or stay within bounds, the latter would mean that the current model for the human operator already is sufficient to handle the new system. Otherwise, the next step in the decision tree is reached and the human operator model is adjusted again. This process continues until the system is stable and the error values reduce to normal levels. The decision regions were empirically determined and depend on the controlled element dynamics which are being considered. Thus, there is no concrete basis to formulate a strategy to come up with these regions without performing experiments first.

Experiment

To verify their model, Phatak and Bekey [5] performed an experiment and compared the data with their model. For the time-varying control situation they used the failure of the stability augmentation of an aircraft. This augmentation system consists of two feedback loops, where either or both could be failed to induce the time-varying component. The participants were well-trained in all the possible system dynamics, however, they did not have any information about the dynamics, nor were they signaled when a failure would occur. The runs would last three to four minutes, where the failure would occur randomly during the run. A more detailed overview of the experiment is given in Table 2-4.

Table 2-4: Experiment overview Phatak and Bekey [5, 10]

Experiment description	Runs lasted three to four minutes, one to three minutes before end of run the dynamics would instantaneously change
Apparatus	NA
Display	Single-axis compensatory (roll control task)
CE dynamics	Dynamics based on different augmentation levels of a VTOL aircraft
Forcing Function(s)	Low frequency random appearing input (sum of sinusoids) with 1.5 rad/s cutoff. RMS value of signal on display was 5°
# Participants	1 participant (well-trained pilot)

Figure 2-7 shows the results of one of the runs of the experiment and the corresponding model output. TF, Time of Failure, is the moment the system dynamics change. In this example

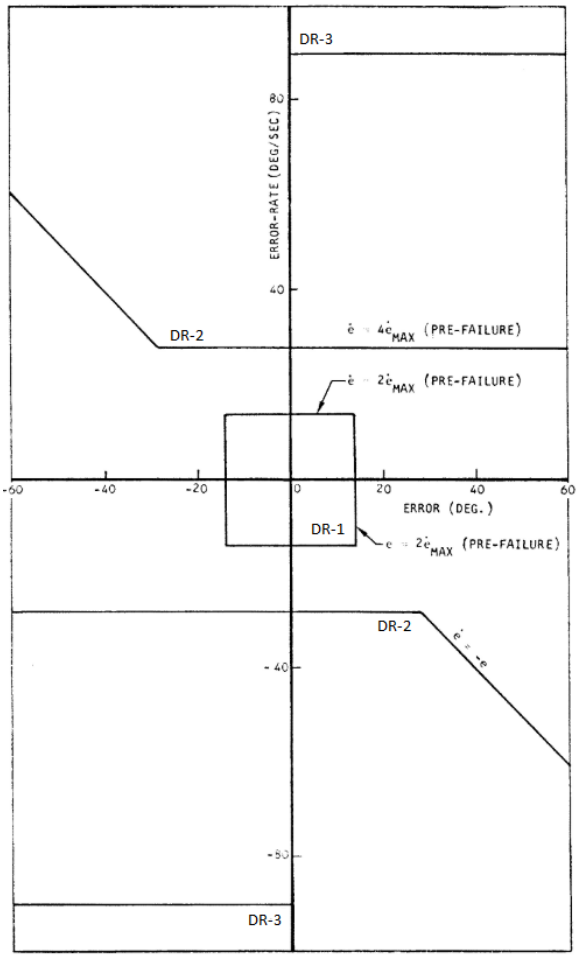

Figure 2-6: Decision regions in phase plane from supervisory control algorithm [5]

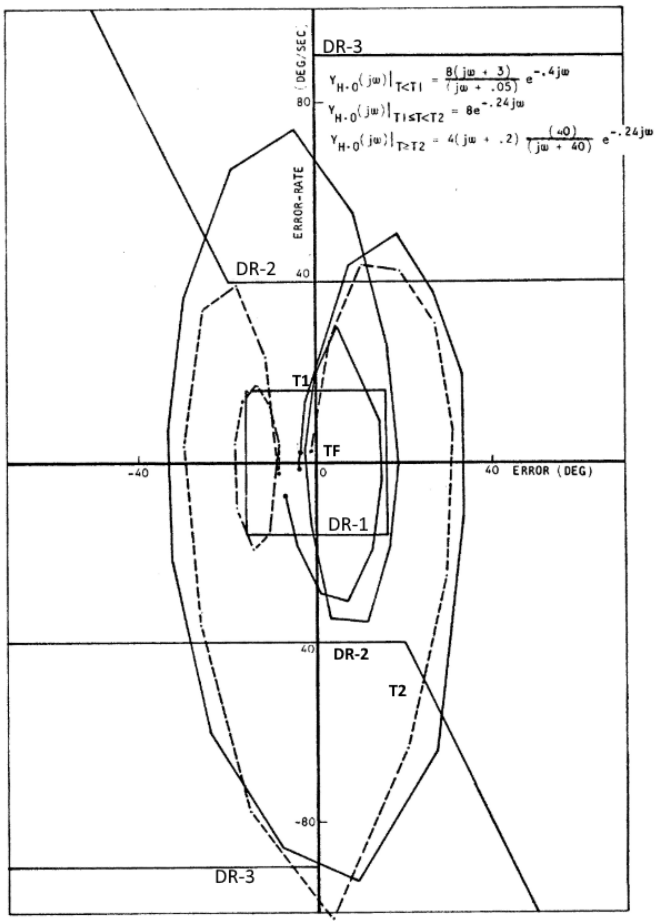

Figure 2-7: Model (dashed line) and experimental (solid line) data in phase plane [5]

both feedback loops failed. It can be seen that both trajectories immediately pass the first decision region (at T1) and on the way back also pass the second decision region (at T2), after which the error and error rate reduce to zero. This shape of the trajectory is as expected, the operator model is adjusted to fit the controlled dynamics without an augmentation system. After the second change of sign of the error rate the model and experiment data do diverge. This can be explained by the model being a more optimal controller than a human, therefore the human has a bit of higher delay. Due to the stochastic nature of the human response to failure, more experiments have to be conducted to draw conclusions on the validity of the model.

2-2-5 Experimental deduction of detection timing of a change in controlled element dynamics by Niemela and Krendel

In 1975 Niemela and Krendel [6] performed an experiment to accurately determine the time that a human operator requires to detect a change in controlled element dynamics. The

experiment consisted of a compensatory tracking task, with a continuous input. One run would take about two minutes, in the middle of the run the dynamics of the controlled element would be reversed. For the dynamics they took a double integrator. The experiment was split in two parts. One part with five participants where the experiment was performed as described, to give an idea on the general process of reacting to a change in controlled element dynamics. The other part of the experiment was conducted with one participant where the participant was alerted by a tone when a change in dynamics had occurred, this part focused on determination of the detection boundaries. The details of the experiment are given in Table 2-5.

Table 2-5: Experiment overview Niemela and Krendel [6]

Experiment description	Two types of experiments were conducted. In both experiments the runs were two minute tracking tasks during during which an instantaneous polarity reversal of the CE dynamics would occur. In the supplemental experiment the participant was alerted at different moments around a transition by an audio tone, this was used to analyze the detection behavior.
Apparatus	Lightly damped single-axis sidearm controller
Display	Single-axis compensatory
CE dynamics	Double integrator (transitions consisted of polarity reversals)
Forcing Function(s)	Low-pass filtered white noise with an equivalent statistical bandwidth of 1.5 rad/s
# Participants	6 participant (5 in main experiment, 1 in supplemental experiment)

From the first part of the experiment it was clear that after detection by the human operator a steep peak of the error rate occurs, which was also found by [2, 3]. There were a few exceptions were the error did not get out of bound, which was probably caused by the error rate pushing the error directly back to the origin, causing the operator to not note the change in dynamics at all. Eventually, it could be concluded from the data that detection only occurred when the error and error rate were relatively large and were both in the first or third quadrant of the phase plane, which confirms the findings of [4, 5].

In the second part the participant was alerted when a change in dynamics had occurred. The time of the alert would be varied to find when the alert would still be useful for the operator to lower the average peak error. From this the detection boundaries could be determined. When the alert was useful the human detection threshold was not met yet and the average peak error would be lower than without an alert. When the alert did not yield a lower average peak error the operator had detected the change already himself. With these average peak errors, reached with the different alerting tone occasions, Figure 2-8 was produced, where the values are based on multiples of the root mean square steady-state error and error rate. These subfigures show the areas in which it is very likely that detection will or will not occur. Therefore the transition region for detection is in between the shaded shapes of the two subfigures. It can be concluded that for this specific system detection by the human

operator occurs when both error and error rate move outside the steady-state tracking region at the same time. In Figure 2-9 the combined results of both the main experiment, from which the steady-state tracking boundaries are deduced, and the supplementary experiment, from which the detection boundaries are deduced, are shown.

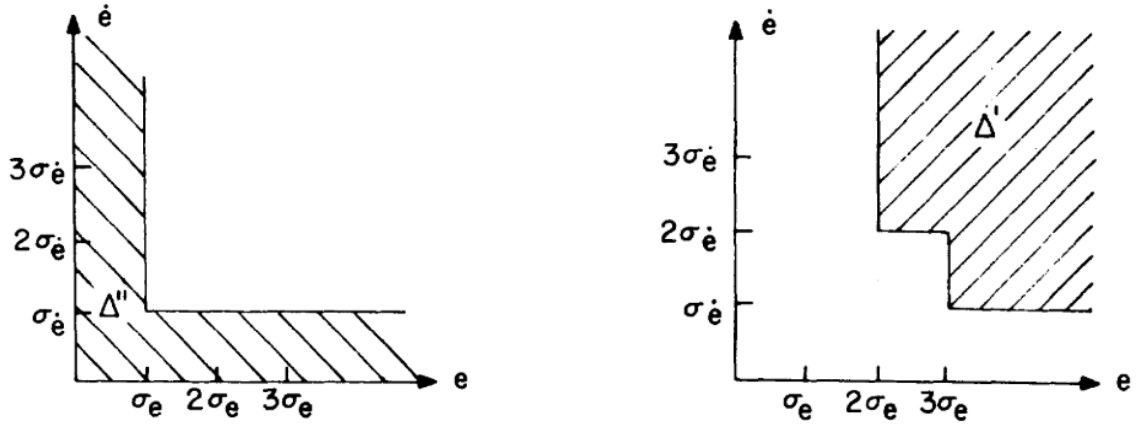

Figure 2-8: Alerting boundaries which did (left) and did not (right) reduce average peak error [6]

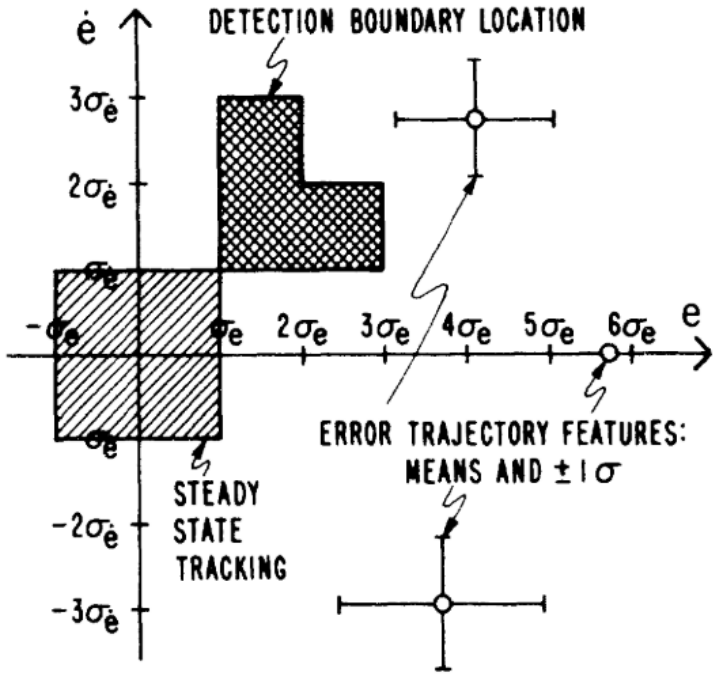

Figure 2-9: Findings of both experiments combined [6]

2-2-6 An adaptive human pilot model for multi-axis tracking tasks by Hess

More recent research on the human behavior in loss-of-control situations was performed by Hess [7, 8, 19, 25, 26, 27]. He came up with a pursuit display human operator model, where the pilot uses both the vehicle output (M) and output rate ($\dot{M}$) to perform a tracking task, as is displayed in Figure 2-10. K_p and K_r are the pilot gains in the position and rate loops, respectively. G_{nm} are the neuromuscular dynamics of the human operator. Additionally, in this same figure the adaptive structure of the model is shown, where the output rate and error are directly fed into an 'adaptive logic', which is used to modify the gains whenever there is a change in controlled element dynamics or other situations where adaptation is required. The fundamental principle of this model is that adaptation mainly occurs by modifying the gain of the inner loop, whereas adjustment of the outer loop gain is more suitable for tuning the overall performance. In [19] four guidelines are presented that are at the basis of this model. Firstly, K_p and K_r have to stay within realistic bounds, there is a limit on the human capabilities. Second, detection during the adaptive process can only occur based on information evident to the human operator. Third, pre- and post-transition operator parameters follow the crossover model [12]. Lastly, adaptation occurs relatively quickly after detection by the human operator of a change in controlled element dynamics.

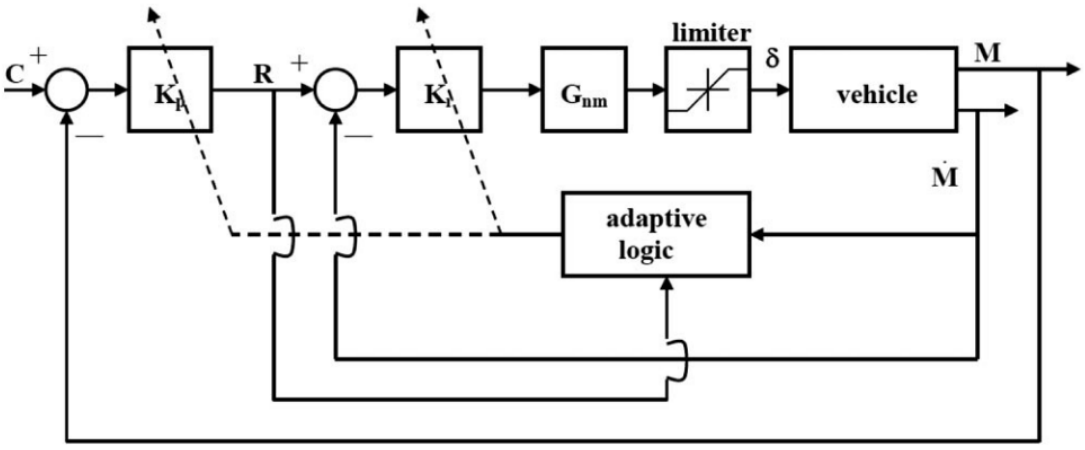

Figure 2-10: Adaptive form of a simplified pursuit control model of a human operator [7]

In this model detecting a change in system dynamics relies on the magnitude and sign of $R - \dot{M}$, i.e., the inner-loop gain. Hess [8] empirically came up with relations between this quantity and the associated gain magnitudes. The signal that is perceived by humans in the adaptation logic is described by Equation 2-3 in the shape of a criterion signal (x). The last part of this relation is a second-order filter, which simulates the human way of smoothing and lag in the process [28].

$$x = sgn\{|R| - |\dot{M}|\} \cdot [|R| - |\dot{M}|]^2 \cdot \frac{1.5^2}{s^2 + 1(1.5)s + 1.5^2} \tag{2-3}$$

The next part, Equation 2-4, is necessary to determine if adaptation is required. The square root of x is used for the reason that the square of the error was used to come up with x.

The factor of three defines the magnitude of $\sqrt{x}$ compared to the root mean square of $\sqrt{x}$ (determined by a tracking run without transitions), that is required for a human operator to detect a change in controlled element dynamics. Furthermore, t_c is the moment of transition and t_s is a small time value to not take into account the run-in time of the run [7].

$$K_{trigger} = \begin{cases} 0 \text{ if the instantaneous value of } \sqrt{|x|} < 3 \cdot rms\left[\sqrt{|x|}\right] & \text{or } t < t_c \\ 1 \text{ if the instantaneous value of } \sqrt{|x|} \geq 3 \cdot rms\left[\sqrt{|x|}\right] & \text{or } t \geq t_s \end{cases} \tag{2-4}$$

The change in the inner loop gain, K_r, is then given by Equation 2-5. x_n is given by Equation 2-6. In these relations the second-order filter is again used to simulate the human adaptation process. The number of variables controlled by the human operator is denoted by the variable N, which is based on the principle that an operator will control less aggressively in multi-axis control tasks [8].

$$\Delta K_r = x_n K_{trigger} \cdot \frac{1}{s^2 + 2s + 1} \tag{2-5}$$

$$x_n = \frac{x}{rms[R^2]} \cdot \frac{1}{s^2 + 2s + 1} \cdot \frac{1}{N} \tag{2-6}$$

The last part, introduced by Hess [25], is the relation that is used to determine the change in outer loop gain, K_p. This is given in Equation 2-7. Hess [7] explains this relation by saying that when K_r is reduced, it does not necessarily have an effect on the stability of the whole system and therefore does not require a change in K_p. While, when K_r increases, the vehicle dynamics might be such that a change in outer loop is required to compensate for a possibly lower phase margin. Lastly, both K_p and K_r have limits on their magnitudes of 2 and 10 times their initial values, respectively. These values are based on findings from [25].

$$\Delta K_p = \begin{cases} 0.35 \cdot \Delta K_r & \text{if } \Delta K_r > 0 \\ 0 & \text{if } \Delta K_r \leq 0 \end{cases} \tag{2-7}$$

Hess shows the capabilities of his model using computer simulations. One such example is given in Figure 2-11. However, only few of his researches are backed-up with experimental data, which therefore makes it difficult to verify some of the empirically derived values.

2-3 Phase plane analysis

Frequency analyses are not useful when investigating the adaptive process: the human model is time-invariant and the duration of the process is too short. Therefore, an analysis in the time-domain is required to gain a better understanding of how a human operator adapts. There exist time-varying identification methods using the time-domain, like Kalman filtering [29], recursive least squares [30] or wavelets [9], which are useful for identifying the human operator dynamics for "slow" adaptations (e.g. due to fatigue). However, in this research there is a focus on situations where there is a sudden change in controlled element dynamics,

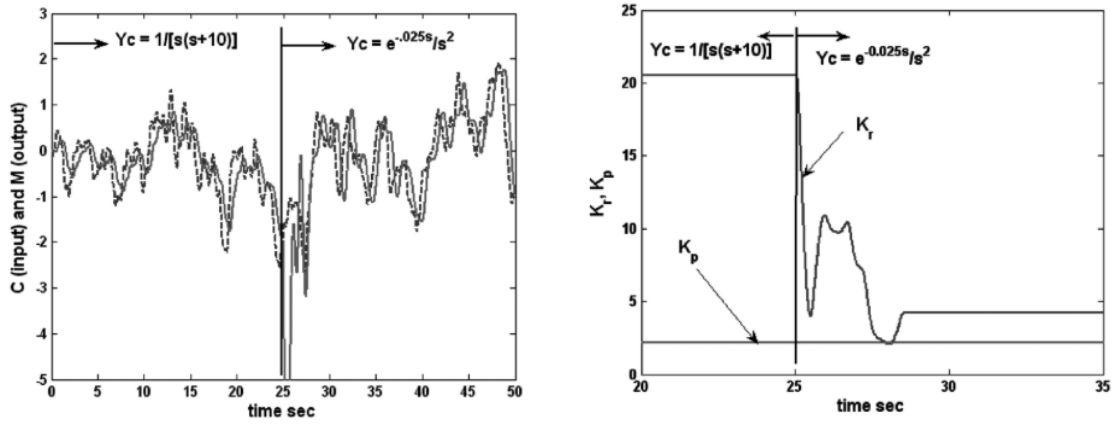

Figure 2-11: Computer simulation of adaptation logic from Hess [8], with the time history of input (dashed) and output (solid) on the left and the corresponding time histories of the gains on the right

hence when "fast" adaptation is required. In these situations only limited data are available, yielding bad results when using these proposed time-varying identification methods.

Another analysis method is desired. In this chapter multiple researches were presented which used the phase plane as a tool to analyze the response to a transition. In these phase planes the position is on the x-axis and the velocity is on the y-axis. Phase planes can immediately show the type of stability and class of a system [31]. Depending on the direction and steepness of the spiraling or circular curve conclusions can be drawn about the stability of a system. Since error in a compensatory tracking task is the only information available to the human operator, the error signal is the most interesting response to inspect when trying to find out more about the adaptive process [2]. The phase planes therefore have the error $e(t)$ on the x-axis and error rate $\dot{e}(t)$ on the y-axis.

A way to analyze the shape of a phase plane is presented in [32], where the characteristics of the curve are indications of the control strategy of an operator. Figure 2-12 shows a phase plane of an adaptive process. The gain is instantaneously increased from two to eight for a single integrator controlled element. The curve is recorded from the moment of the transition. The error had an immediate 'jump' up due to the transition (at 'T' in figure), which explains the relatively large starting value. Every circle indicates a second of elapsed time, after a little more than three seconds the curve is back to its normal tracking behavior. In this same figure also some characteristics are indicated: maximum error rate, maximum error and number of overshoots. As explained, these values might be helpful in understanding the human operator's adaptive behavior. Furthermore, from the researches presented in this chapter it is clear that the critical areas of a phase plane are the first and third quadrant [6], where the error and error rate have the same sign and, consequently, only increase the error even further if not obstructed by the operator.

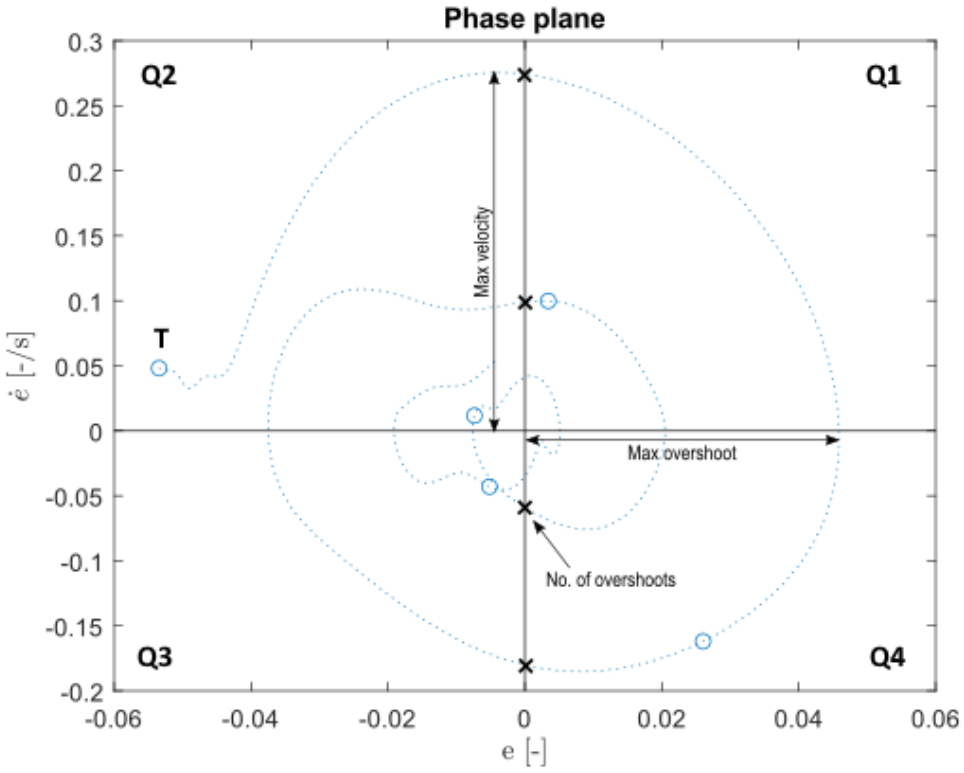

Figure 2-12: Error response phase plane of a computer simulation of an adaptive process showing specific characteristics

2-4 Conclusions

In this chapter a literature review of previous research on human adaptation in manual control was presented. To continue on this previous work a clear understanding of what has been done and what has not been done is required. In this last part a quick overview of the previous sections will be given, from which a conclusion will be drawn as a foundation for the rest of this research.

The basis of the adaptive process is the crossover model [12]. Pretransition and postransition steady-state tracking happens in compliance with this model [1, 3, 5, 26], from which the simple form is given in Equation 2-8. The interesting part of the adaptive process is what happens in between these two phases. How does a human operator detect changes, identify the correct new situation and modify his own parameters to fit the new situation?

$$Y_p(j\omega) = \frac{\omega_c}{j\omega} \cdot e^{-j\omega\tau_e} \cdot \frac{1}{Y_c(j\omega)} \tag{2-8}$$

In Section 2-1 the different factors responsible for adaptation were introduced. The only factor that is considered in the researches presented in this chapter, is the adaptive process as a consequence of a change in controlled element dynamics. In addition, only "fast" adaptive behavior is investigated, caused by a step or nearly step change in controlled element dynamics.

It was found that the error signal is an important measure for the human operator to detect and identify a change in controlled element dynamics [2]. For this reason the analysis of the adaptive process is generally concentrated on patterns in the error and error rate response. One of the interesting tools to analyze adaptation processes found in literature is the average error waveform [2]. The advantage of this way of analyzing such data is that it filters out the influence of the input signal, while showing the anomalies in the shape of the waveforms which are caused by the adaptive behavior of the human operator. Another way of analyzing and visualizing the error response which is widely used in the literature about this subject is the phase plane [3, 5, 6]. In the phase plane the error is on the x-axis and the error rate is on the y-axis. In [3, 5] specific patterns and shapes were found when visualizing the error in a phase plane for certain transitions in controlled element dynamics. For all experiments these patterns were best visible with well-trained participants, only few experiments with less-trained participants were performed [3].

The phases which a human operator encounters during an adaptive process are: $detection \Rightarrow identification \Rightarrow modification$ [2]. In further research this same structure is assumed. Later, Weir and Phatak [3] expanded on this process for destabilizing transitions. Immediately after the transition the operator controls according to the pretransition dynamics while actually controlling the new dynamics (pretransition retention) and after detection the operator reacts as an optimal controller by a bang-bang maneuver to compensate for the created error. Table 2-6 gives an overview of the applicability per phase of each of the presented models and research papers presented in this chapter.

Table 2-6: Overview of applicability of each model/research

	Detection	Identification	Modification
Young et al. [2]			
Weir and Phatak [3]	X	X	
Miller and Elkind [4]	X	X	
Phatak and Bekey [5]	X	X	X
Niemela and Krendel [6]	X		
Hess [25]	X	X	X

On the first phase, detection, the most research was done. According to Miller and Elkind [4] detection occurs when the expected and actual error deviate past a certain limit. While Phatak and Bekey [5] empirically found that when the error and error rate passed two times the maximum error rate the operator would notice a change. Niemela and Krendel [6] conducted some experiments from which the detection limits could be determined, which gave a similar result as the findings of [5]. More recently, Hess [25] came up with some concrete mathematical relations for this too, similar to the ideas of [4].

For the second and third phase, identification and modification, some interesting models were constructed. Miller and Elkind [4] came up with a model where the human operator, if well-trained, could determine what the new system was by internally calculating the expected errors for every known system and comparing it to the actual displayed error. They deduced some relations showing this internal process. However, these relations are only suitable for single integrator controlled element dynamics transitions, it is not yet clear if this could easily be expanded to different order systems. Later, Phatak and Bekey [5] presented a model, where the human operator sequentially identifies the correct system after transition based on

recognizing patterns in the error and error rate, which is in contrast to [4] where identification of the correct system happens immediately and simultaneously. They empirically found the decision regions that define the identification process. However, they did not give a strategy on how they defined these regions exactly, making it impossible to apply this model to different situations without further research. Lastly, Hess [25] designed a pursuit tracking model, where two loops, containing two human operator gains, are responsible for controlling the system. He empirically formulated relations which show the human adaptive behavior when a change in controlled element is introduced. His model can also be extended to multi-axis situations, making it interesting for more complex (real-life) scenarios [7].

Despite the extensive research which has been performed the past 70 years, there is still much unknown about the human adaptive process. The difficult part is that adaptation happens within a few seconds and that the human model in this period is time varying, making the popular pilot identification methods (e.g. analyzing the frequency response) useless [1]. Separate models do not yet give an explanation on what exactly happens during the whole process. Moreover, the relations, on which these models are based, are difficult to trace back and it is mostly unclear how they were obtained [4, 25]. The next step in this research field is to make the models more concrete and better applicable to general cases.

Chapter 3

Computer Simulations

In the previous chapter the literature review on adaptive manual control was presented. Several researchers have come up with frameworks to model the human adaptive process. In this chapter computer simulations will be used to show the applicability of the models and phase plane analysis presented in the previous chapter.

For the simulations it was initially decided to use step inputs. The benefit of a step input is that the response only consists of a transition, with a very clear beginning and ending. When this is combined with a change in dynamics before the initiation of the step, the adaptive process also happens within this step transition. The response to a step is very well-known, which would theoretically make it easy to see the difference between the normal step response and the step response with a change in dynamics. However, little research is performed on the adaptive behavior using a step input. Furthermore, the response to a step input happens too rapidly for good analyses to be performed [2]. For this reason, it was decided to use a continuous input in the later simulations, which is in line with most earlier investigations [1, 3, 5, 26].

In Section 3-1 the time-varying human operator model is presented which is used in the simulations. Section 3-2) contains some initial simulations with a continuous input. A short section about some step input simulations with varying controlled element dynamics and pilot model dynamics can be found in Appendix A. The last section, section 3-3, discusses the conclusions regarding this chapter and presents some recommendations for performing further simulations.

3-1 Time-varying human operator model

The human operator dynamics used in the simulations in the next sections are in accordance with the crossover model for compensatory tracking [12]. Only, in this case the parameters are time-varying, due to the changing controlled element dynamics which need to be compensated by the human operator dynamics. The time-varying human operator model is given by Equation 3-1 [33, 34].

$$H_p(s,t) = K_p(t)[1 + T_L(t)s]e^{-s\tau_e}\frac{\omega_{nms}^2(t)}{\omega_{nms}^2(t) + 2\zeta_{nms}(t)\omega_{nms}(t)s + s^2} \tag{3-1}$$

In the first simulations, fixed human operator parameter values were used for the single and double integrator dynamics of the controlled element. These values are given in Table 3-1. The gains of the single and double integrator dynamics associated with these parameters are 1.5 and 5, respectively. With the step input simulations the controlled element dynamics only switched between these two dynamics. With the continuous input simulations initially only a single integrator controlled element was used, from which the gain would be varied, yielding deviating parameter values from the values in the table.

	K_p	T_L	ω_{mns}	ζ_{mns}	τ_e
SI	1.3	0	10.5	0.35	0.26
DI	0.24	1.5	8	0.45	0.3

Table 3-1: Human operator parameter values for compensatory tracking retrieved from [11]

It was decided for the time being to analyze the adaptive process by only varying the pilot gain (K_p) and lead time constant (T_L) in the simulations. The other parameters (ω_{mns}, ζ_{mns}, τ_e) were kept constant during the transitions (only the single integrator parameter values were considered), as the relative variations of these parameters are lower compared to the required variations in pilot gain and lead time constant [33].

The shape of time-varying pilot model parameters used in the computers simulations presented in the next sections will be that of a sigmoid function, which is given by

$$P(t) = P_1 + \frac{P_2 - P_1}{1 + e^{-G(t-M)}} \tag{3-2}$$

The initial and final values of the time-varying parameters are P_1 and P_2, respectively. G the maximum rate of change and M is the time of maximum rate of change. By varying G the 'steepness' of the function can be defined. In several researches it is suggested that modification of the pilot model to sudden changes in controlled element dynamics happens instantaneously [3, 4, 5], which would require high values for G to simulate the same effect. In the simulations in the next sections, however, this parameter is still varied between smaller and larger values to understand its influence on the whole response. Figure 3-1 gives an example of the time traces of time-varying human operator parameters for a transition from single to double integrator dynamics.

3-2 Simulations with continuous input

In this section the computer simulations using continuous inputs will be presented. For simplicity, only a single integrator controlled element was used in these simulations, from which the gain would be instantaneously varied at certain moments in time. In the pilot model the pilot gain would then be adjusted to compensate for the change in gain of the controlled element dynamics.

For the continuous input a sum of sinusoids is used, that repeats itself every 30 seconds [35]. The benefit of using a repeating forcing function is that it is easy to compare pre- and posttransition tracking. The equation for a sum of sines is given by:

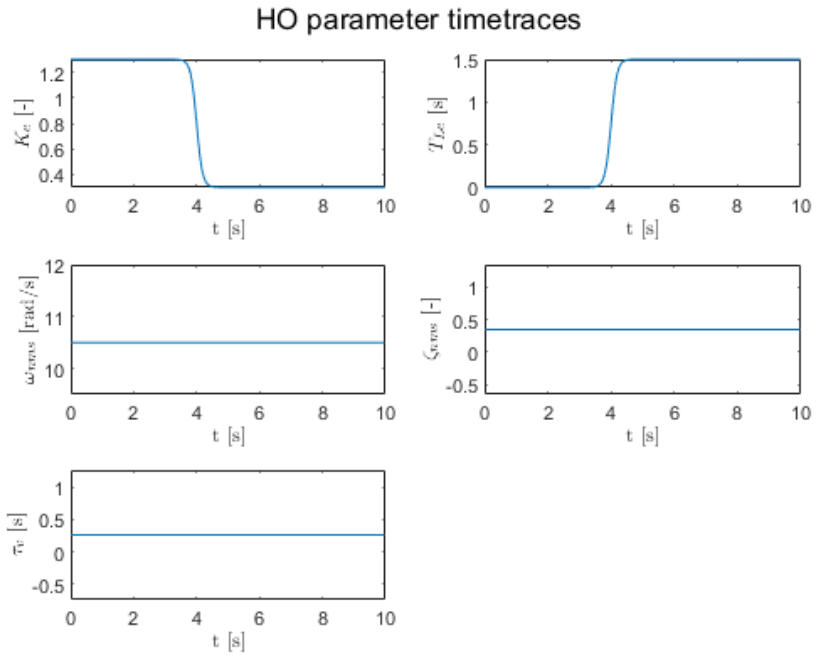

Figure 3-1: Example of the time trace of time-varying human operator parameters

$$f(t) = \sum_{n=1}^{N} A_n sin(\omega_n t + \phi_n) \tag{3-3}$$

In this equation N is the number of sines and A_n, ω_n and ϕ_n are the amplitude, frequency and phase shift of each sine wave. Only a single set of phase shifts was used in the initial computer simulations. All the parameter values are given in Table 3-2.

Table 3-2: Parameter values of forcing function

n	$k_n[-]$	$\omega_n[rad]$	$A_n[-]$	$\phi_n[rad]$
1	3	0.63	1.55e−2	1.80
2	7	1.47	8.40e−3	2.72
3	11	2.30	4.70e−3	0.19
4	17	3.56	2.40e−3	0.05
5	21	4.40	1.80e−3	3.94
6	29	6.07	1.10e−3	0.47
7	41	8.59	0.70e−3	5.60
8	53	11.1	0.60e−3	6.23
9	71	14.9	0.50e−3	0.35
10	87	18.2	0.40e−3	0.77

In Figure 3-2 an example of the consequence of a gain increase, from 1.5 to 4, in the single integrator without a change in pilot model dynamics is shown. The error rises quickly com-

pared to the pretransition tracking. In this example the system is on the edge of stability, in real life a human operator would probably have reacted to such a change in controlled element dynamics.

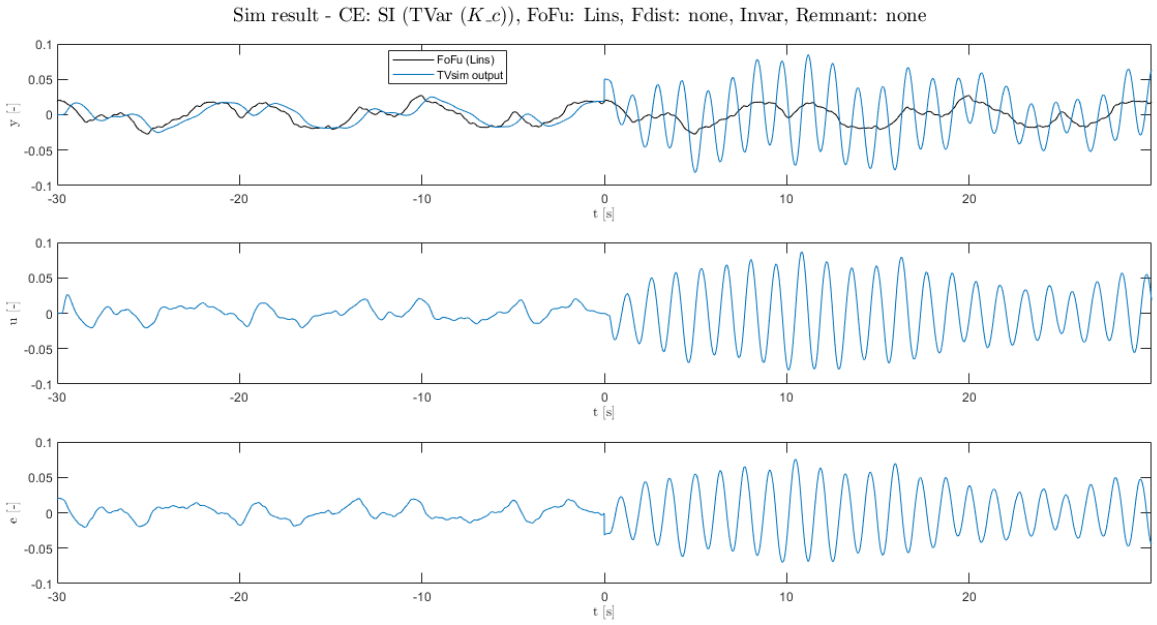

Figure 3-2: Output, control input and error time traces of a system with a gain increase (1.5 to 4) in the controlled element dynamics at t=0, while pilot model stays constant

In the next figure, Figure 3-3, the gain of the controlled element dynamics is increased more than in the previous figure, from 2 to 8, resulting in an unstable system without interference of the human operator. In this case the operator does react by decreasing their own gain. Within three seconds the system is stabilized and the operator is steady-state tracking. The initially large error peak is caused by the instantaneous change in gain of the controlled element dynamics.

The most interesting part of the adaptation process happens within the first couple of seconds after the transition [2]. Therefore, Figure 3-4 gives a zoomed in view of the first ten seconds after the transition. The upper graph is the time response, the lower graph is the phase plane containing the error and error rate. The red lines indicate the period of adjustment from the old pilot model parameter values to the new pilot model parameter values. The phase plane has the distinct shape of a spiral moving inwards in clockwise direction. In this specific simulation the modification of the pilot model takes two seconds, this process in real life probably happens instantly, as indicated in Section 3-1. In future simulations with a continuous input this should be taken into account.

Lastly, the first decision region of Phatak and Bekey [5] is added to the previous simulation (see Section 2-2-4 for more details). The first decision region is defined by two times the maximum error rate in pretransition tracking. The phase plane of the simulation, shown in Figure 3-4, with this decision region is displayed in Figure 3-5. Passing this first decision region will trigger the detection of a change in controlled element dynamics in a human

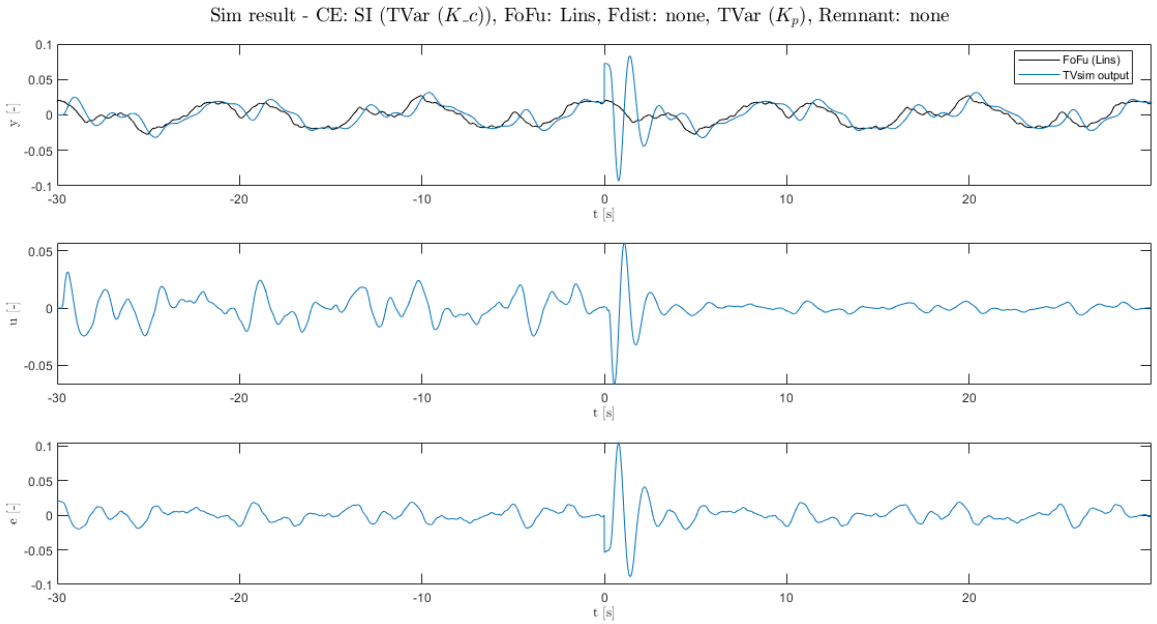

Figure 3-3: Output, control input and error time traces of a system with a gain increase (2 to 8) in the controlled element dynamics at t=0, the pilot model is adjusted to fit the new dynamics

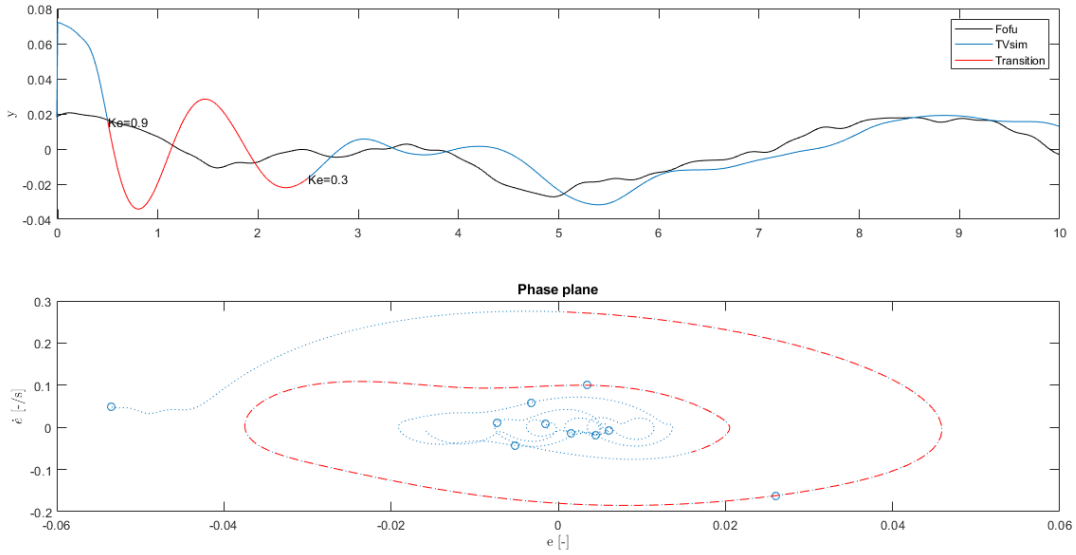

Figure 3-4: Output time trace and phase plane of first ten seconds after transition to new controlled element dynamics(instant gain increase of a single integrator from 2 to 8), operator takes 2 seconds to fully modify to new dynamics (indicated by red line)

operator. In this simulation the graph moves outside this decision region quite quickly (curve moves clockwise) after which the human operator adapts to the new dynamics (red dotted curve). When the human operator has modified their own dynamics to the new dynamics, the curve moves quickly back to steady-state tracking level, within the decision region. In future simulations it will be interesting to see what the effect of moving the boundaries of these regions is and if it can be verified that this specific boundary, assumed by Phatak and Bekey [5], is correct for real life applications.

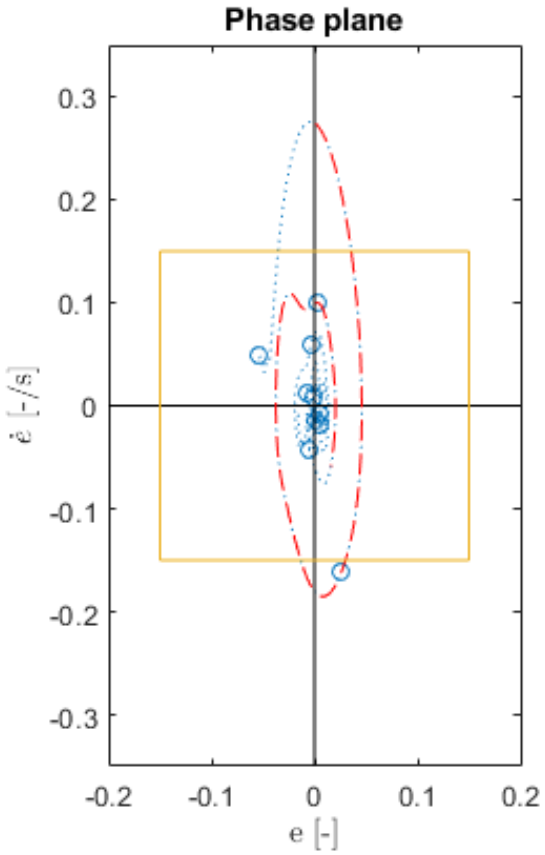

Figure 3-5: Adaptive process phase plane containing first decision region based on model from Phatak and Bekey [5]

3-3 Conclusions

In this chapter the preliminary research on computer simulations was presented. It was used to get a better understanding of the possibilities of simulating and analyzing the human adaptive response. A trade-off between input signals and parameter variations was performed to demarcate the interesting simulation direction.

The first thing that was examined was the influence of the forcing function on the way of analyzing the output. The result of two types of forcing functions, step input and continuous sum of sinusoids input, were compared. It turned out that, although the step input gave a

more clean output, the continuous output with the higher amount of research background would yield the most interesting results to continue to work with.

Several of the simulations performed for this preliminary research were focused on checking the influence of varying particular parameters, in both the controlled element dynamics and the pilot model, on the output. For simplicity, for future simulations it is decided to keep these variations changes simple and clear. This means that only few different controlled element dynamics will be considered and that these will be accompanied by distinct pilot model parameters, such that it will be easier to compare different simulations (e.g., when different forcing functions are applied). Furthermore, it was found in the literature research that a human operator, when detecting a change in controlled element dynamics, adjusts instantly to the new dynamics, therefore the transition of the pilot model parameters will also be instantaneous when performing future computer simulations.

For following simulations a more elaborate set-up is required to find the effect of variations that were not considered in creating the simulations up to now. The following list are interesting options that should be considered for a better assessment of a possible human adaptation model:

- Use dynamics that have been used in previous more recent time-varying research to be able to use the data and correctly compare results [9, 35].
- Use different forcing functions and vary the moment of transition to new controlled element dynamics. It appears that the forcing function can have a significant influence on the adaptation process of the human operator [2].
- Vary the size of the decision regions in the simulations and look at the sensitivity of its influence.

Chapter 4

Conclusions

The aim of this preliminary thesis was to get a better understanding of what has been done and what still needs to be done in the field of adaptive manual control. It was found that the adaptive process of a human operator consists of distinct phases, where different strategies are applied. These phases are detection, identification and modification [2]. By analyzing each phase separately the full process can be modeled.

In the past, several models have been created to try to explain the adaptive process. Early on it was clear that the error and error rate are the main information channels for analyzing the adaptive process [2, 3, 5]. The models of Phatak and Bekey [5] and Hess [19] cover each phase of this process and are therefore the most interesting models to continue looking at. The first model is based on the idea that a human operator sequentially identifies and modifies to different dynamics depending on the magnitude of the error and error rate. The latter came up with mathematical relations based on adaptive laws, that are applicable in pursuit and multi-axis tracking tasks. Unfortunately, both models lack a proper understanding on how the empirical defined relations or boundaries were formed. To better understand if these models give a proper representation of the adaptive process, simulations and experimental data are required. What these two models do not cover is the question if the adaptive process might be different for stable or unstable transitions. Weir and Phatak [3] focused mainly on destabilizing transitions for finding proof for their optimal-control model, since this would require an even more rapid response. However, even with a stable transition the same adaptive strategy seems applicable [2, 3, 17].

The analysis of the adaptive process is mainly performed by using phase planes [3, 5, 6], in which the error is displayed on the x-axis and the error rate on the y-axis. Phase planes have distinct shapes depending on the stability of the system [31]. Furthermore, the specific characteristics, like maximum error and error rate overshoot, can give information on when and how a human operator detects a change in controlled element dynamics. This same information can also be used for understanding the identification and modification phases of the adaptive process.

Some initial computer simulations were used to create a framework for the analysis of the adaptive process. First, the simulations were executed with a step input. However, due to the lack of literature using this type of input and the response following a step being to short, it was decided to continue using continuous outputs. From the simulations some initial idea

of the characteristic values and shape of the phase planes was obtained for varying adaptive and non-adaptive situations.

The next steps of this research consist of verifying the found models and trying to generalize their applicability, as explained in detail in chapter 5. The ultimate goal is to come up with an initial framework or mathematical model, that is able to predict the human behavior following sudden changes in controlled element dynamics.

Chapter 5

Future Research

After the extensive literature research on adaptive manual control, the coming phase of this research consists of extending the current frameworks and models. In Figure 5-1 the processes of this next phase are displayed in a flowchart.

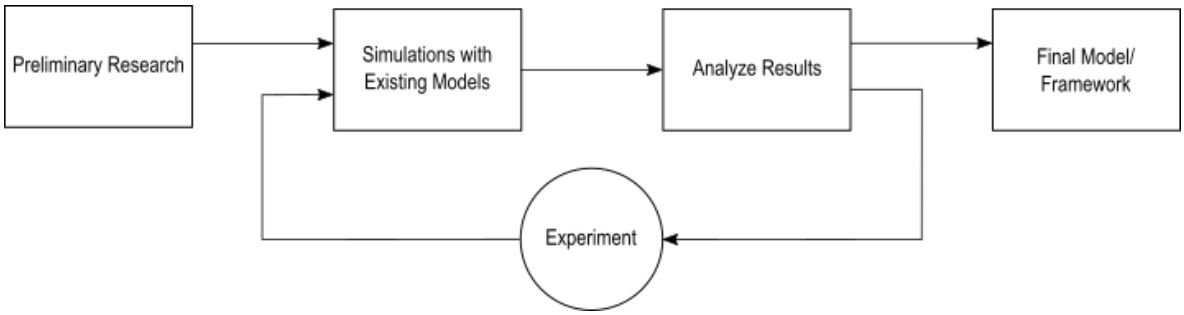

Figure 5-1: Flowchart of next research phase

First, more simulations of the existing models are required. Since, there is only limited time in the second phase of this research, it is decided to only focus on the sequential identification model of Phatak and Bekey [5]. Their model seems less complex and is less based on empirical relations in comparison to the model of Hess [19]. Then, these simulations will be analyzed and a general framework or model will be formulated. Based on this a small experiment will be executed, which will be used to validate and tweak this model. This validated and tweaked model will then be simulated again to come up with some final results. At the end of this process a final model or framework will be defined as an initial attempt to model the adaptive process of a human operator.

5-1 Computer simulations with sequential identification model of Phatak and Bekey

Since the research of Phatak and Bekey [5] is over 50 years ago, when the equipment for creating simulations was not as advanced as now, it is very interesting to conduct simulations based on their model and compare it to their results.Depending on how much time is

available during the next phase determines what kind of simulations will be executed. The first simulations with the sequential identification model will consist of identifying the first decision region. For these simulations the first decision region defined by [5] will be used initially. Several transitions with different dynamics (specified in the next section) will be used to simulate the response of the human operator with this decision region. Then, the boundaries of the decision region will be varied, this will at some point cause many false positives (eg. the human operator reacts to an outlier in the input) or false negatives (eg. the human operator is not able to detect the transition). This data will be used to find the decision region which induces the most realistic human behavior based on previous research [1, 3, 4, 5, 14, 15, 16, 17, 18]. If time permits, later simulations can be dedicated on finding and potentially verifying other decision regions of the sequential identification model.

5-2 Initial experiment set-up

A small tracking task experiment will be executed to validate and tweak the final values of the decision region(s) of the model. The decision regions of Phatak and Bekey [5] are based on assumptions and based on a specific set of controlled element dynamics. It is the goal of the experiment data to show if these assumptions are correct and if not, how they should be altered to yield a more robust model. *It is hypothesized that the framework of Phatak and Bekey [5] gives a good representation of the true adaptive process of a human operator in a response to a sudden change in controlled element dynamics.* The error and error rate are the leading information sources for an operator to detect this change and act upon it. Some parts of the experiment set-up will be decided upon based on what comes out of the simulations (e.g., forcing functions, moments of transition to new controlled element dynamics within the forcing functions).

Single-Axis Adaptive Control Task

The experiment task will consist of single-axis compensatory tracking runs during which the controlled element dynamics will suddenly and at random moments change. The participant will therefore only be able to see the error and their objective will be to keep that as low as possible during the whole run. The display will be that of an attitude indicator of an aircraft's primary flight display and simulates pitch maneuvers, the aircraft icon is required to stay level as much as possible.

Controlled Element Dynamics

As explained in section 3-3 it might be useful to consider controlled element dynamics of recent research on time-varying control tasks to be able to compare data. A recent research is that of [9], in which the following dynamics are considered:

$$H_c, 1 = \frac{90}{s(s+6)} \tag{5-1}$$

$$H_c, 2 = \frac{30}{s(s+0.2)} \tag{5-2}$$

$H_c, 1$ approaches single integrator dynamics in the crossover region and $H_c, 2$ approaches double integrator dynamics in the crossover region, as can be seen in Figure 5-2. The transition from the first to the second equation is considered to be destabilizing enough to induce proper adaptive behavior that can be more easily analyzed by using phase planes.

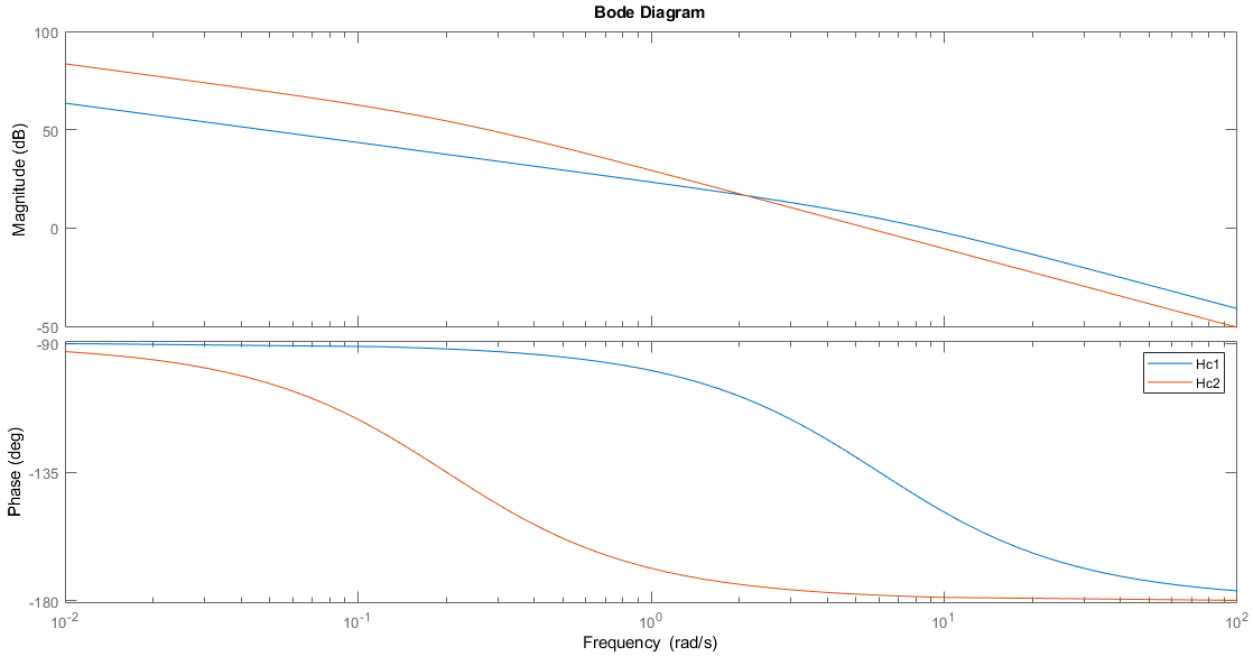

Figure 5-2: Bode plots of controlled element dynamics [9]

Apparatus

The experiment will be performed in the HMI-lab of the faculty of Aerospace Engineering at TUDelft. The set-up is that of a fixed-based aircraft simulator with a side-stick on the right arm rest. The side-stick is a hydraulically loaded control stick with 22 degrees moving space in the 'up-down' direction. Moving the side stick yields the same movements on the attitude displays as in an aircraft, moving the stick forwards pushes nose down, pulling the stick backwards will make the nose pitch up.

Participants

Probably only few participants are required, there is only a limited amount of conditions that will be tested, mainly testing the same dynamics transitions for different forcing functions. The participants should be right handed and well-trained, therefore it is beneficial to have

people who already have some experience with similar tracking task and have proven to be skillful in these types of task, which reduces the training time and makes sure the performance is high.

Bibliography

[1] L. R. Young. On adaptive manual control. *Ergonomics*, 10(4):292–331, 1969.

[2] L. R. Young, D. M. Green, J. I. Elkind, and J. A. Kelly. Adaptive dynamic response characteristics of the human operator in simple manual control. *IEEE Transactions on Human Factors in Electronics*, HFE-5(1), 1964.

[3] D. H. Weir and A. V. Phatak. *Model of human operator response to step transitions in controlled element dynamics*, volume 671. NASA, 1967.

[4] D. C. Miller and J. I. Elkind. The adaptive response of the human controller to sudden changes in controlled process dynamics. *IEEE Transactions on Human Factors in Electronics*, (3):218–223, 1967.

[5] A. V. Phatak and G. A. Bekey. Model of the adaptive behavior of the human operator in response to a sudden change in the control situation. *IEEE Transactions on Man-Machine Systems*, 10(3):72–80, 1969.

[6] R. J. Niemela and E. S. Krendel. Detection of a change in plant dynamics in a man-machine system. *IEEE Transactions on Systems, Man, and Cybernetics*, SMC-5(6): 615–617, 1975.

[7] R. A. Hess. Modeling human pilot adaptation to flight control anomalies and changing task demands. *Journal of Guidance, Control, and Dynamics*, 39(3):655–666, 2016.

[8] R. A. Hess. Modeling pilot control behavior with sudden changes in vehicle dynamics. *Journal of Aircraft*, 46(5):1584–1592, 2009.

[9] P. Zaal and B. Sweet. Estimation of time-varying pilot model parameters. In *AIAA Modeling and Simulation Technologies Conference*, page 6474, 2011.

[10] A. V. Phatak and G. A. Bekey. Decision processes in the adaptive behavior of human controllers. *IEEE Transactions on Systems Science and Cybernetics*, 5(4):339–351, 1969.

[11] K. Van Der El, S. Padmos, D. M. Pool, M. M. Van Paassen, and M. Mulder. Effects of preview time in manual tracking tasks. *IEEE Transactions on Human-Machine Systems*, 48(5):486–495, 2018.

[12] D.T. McRuer and H. R. Jex. A review of quasi-linear pilot models. *IEEE transactions on human factors in electronics*, (3):231–249, 1967.

[13] M. Mulder, D. M. Pool, D. A. Abbink, E. R. Boer, P. M. T. Zaal, F. M. Drop, K. Van Der El, and M. M. Van Paassen. Manual control cybernetics: State-of-the-art and current trends. *IEEE Transactions on Human-Machine Systems*, 48(5):468–485, 2018.

[14] J. D. McDonnell. A preliminary study of human operator behavior following a step change in the controlled element. *IEEE Transactions on Human Factors in Electronics*, HFE-7(3):125–128, 1966.

[15] T. B. Sheridan. Experimental analysis of time-variation of the human operator's transfer function. *IFAC Proceedings Volumes*, 1(1):639–645, 1960.

[16] D. H. Weir and W. A. Johnson. *Pilot Dynamic Response to Sudden Flight Control System Failures and Implications for Design*, volume 1087. National Aeronautics and Space Administration, 1968.

[17] P. G. Katona, L. Stark, A. Taub, R. Taub, and L. R. Young. Biological control systems-a critical review and evaluation. 1966.

[18] J. I. Elkind, J. A. Kelly, and R. A. Payne. Adaptive characteristics of the human controller in systems having complex dynamics. 1964.

[19] R. A. Hess. A model for pilot control behavior in analyzing potential loss-of-control events. *Proceedings of the Institution of Mechanical Engineers, Part G: Journal of Aerospace Engineering*, 228(10):1845–1856, 2014.

[20] S. S. Tohidi and Y. Yildiz. Adaptive human pilot model for uncertain systems. In *2019 18th European Control Conference (ECC)*, pages 2938–2943. IEEE, 2019.

[21] J. I. Elkind. Characteristics of simple manual control systems. *Thesis (Sc.D.) Massachusetts Institute of Technology*, 1956.

[22] L. R. Young and J. Meiry. Bang-bang aspects of manual control in high-order systems. *IEEE Transactions on Automatic Control*, 10(3):336–341, 1965.

[23] R. G. Costello. The surge model of the well-trained human operator in simple manual control. *IEEE Transactions on Man-Machine Systems*, 9(1):2–9, 1968.

[24] D. C. Miller and J. I. Elkind. *The adaptive response of the human controller to sudden changes in controlled process dynamics*. PhD thesis, 1967.

[25] R. A. Hess. Simplified approach for modelling pilot pursuit control behaviour in multi-loop flight control tasks. *Proceedings of the Institution of Mechanical Engineers, Part G: Journal of Aerospace Engineering*, 220(2):85–102, 2006.

[26] R. A. Hess. Modeling the pilot detection of time-varying aircraft dynamics. *Journal of Aircraft*, 49:2100–2104, 2012. doi: 10.2514/1.C031805.

[27] R. A. Hess. A preliminary study of human pilot dynamics in the control of time-varying systems. In *AIAA modeling and simulation technologies conference*, page 6554, 2011.

[28] A. B. Farjadian and A. M. Annaswamy. Towards a resilient control architecture : A demonstration of bumpless reengagement following an anomaly in flight control.

[29] E. R. Boer and R. V. Kenyon. Estimation of time-varying delay time in nonstationary linear systems: an approach to monitor human operator adaptation in manual tracking tasks. *IEEE Transactions on Systems, Man, and Cybernetics - Part A: Systems and Humans*, 28(1):89–99, 1998.

[30] M. Olivari, F. M. Nieuwenhuizen, H. H. Bülthoff, and L. Pollini. Identifying time-varying neuromuscular system with a recursive least-squares algorithm: a monte-carlo simulation study. In *2014 IEEE International Conference on Systems, Man, and Cybernetics (SMC)*, pages 3573–3578. IEEE, 2014.

[31] E. R. Kalman. Phase-plane analysis of automatic control systems with nonlinear gain elements. *Transactions of the American Institute of Electrical Engineers, Part II: Applications and Industry*, 73(6):383–390, 1955.

[32] J. Ellerbroek, O. Stroosma, M. Mulder, and M. M. Van Paassen. Role identification of yaw and sway motion in helicopter yaw control tasks. *Journal of Aircraft*, 45(4): 1275–1289, 2008.

[33] W. Plaetinck, D. M. Pool, M. M. Van Paassen, and M. Mulder. Online identification of pilot adaptation to sudden degradations in vehicle stability. *IFAC-PapersOnLine*, 51 (34):347–352, 2019.

[34] P. M.T. Zaal. Manual control adaptation to changing vehicle dynamics in roll–pitch control tasks. *Journal of Guidance, Control, and Dynamics*, 39(5):1046–1058, 2016.

[35] M. Linssen. Identifying time-varying multimodal manual control using recursive arx model techniques. *MSc Thesis*, 2020.

[36] C. Vertregt. Estimation of time-varying human manual control behaviour in preview tracking tasks using a dual extended kalman filter. *MSc Thesis*, 2020.

[37] MATLAB. *version 9.8.0.1323502 (R2020a)*. The MathWorks Inc., Natick, Massachusetts, 2020.

Appendix A

Simulations with Step Input

The first part of the step input simulations consisted of mapping the constant behavior of a human operator to such an input[1]. For modeling the human model during steady-state tracking the crossover model [12] is used. First, the maximum reached velocities for different lead and gain constants for time-invariant simulations were investigated, where the operator is controlling a double integrator system (Kc=1), which is subjected to a step input with a magnitude of one. From this a linear relation could be deduced between the lead, gain and maximum velocity of the output of this system. Similar results were found for single integrator dynamics (Kc=1), where only the gain of the pilot model was varied. These findings give a better understanding of what the consequences are of changing certain parameters in the pilot model on the shape and characteristic values of the phase plane with a time-invariant system. In the second phase these simulations should be expanded to time-varying controlled element dynamics and time-varying pilot dynamics to come closer to see if these characteristics are also distinct in the adaptive processes.

Figure A-1 shows the characteristic values for time-varying pilot dynamics simulations in response to a step input. The controlled element dynamics in this system are equal to a double integrator, while the pilot model initially consists of the parameters to control a single integrator. The parameters of the pilot model need to be adapted for the system to not become unstable. In this figure multiple starting times of the adaptation process were used to come up with the characterizing values, that are shown in the bottom four graphs in the figure. The two upper graphs only display the simulation with the last starting time (four seconds). In this simulation the human operator took five seconds to adapt to the new dynamics. From this simulation trends are visible in the relation between the varying starting time and the characteristic values, however a higher resolution is required before being able to mathematically define these relations. Furthermore, due to the many variable options in tweaking the human model to perform the adaptation process differently, this will take many more different simulations to result in actual useful conclusions about the adaptation process. Due to the decision to continue investigating only continuous input simulations, it was decided to not continue spending more time on creating more and more detailed simulations with a step input. If, in future research, it is deemed to be more interesting than it seems from the investigated literature in this research, this should be the starting point.

[1]With a step input the error and output response have the same shape. For this reason only the output values are used in the analyses of the step input simulations

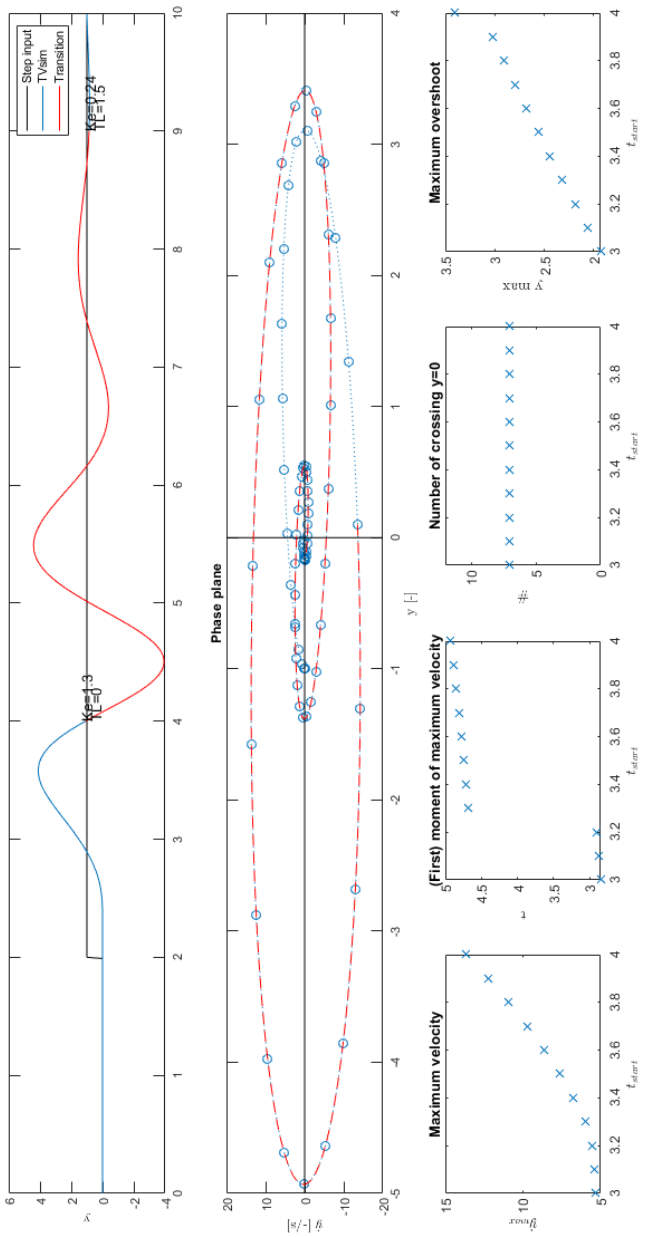

Figure A-1: Time-varying human operator simulations in response to a step input with varying starting times for the varying parameters. The upper two graphs only show the last simulation. The red dotted line indicates the transition of the pilot model. The circles in the phase plane indicate 0.1s of elapsed time.

Part III

Final Thesis Report Appendices

Appendix B

Experiment Documents

The following documents were used in the execution of the experiment presented in the paper. The first document (Figure B-1) is the consent form every participant had to sign to be able to participate in the experiment. The experiment briefing is the document that informed the participants about the exact procedures, their rights and length of the experiment, this document is shown in Figure B-2. The last document, Figure B-3, shows training schedule and distribution and order of conditions per participant.

Experiment Consent Form

Adaptive Manual Control Experiment

I hereby confirm, by ticking each box, that:

1. I volunteer to participate in the experiment conducted by the researcher (**Jacomijn van Ham**) under supervision of **Dr.ir. Daan Pool** from the Faculty of Aerospace Engineering of TU Delft. I understand that my participation in this experiment is voluntary and that I may withdraw and discontinue participation at any time, for any reason. ☐
2. I have read the experiment briefing and confirm that I understand the instructions and have had all remaining questions answered to my satisfaction. ☐
3. I understand that my participation involves performing a tracking task in a fixed-based simulator. ☐
4. I confirm that the researcher has provided me with detailed safety and operational instructions for the hardware (simulator setup, control-loaded stick, fire escape) used in the experiment. ☐
5. I understand that (though very unlikely) it is possible that I may develop some feelings of discomfort caused by focussing on the display. If this is the case, I will inform the experimenter. I also understand that the experiment may be discontinued for this reason. ☐
6. I understand that the researcher will not identify me by name in any reports or publications that will result from this experiment, and that my confidentiality as a participant in this study will remain secure. ☐
7. I understand that this research study has been reviewed and approved by the TU Delft Human Research Ethics Committee (HREC). To report any problems regarding my participation in the experiment, I know I can contact the researchers using the contact information below or, if necessary, the TU Delft HREC (hrec@tudelft.nl). ☐

My Signature	Date
My Printed Name	Signature of researcher

Contact information researcher:	Contact information research supervisor
Jacomijn van Ham	Dr. ir. Daan M. Pool
j.m.vanham@student.tudelft.nl	d.m.pool@tudelft.nl
+31 6 22038572	+31 15 2789611

Figure B-1: Consent form

Experiment Briefing

ADAPTIVE MANUAL CONTROL

Thank you for participating in this experiment! The experiment, conducted in the Human-Machine Interaction Laboratory (HMI-Lab), analyses human tracking behavior. The experiment consists of a simple tracking task. This briefing will introduce you to the experiment and what is expected of you as a participant.

Experiment Goal

The goal of this experiment is to investigate human adaptive behaviour. A simple tracking task, containing variations in controlled element dynamics, will be performed to gather data on this adaptive behaviour. With this data an existing mathematical model will be tested and adjusted if necessary.

Experiment Task

The task you will be carrying out is a tracking task with a compensatory display (i.e. you can only see the error). It is your task to keep the error as low as possible by moving the side-stick on your right hand-side to left or right. A button on the back of the side-stick will be used to indicate if you detect a change in the dynamics you are controlling.

Experiment Procedures

Each tracking run lasts 95 seconds. During each run the controlled element dynamics of the system might suddenly change. It is important that you continue to focus on keeping the error as low as possible each time and try to quickly stabilize the system after such a change occurs. Furthermore, when you are confident such a change has occurred, you are required to indicate this by pushing a button on the front of the side-stick. The researcher will keep track of your performance and will announce when the experiment has been completed. You will start the experiment by doing a couple of practice runs to familiarise yourself with the different controlled element dynamics.

Short breaks can be taken between runs to alleviate any discomfort that might occur due to controlling the side-stick or after sitting in a fixed position for a prolonged period of time. The experiment will last approximately 60 minutes.

For each driving trial, the subsequent procedure will be followed:

1. The researcher applies the settings for the next run.
2. The researcher checks whether the participant is ready to proceed and initiates the run after a countdown from 3 (3-2-1-go).
3. The participant performs the tracking task.
4. The participant will be notified of their performance in the run in terms of error score after the completed run.

COVID-19 protocol

Due to the ongoing COVID-19 ('coronavirus') pandemic, several measures are taken to reduce the risk of spreading it. First and foremost, researcher and participant will follow the guidelines as indicated on the Dutch government website[1] on the day of the experiment. Related to this experiment, the following four measures are taken:

- Both researcher and participants confirm they do not have symptoms related to COVID-19.
- 1.5 meter distance will be kept between researcher and participant at all times.
- All touched objects in the simulator will be disinfected by the researcher before and after the experiment.
- Before and after the experiment both researcher and participant will wash or disinfect their hands.

This experiment will be performed following the most recent "COVID-19 Protocols for Human Subject Experiments" of the Control and Simulation department.

Your rights

Participation in the experiment is voluntary. This means that you can terminate your cooperation at any time. By participating in the experiment you agree that the collected data may be published. Your data will remain confidential and anonymous, so only the experimenter can link the results to a particular participant. To make sure that you understand and comply with the conditions of the experiment, you will be asked to sign an informed consent form.

Contact information researcher:	Contact information research supervisor
Jacomijn van Ham	Dr. ir. Daan Pool
j.m.vanham@student.tudelft.nl	d.m.pool@tudelft.nl
+31 6 22038572	+31 15 2789611

Thank you for participating!

[1] https://www.rijksoverheid.nl/coronavirus

Figure B-2: Experiment briefing document

Run	Dyn	Participant	1	2	3	4	5	6
1	SI	Training	N1	N1	N1	N1	N1	N1
2	SI		N2	N2	N2	N2	N2	N2
3	SI		N3	N3	N3	N3	N3	N3
4	DI		N4	N4	N4	N4	N4	N4
5	DI		N5	N5	N5	N5	N5	N5
6	DI		N6	N6	N6	N6	N6	N6
7	SI>DI	Training	C3	C3	C3	C3	C3	C3
8	SI>DI		C3	C3	C3	C3	C3	C3
9	SI>DI		C3	C3	C3	C3	C3	C3
10	SI>DI		C3	C3	C3	C3	C3	C3
11	SI>DI	Exp	C1	C15	C14	C11	C10	C7
12	SI>DI		C4	C1	C15	C14	C11	C10
13	SI>DI		C5	C4	C1	C15	C14	C11
14	SI>DI		C8	C5	C4	C1	C15	C14
15	SI>DI		C9	C8	C5	C4	C1	C15
16	SI>DI		C12	C9	C8	C5	C4	C1
17	SI>DI		C13	C12	C9	C8	C5	C4
18	SI>DI		C16	C13	C12	C9	C8	C5
19	SI>DI		C2	C16	C13	C12	C9	C8
20	SI>DI		C3	C2	C16	C13	C12	C9
21	SI>DI		C6	C3	C2	C16	C13	C12
22	SI>DI		C7	C6	C3	C2	C16	C13
23	SI>DI		C10	C7	C6	C3	C2	C16
24	SI>DI		C11	C10	C7	C6	C3	C2
25	SI>DI		C14	C11	C10	C7	C6	C3
26	SI>DI		C15	C14	C11	C10	C7	C6

Figure B-3: Experiment planning of conditions

Appendix C

Individual and Extra Experiment Results

This appendix presents the individual and extra experiments results. Section C-1 presents some of the open loop stability characteristics obtained from analyzing the experiment data. Section C-2 contains the time traces of each participant and each condition. In Section C-3 the classification of simulated detection per participant using general and individual standard deviations of the error and error rate as limits are presented. In the last section, Section C-4, an analysis is performed on the effect of using different reaction time window sizes on the predicted moments of detection.

C-1 Open loop stability characteristics

The crossover frequencies, phase margins and time delays of each participant during the SI and DI tracking phases are presented in Figures C-1, C-2 and C-3, respectively. The reference lines in each plot were determined using the verbal adjustment rules of McRuer and Jex [12].

It can be observed that the crossover frequencies are relatively low compared to the reference for both phases and that the phase margins are relatively high compared to the reference for both phases. The crossover frequencies and phase margins do follow the trend described by the crossover model [12], i.e., lower crossover frequency and phase margin for DI tracking compared to SI tracking. The time delays for the SI phase yield erroneous results with negative and very large time values. The time delays for the DI phase are more realistic.

The unexpected results for the crossover frequencies and phase margins can be caused by an inaccurate estimate due to the low number of data points used. For both the SI phase and DI phase only 30 s of data was available to do this identification. Another reason for these results might be found in participants not having a constant performance, which could produce a disturbed frequency response.

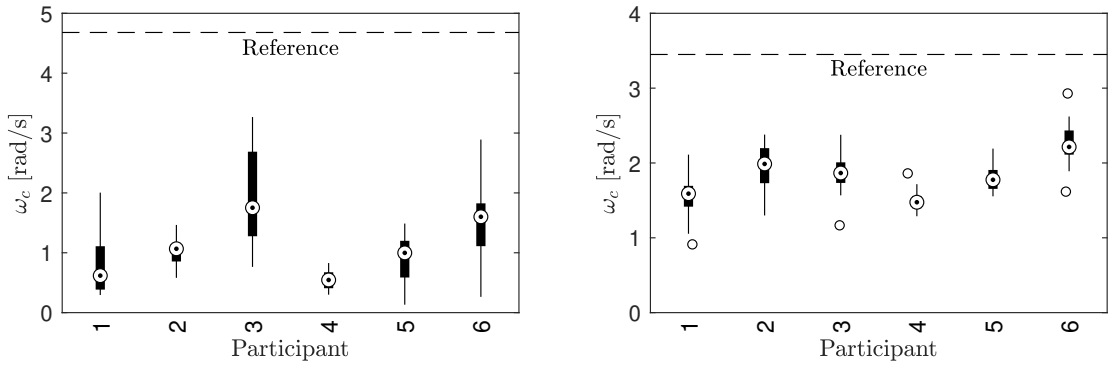

(a) SI tracking (b) DI tracking

Figure C-1: Crossover frequencies of each participant for the SI and DI tracking phases

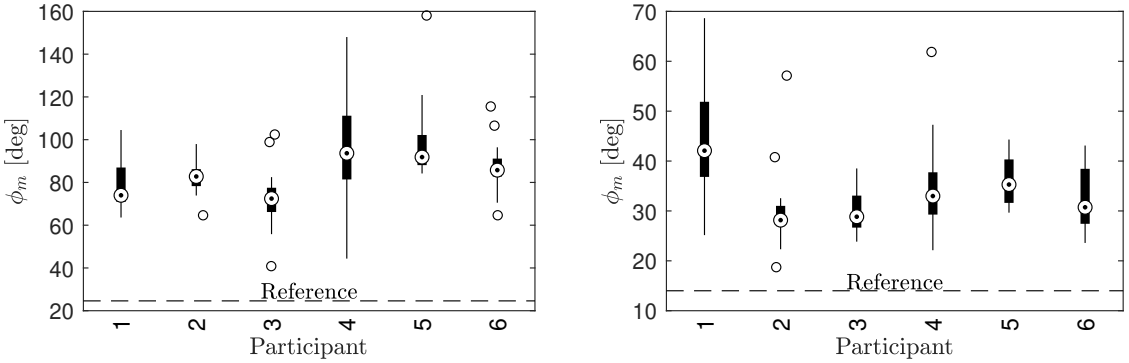

(a) SI tracking (b) DI tracking

Figure C-2: Phase margins of each participant for the SI and DI tracking phasess

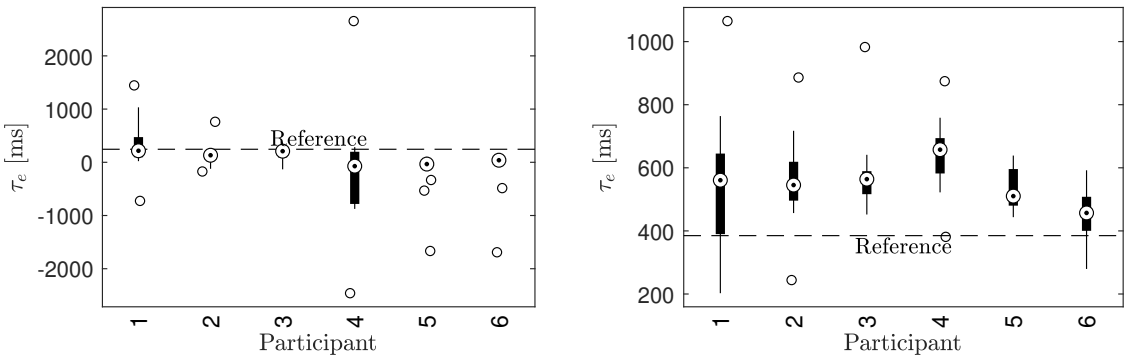

(a) SI tracking (b) DI tracking

Figure C-3: Time delays of each participant for the SI and DI tracking phases

C-2 Individual time traces per condition

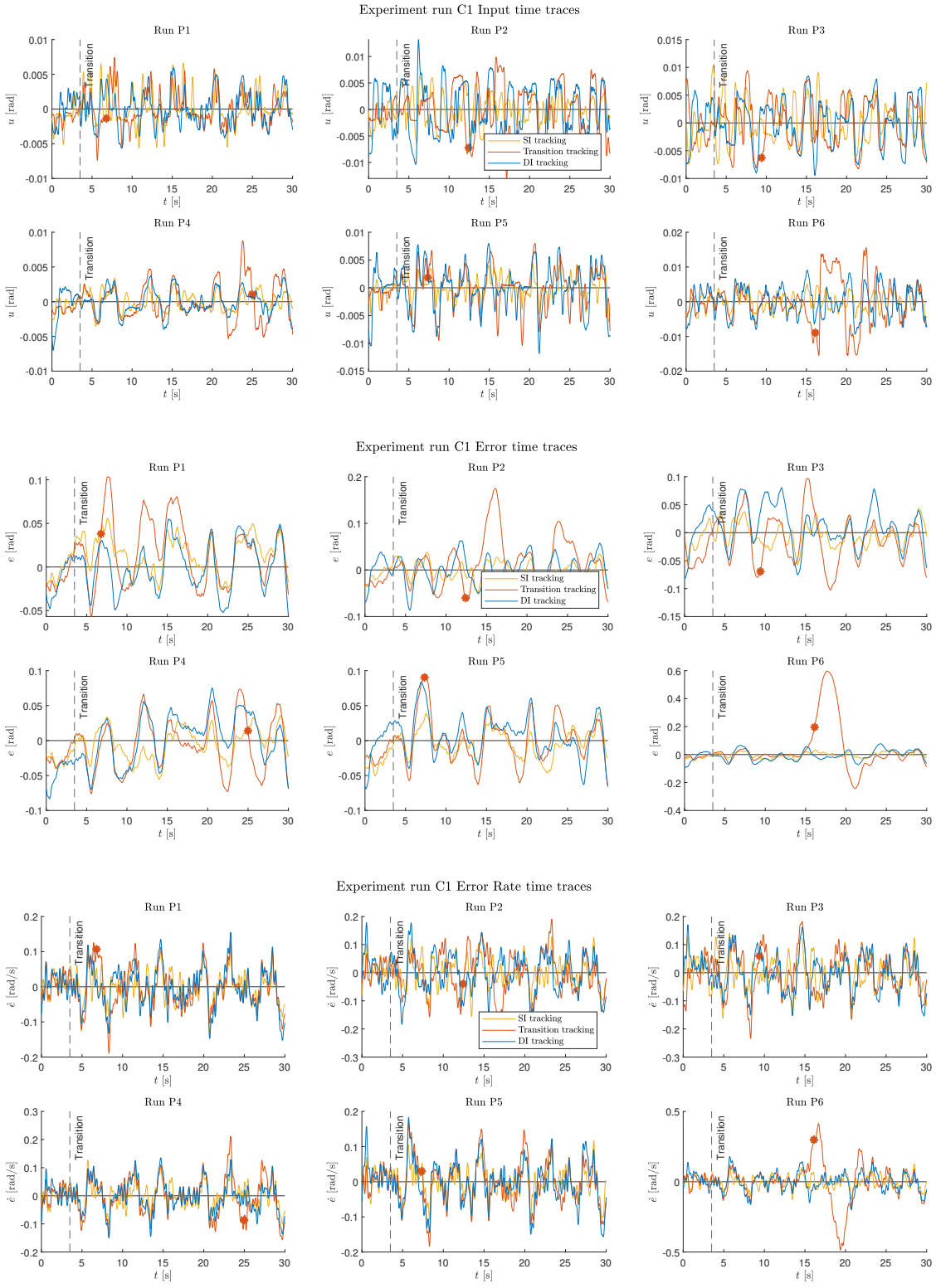

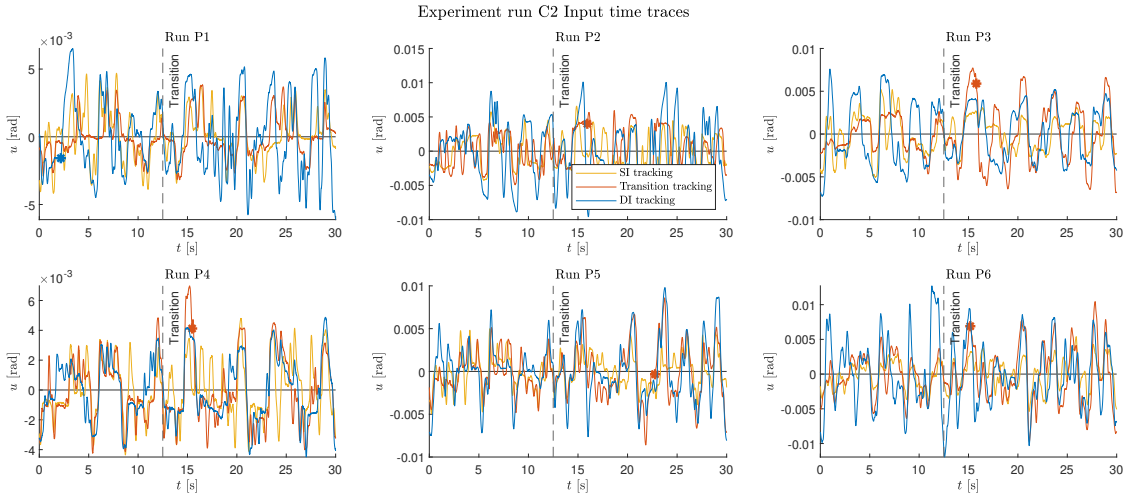
Experiment run C2 Input time traces
Run P1
Run P2
Run P3
Run P4
Run P5
Run P6
Transition
SI tracking
Transition tracking
DI tracking
u [rad]
t [s]

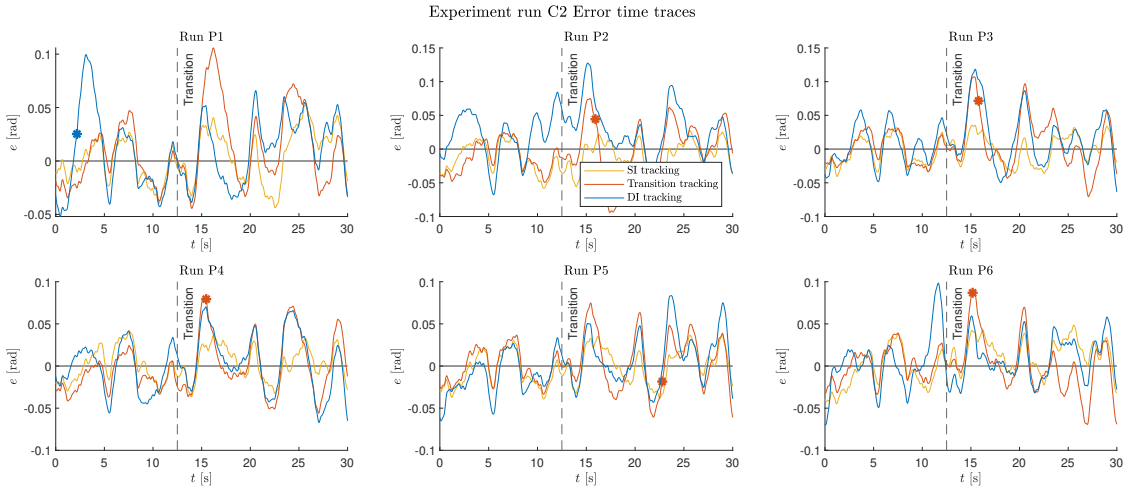
Experiment run C2 Error time traces
Run P1
Run P2
Run P3
Run P4
Run P5
Run P6
Transition
SI tracking
Transition tracking
DI tracking
e [rad]
t [s]

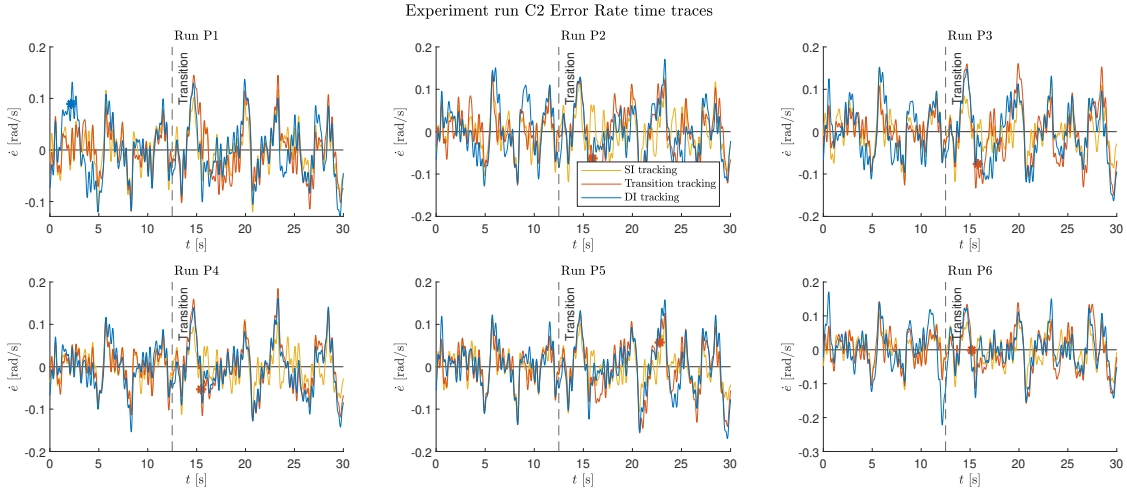
Experiment run C2 Error Rate time traces
Run P1
Run P2
Run P3
Run P4
Run P5
Run P6
Transition
SI tracking
Transition tracking
DI tracking
ė [rad/s]
t [s]

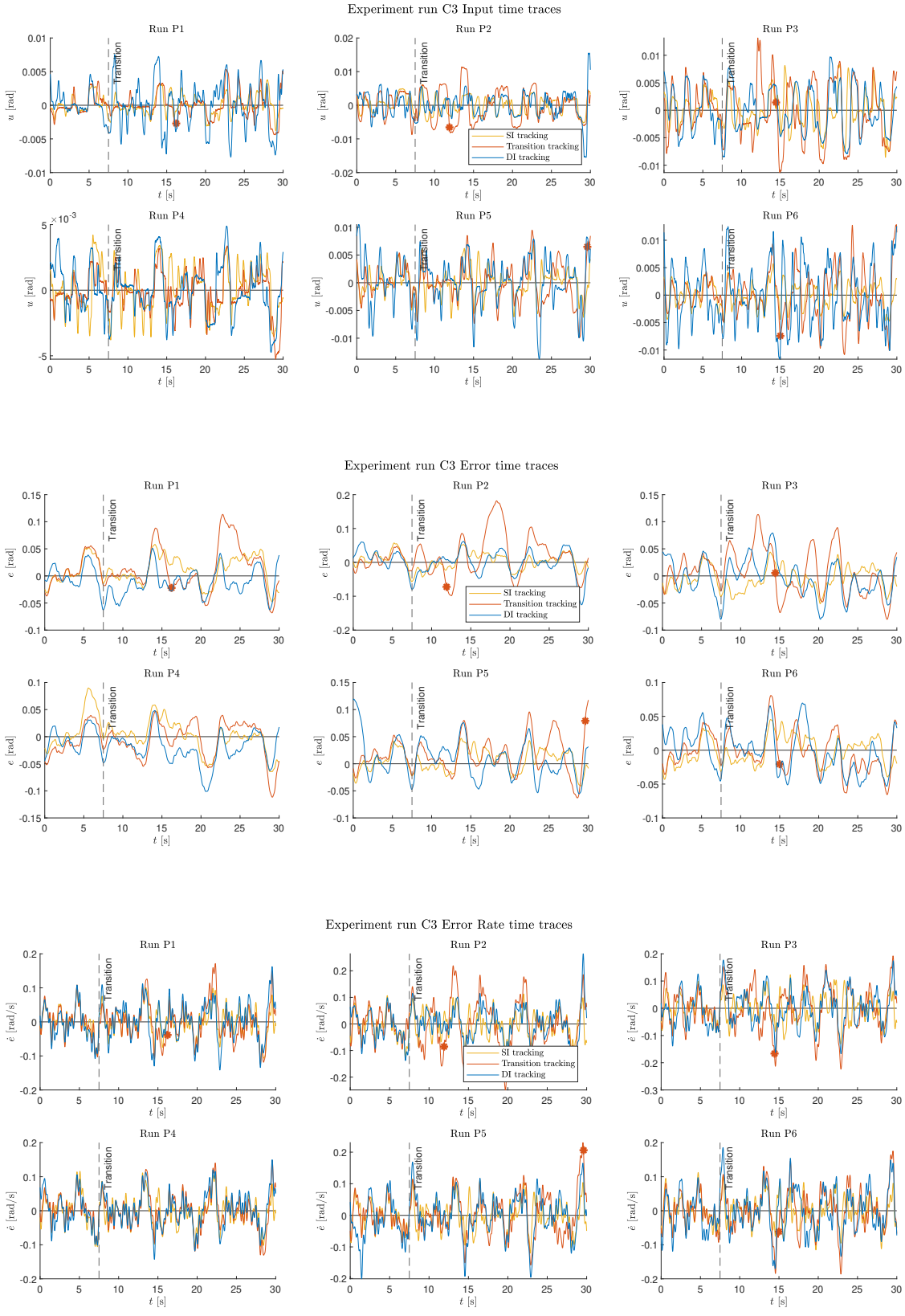
Experiment run C3 Input time traces
Run P1
Run P2
Run P3
Run P4
Run P5
Run P6
Transition
SI tracking
Transition tracking
DI tracking
u [rad]
t [s]
Experiment run C3 Error time traces
e [rad]
Experiment run C3 Error Rate time traces
ė [rad/s]

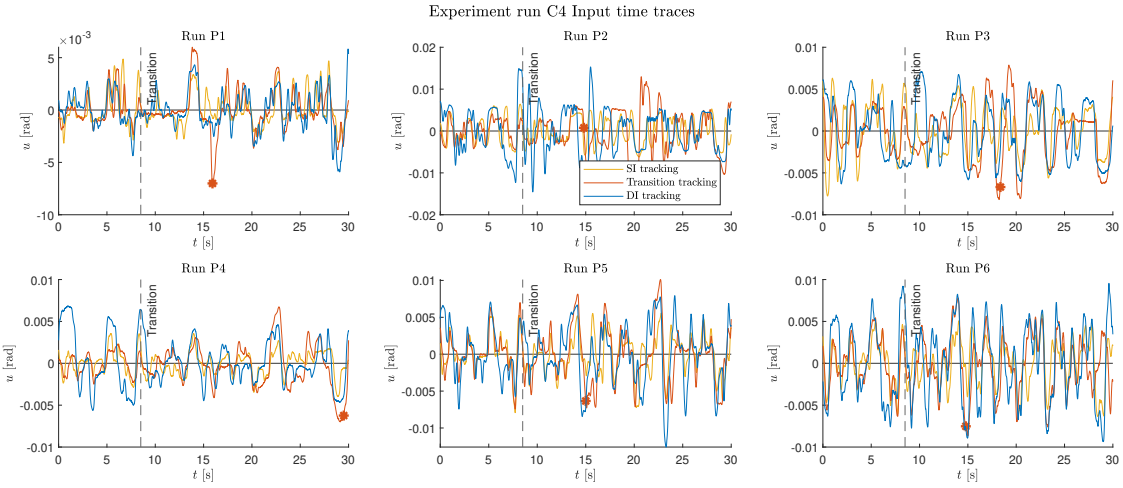
Experiment run C4 Input time traces
Run P1
Run P2
Run P3
Run P4
Run P5
Run P6
Transition
SI tracking
Transition tracking
DI tracking
u [rad]
t [s]

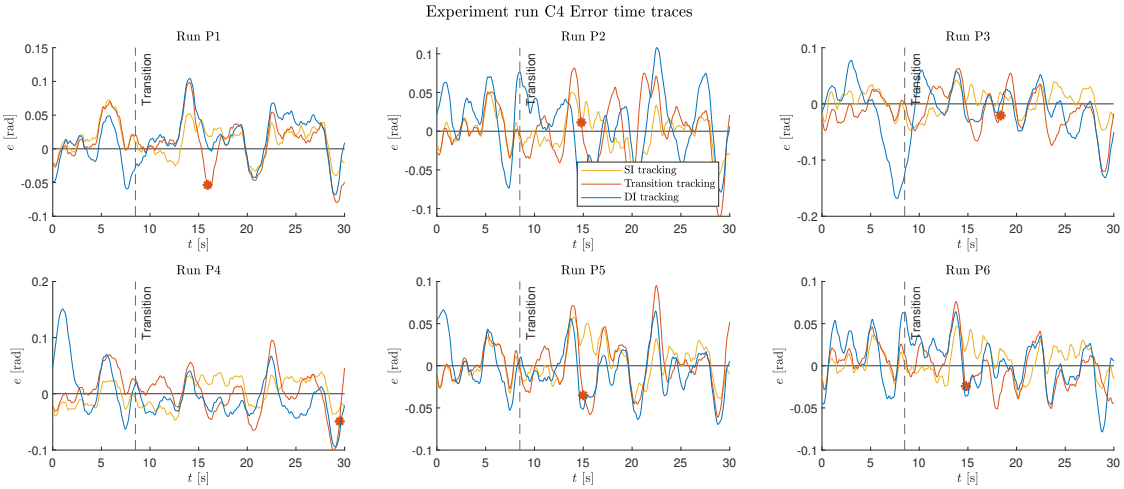
Experiment run C4 Error time traces
Run P1
Run P2
Run P3
Run P4
Run P5
Run P6
Transition
SI tracking
Transition tracking
DI tracking
e [rad]
t [s]

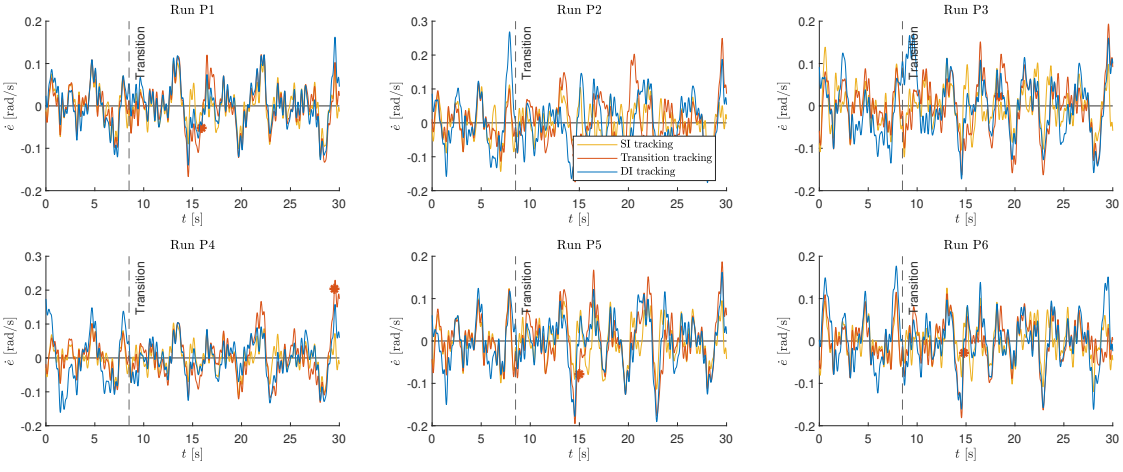
Experiment run C4 Error Rate time traces
Run P1
Run P2
Run P3
Run P4
Run P5
Run P6
Transition
SI tracking
Transition tracking
DI tracking
ė [rad/s]
t [s]

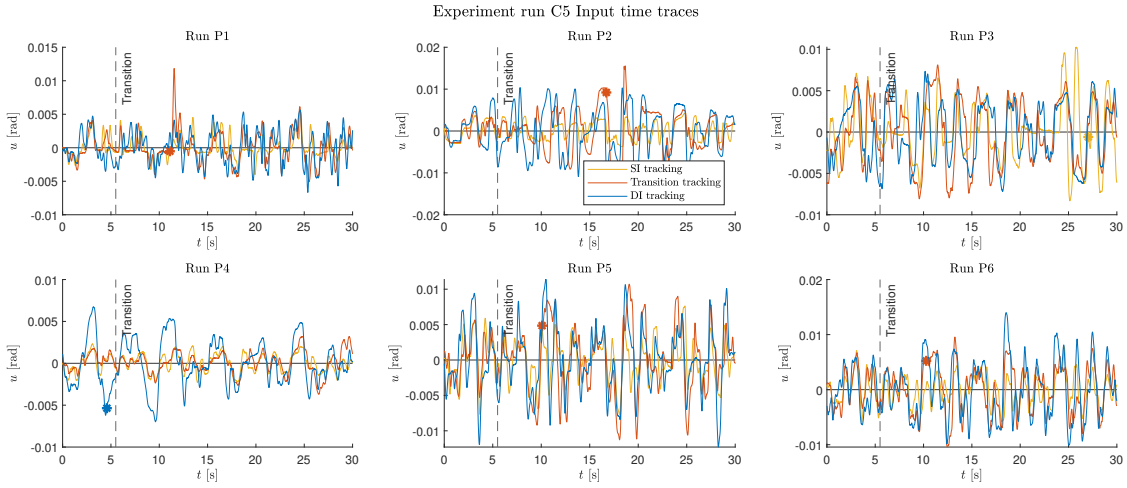
Experiment run C5 Input time traces
Run P1
Run P2
Run P3
Run P4
Run P5
Run P6
Transition
SI tracking
Transition tracking
DI tracking
u [rad]
t [s]

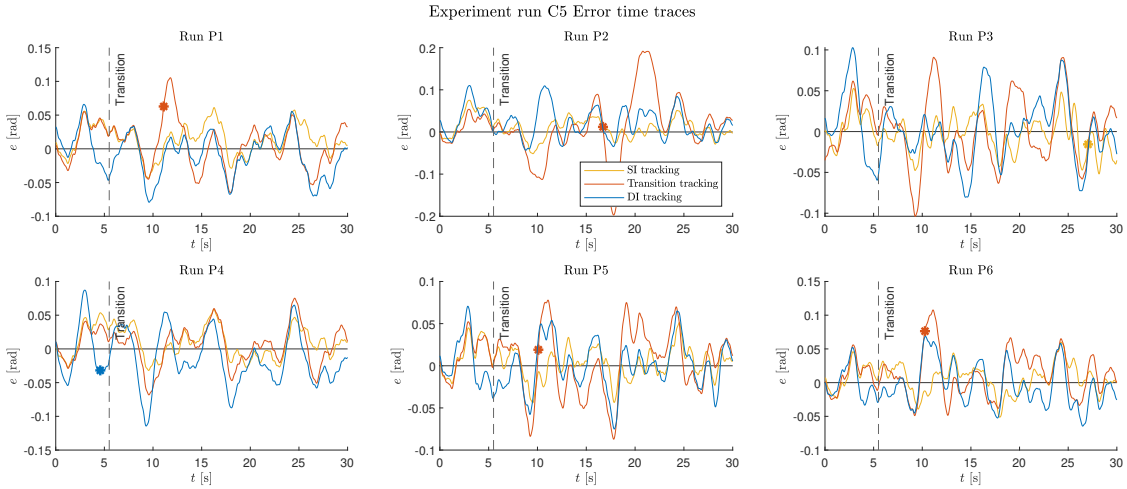
Experiment run C5 Error time traces
Run P1
Run P2
Run P3
Run P4
Run P5
Run P6
Transition
SI tracking
Transition tracking
DI tracking
e [rad]
t [s]

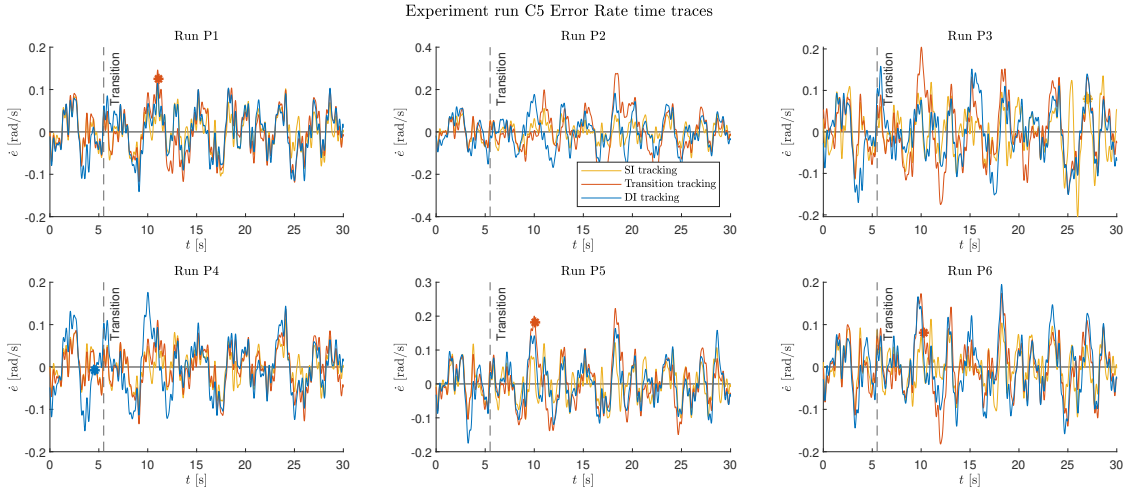
Experiment run C5 Error Rate time traces
Run P1
Run P2
Run P3
Run P4
Run P5
Run P6
Transition
SI tracking
Transition tracking
DI tracking
ė [rad/s]
t [s]

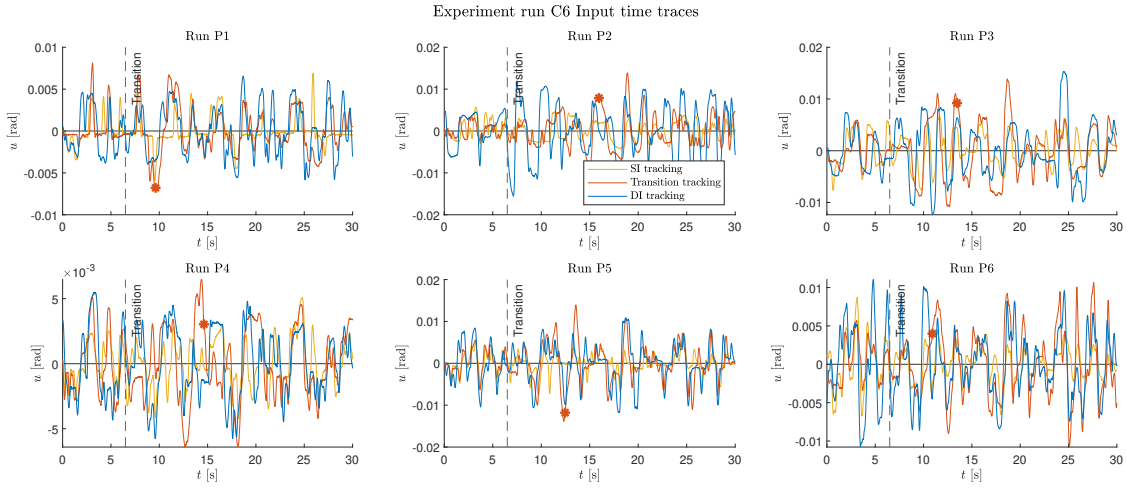
Experiment run C6 Input time traces
Run P1
Run P2
Run P3
Run P4
Run P5
Run P6
Transition
SI tracking
Transition tracking
DI tracking
u [rad]
t [s]

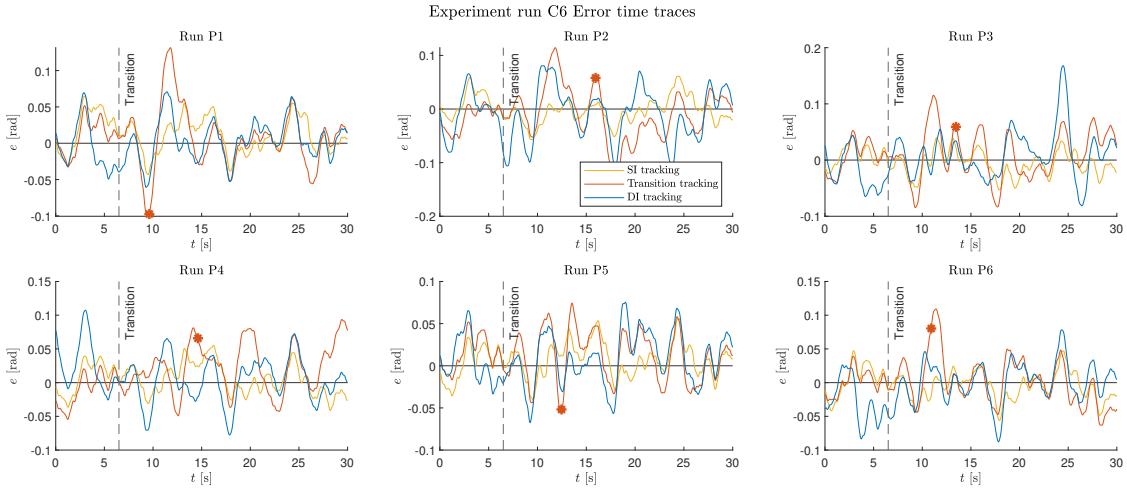
Experiment run C6 Error time traces
Run P1
Run P2
Run P3
Run P4
Run P5
Run P6
Transition
SI tracking
Transition tracking
DI tracking
e [rad]
t [s]

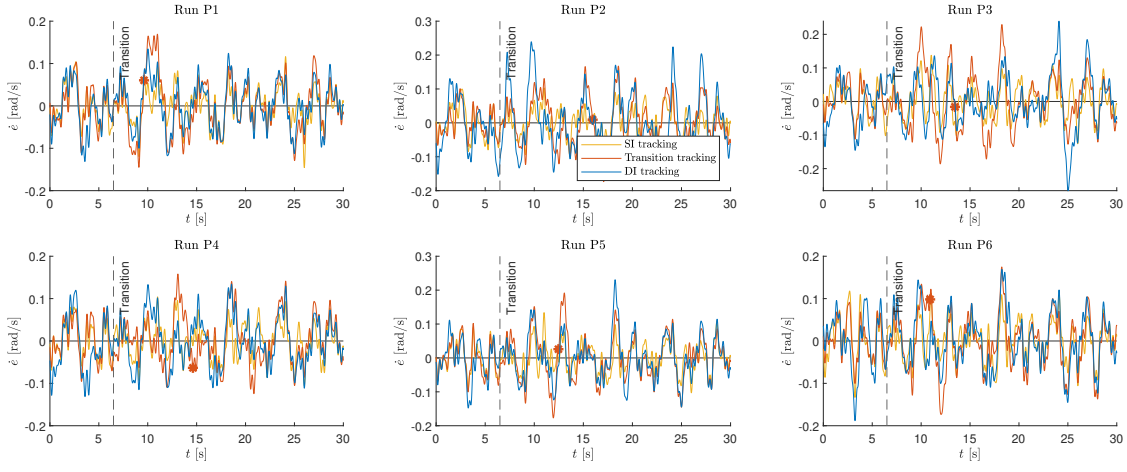
Experiment run C6 Error Rate time traces
Run P1
Run P2
Run P3
Run P4
Run P5
Run P6
Transition
SI tracking
Transition tracking
DI tracking
ė [rad/s]
t [s]

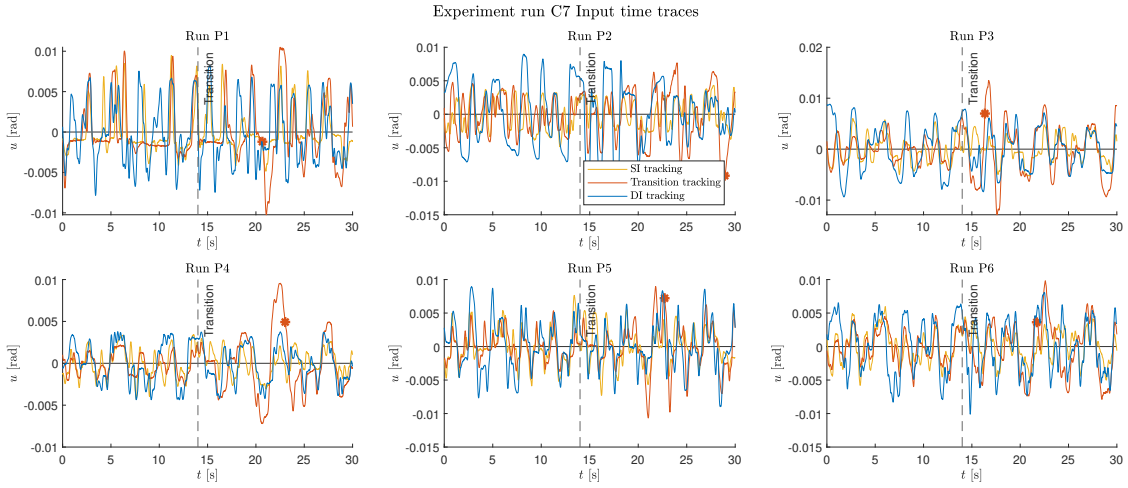
Experiment run C7 Input time traces
Run P1
Run P2
Run P3
Run P4
Run P5
Run P6
Transition
SI tracking
Transition tracking
DI tracking
u [rad]
t [s]

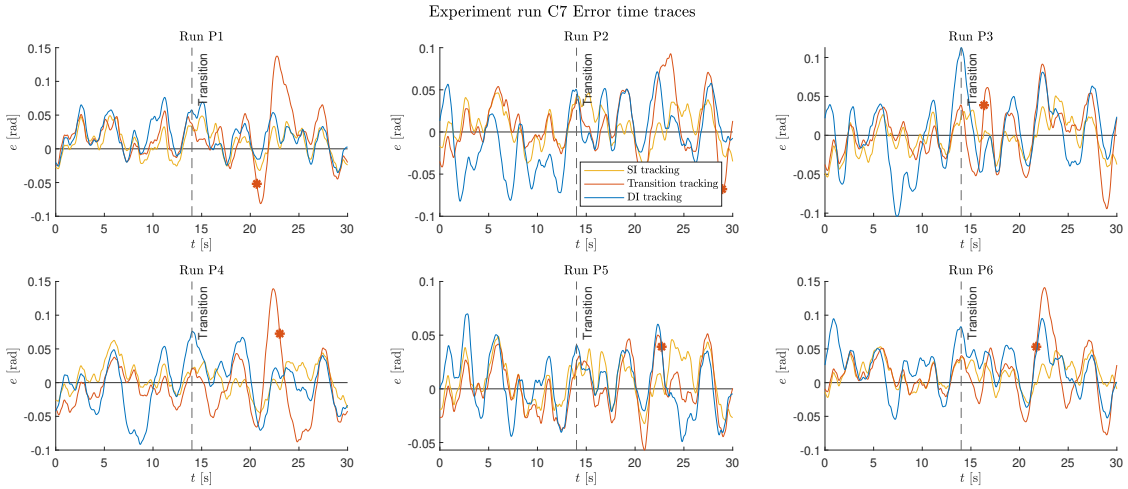
Experiment run C7 Error time traces
Run P1
Run P2
Run P3
Run P4
Run P5
Run P6
Transition
SI tracking
Transition tracking
DI tracking
e [rad]
t [s]

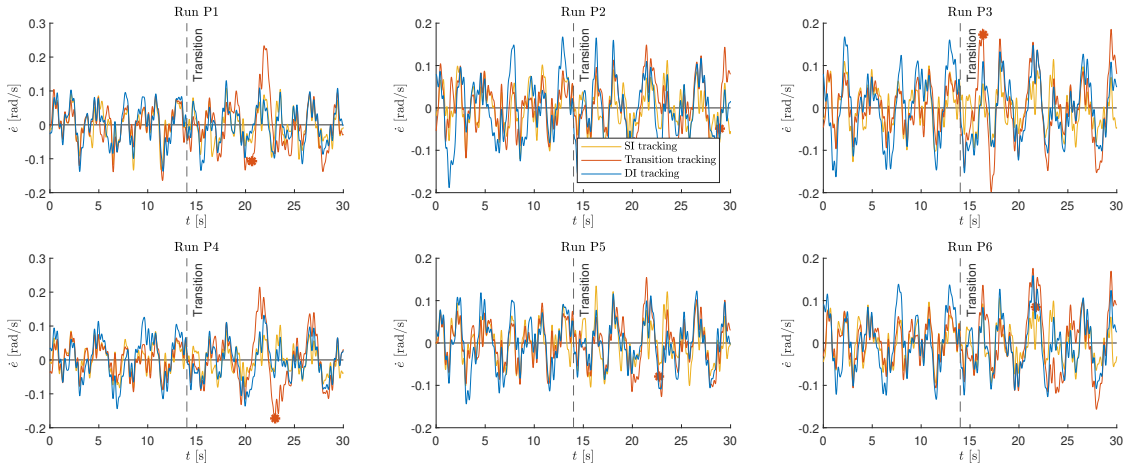
Experiment run C7 Error Rate time traces
Run P1
Run P2
Run P3
Run P4
Run P5
Run P6
Transition
SI tracking
Transition tracking
DI tracking
ė [rad/s]
t [s]

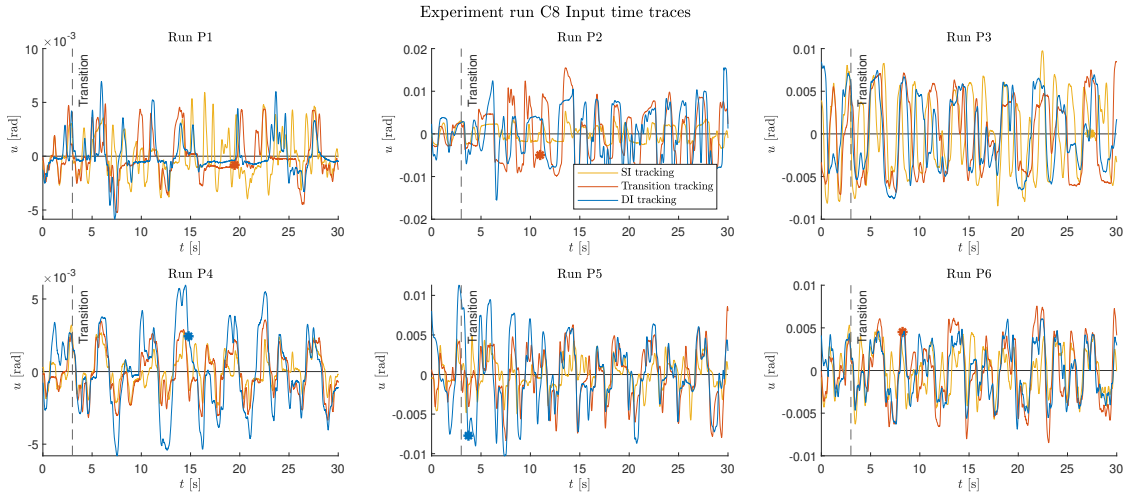
Experiment run C8 Input time traces
Run P1
Run P2
Run P3
Run P4
Run P5
Run P6
Transition
SI tracking
Transition tracking
DI tracking
u [rad]
t [s]

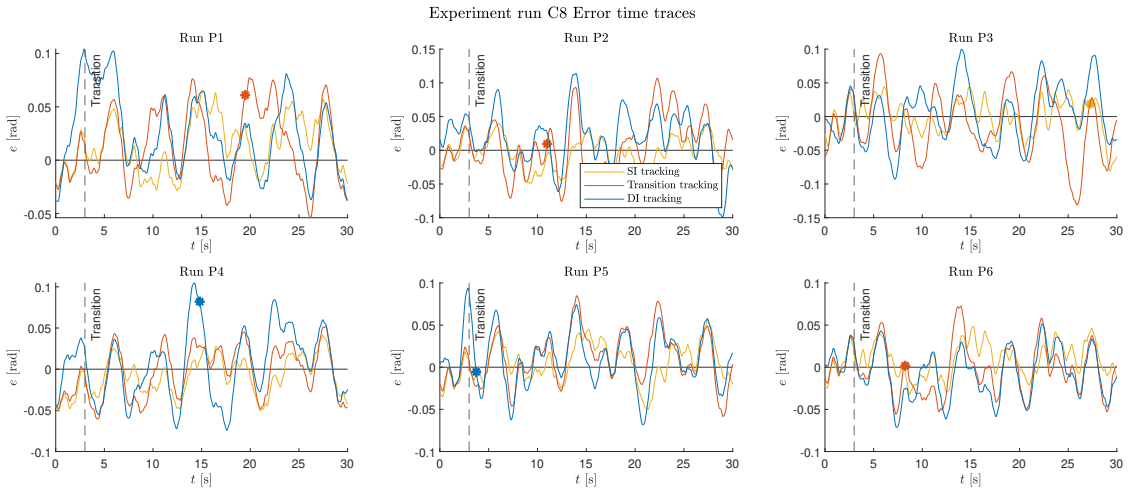
Experiment run C8 Error time traces
Run P1
Run P2
Run P3
Run P4
Run P5
Run P6
Transition
SI tracking
Transition tracking
DI tracking
e [rad]
t [s]

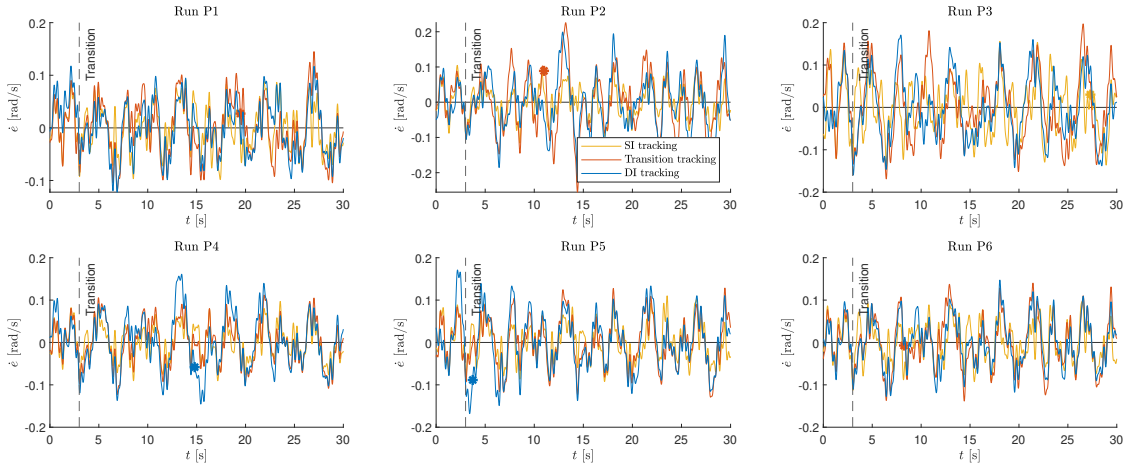
Experiment run C8 Error Rate time traces
Run P1
Run P2
Run P3
Run P4
Run P5
Run P6
Transition
SI tracking
Transition tracking
DI tracking
ė [rad/s]
t [s]

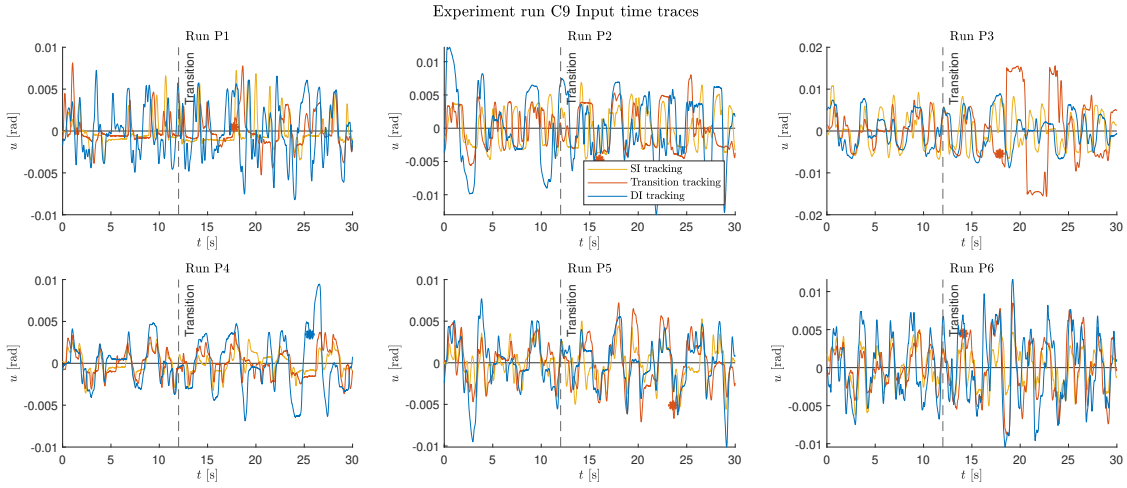
Experiment run C9 Input time traces
Run P1
Run P2
Run P3
Run P4
Run P5
Run P6
Transition
SI tracking
Transition tracking
DI tracking
u [rad]
t [s]

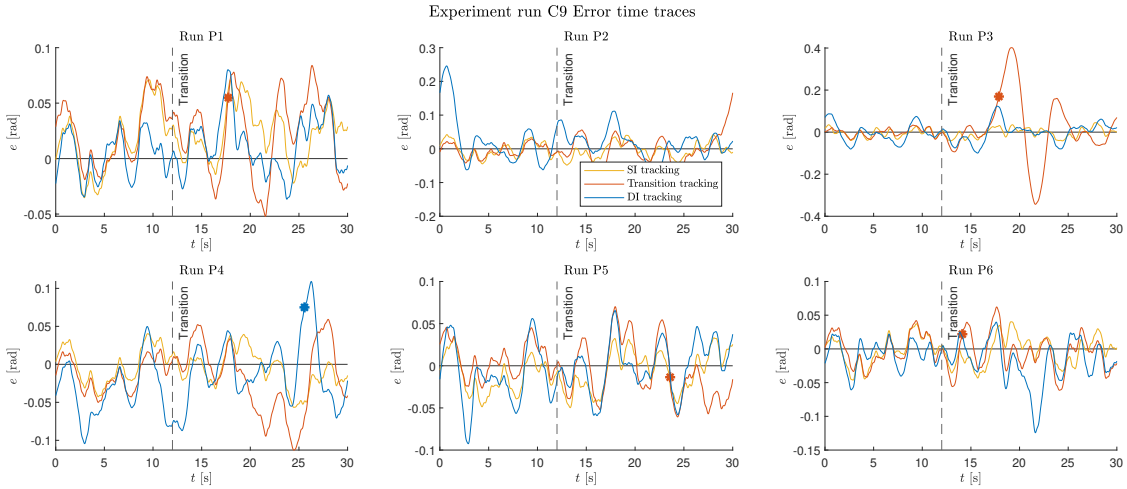
Experiment run C9 Error time traces
Run P1
Run P2
Run P3
Run P4
Run P5
Run P6
Transition
SI tracking
Transition tracking
DI tracking
e [rad]
t [s]

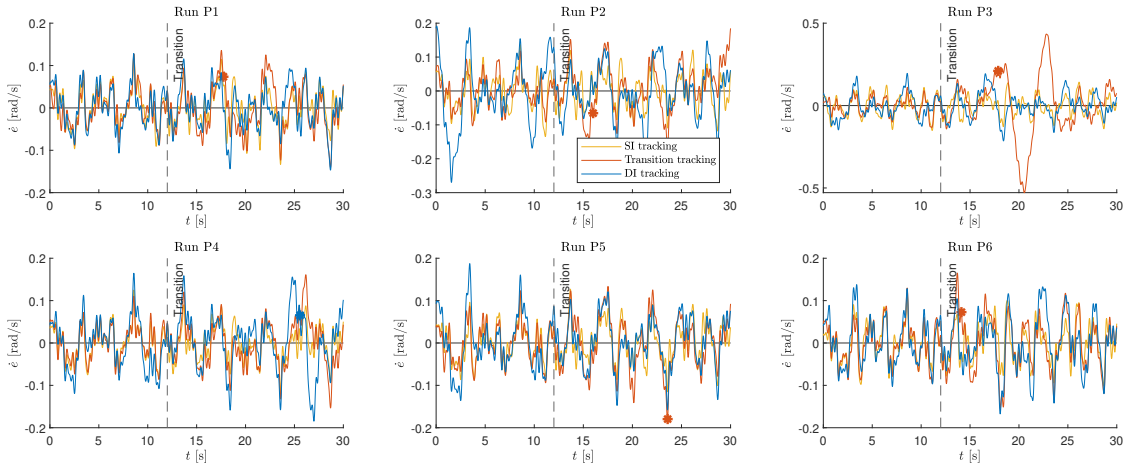
Experiment run C9 Error Rate time traces
Run P1
Run P2
Run P3
Run P4
Run P5
Run P6
Transition
SI tracking
Transition tracking
DI tracking
ė [rad/s]
t [s]

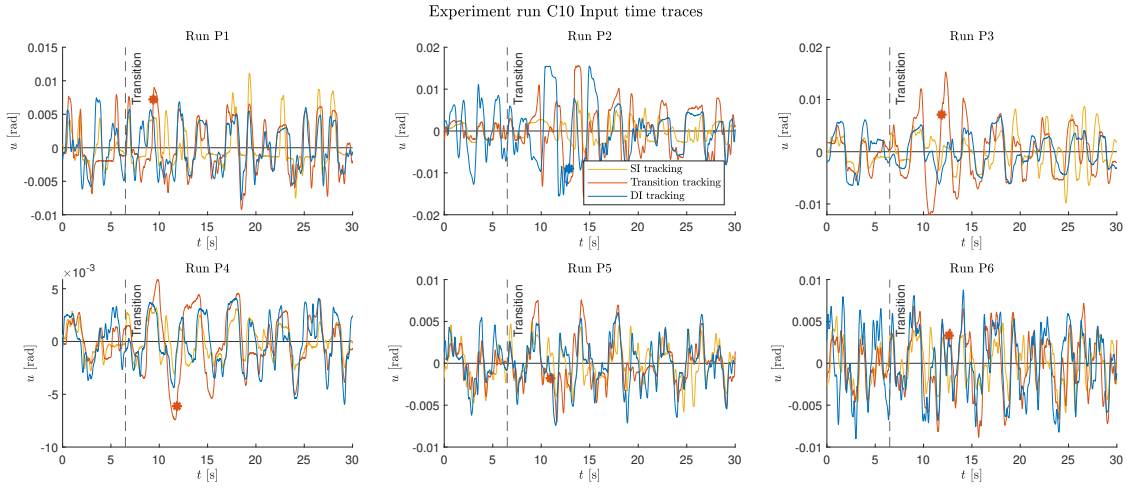
Experiment run C10 Input time traces
Run P1
Run P2
Run P3
Run P4
Run P5
Run P6
Transition
SI tracking
Transition tracking
DI tracking
u [rad]
t [s]

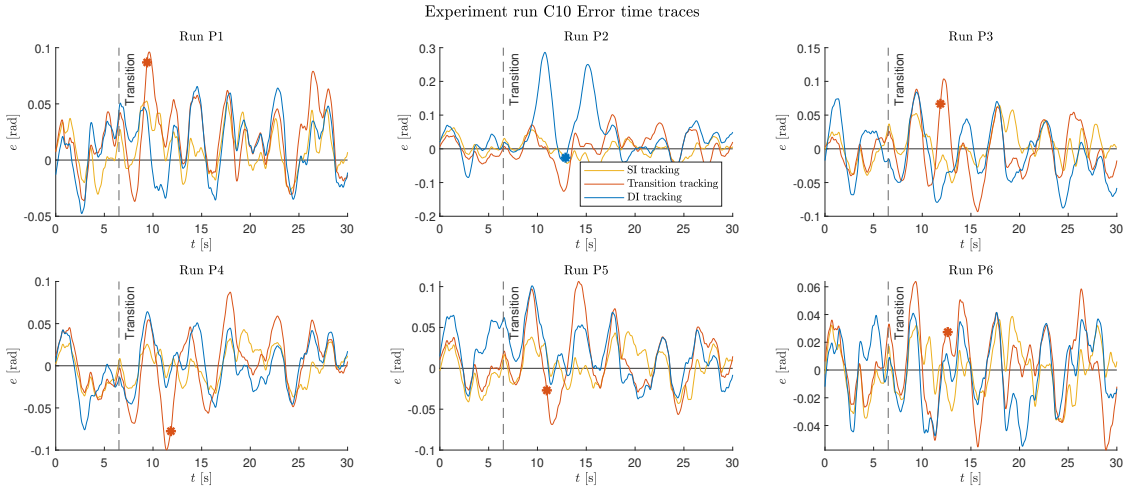
Experiment run C10 Error time traces
Run P1
Run P2
Run P3
Run P4
Run P5
Run P6
Transition
SI tracking
Transition tracking
DI tracking
e [rad]
t [s]

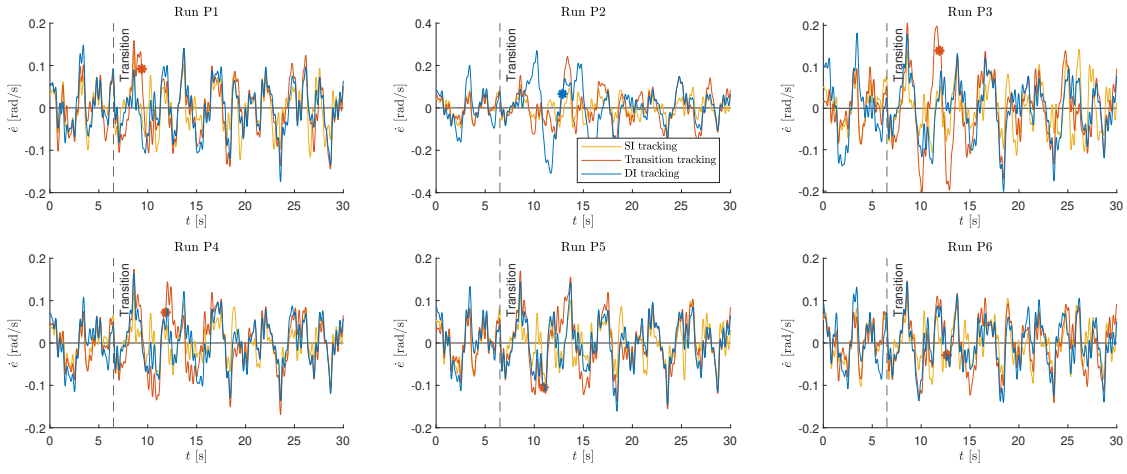
Experiment run C10 Error Rate time traces
Run P1
Run P2
Run P3
Run P4
Run P5
Run P6
Transition
SI tracking
Transition tracking
DI tracking
ė [rad/s]
t [s]

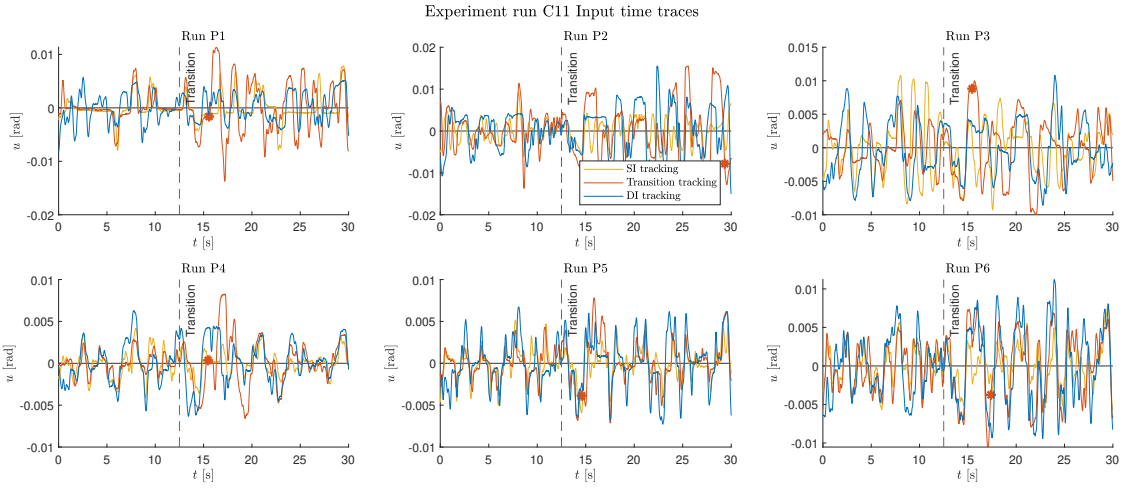
Experiment run C11 Input time traces
Run P1
Run P2
Run P3
Run P4
Run P5
Run P6
Transition
SI tracking
Transition tracking
DI tracking
u [rad]
t [s]

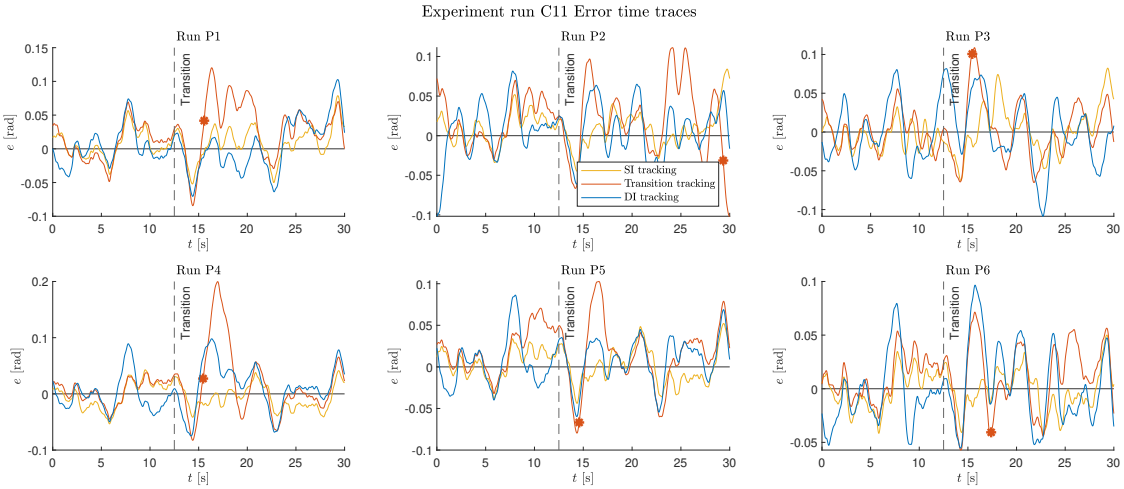
Experiment run C11 Error time traces
Run P1
Run P2
Run P3
Run P4
Run P5
Run P6
Transition
SI tracking
Transition tracking
DI tracking
e [rad]
t [s]

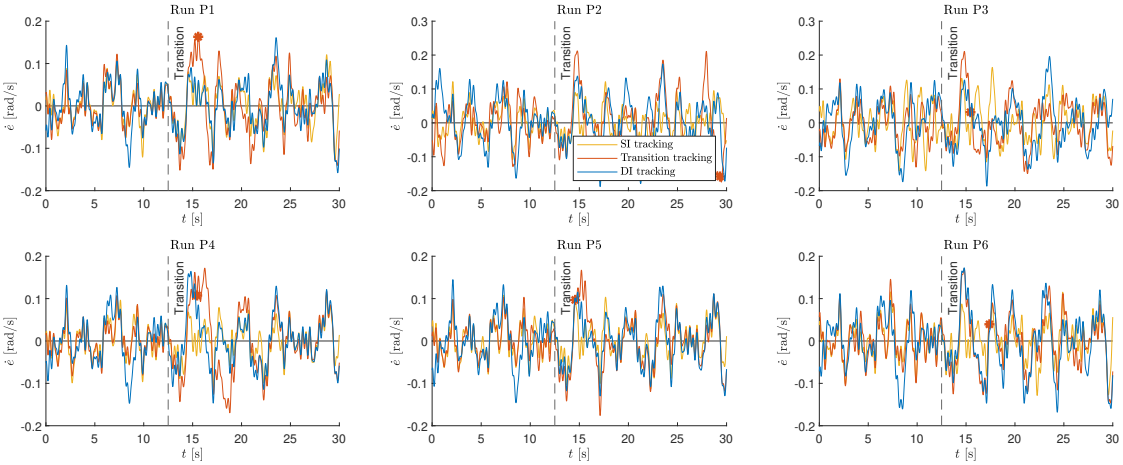
Experiment run C11 Error Rate time traces
Run P1
Run P2
Run P3
Run P4
Run P5
Run P6
Transition
SI tracking
Transition tracking
DI tracking
ė [rad/s]
t [s]

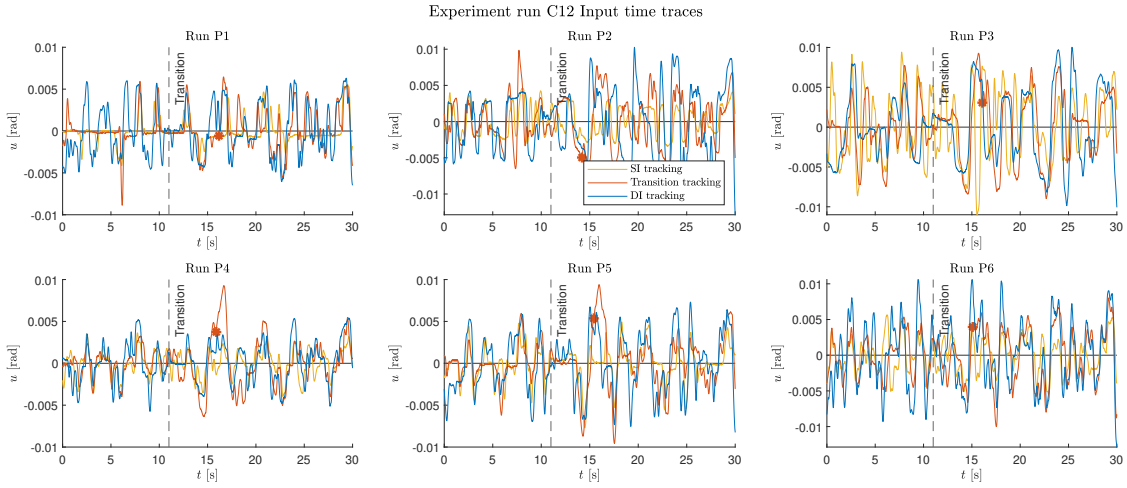
Experiment run C12 Input time traces
Run P1
Run P2
Run P3
Run P4
Run P5
Run P6
Transition
SI tracking
Transition tracking
DI tracking
u [rad]
t [s]

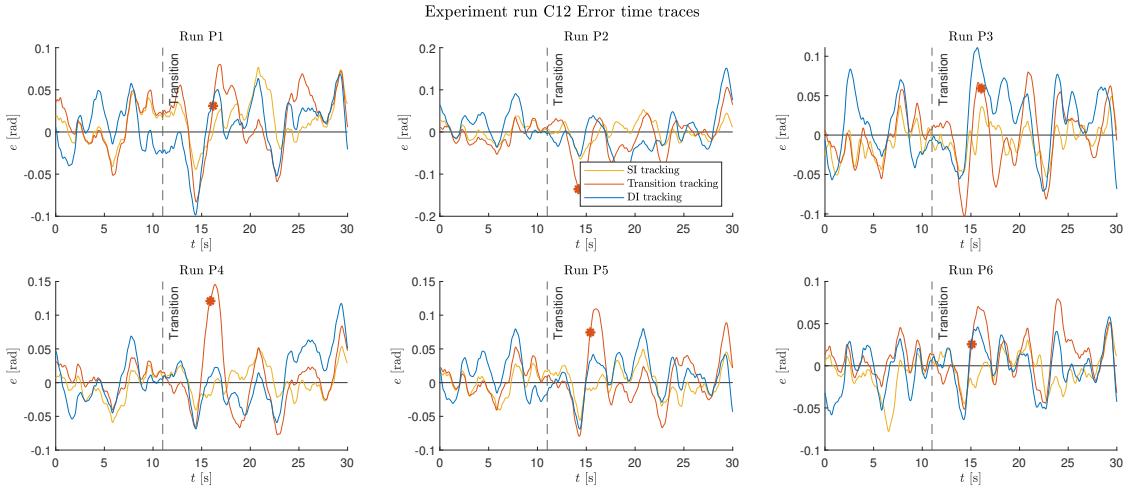
Experiment run C12 Error time traces
Run P1
Run P2
Run P3
Run P4
Run P5
Run P6
Transition
SI tracking
Transition tracking
DI tracking
e [rad]
t [s]

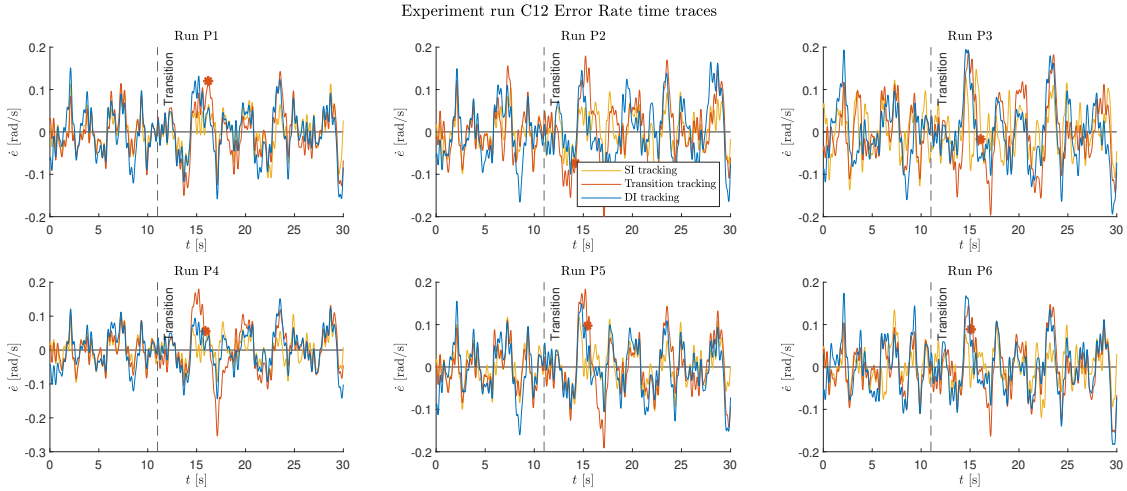
Experiment run C12 Error Rate time traces
Run P1
Run P2
Run P3
Run P4
Run P5
Run P6
Transition
SI tracking
Transition tracking
DI tracking
ė [rad/s]
t [s]

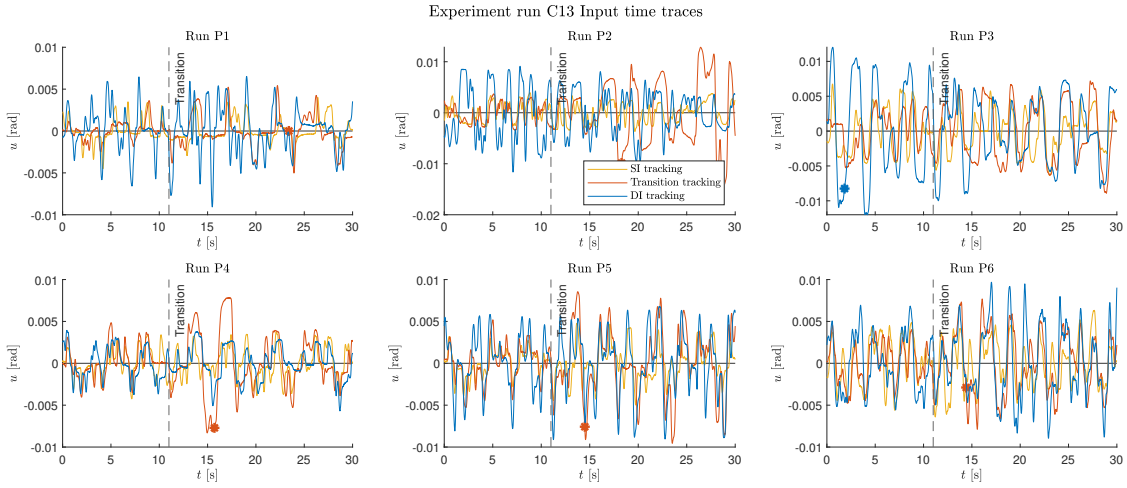
Experiment run C13 Input time traces
Run P1
Run P2
Run P3
Run P4
Run P5
Run P6
Transition
SI tracking
Transition tracking
DI tracking
u [rad]
t [s]

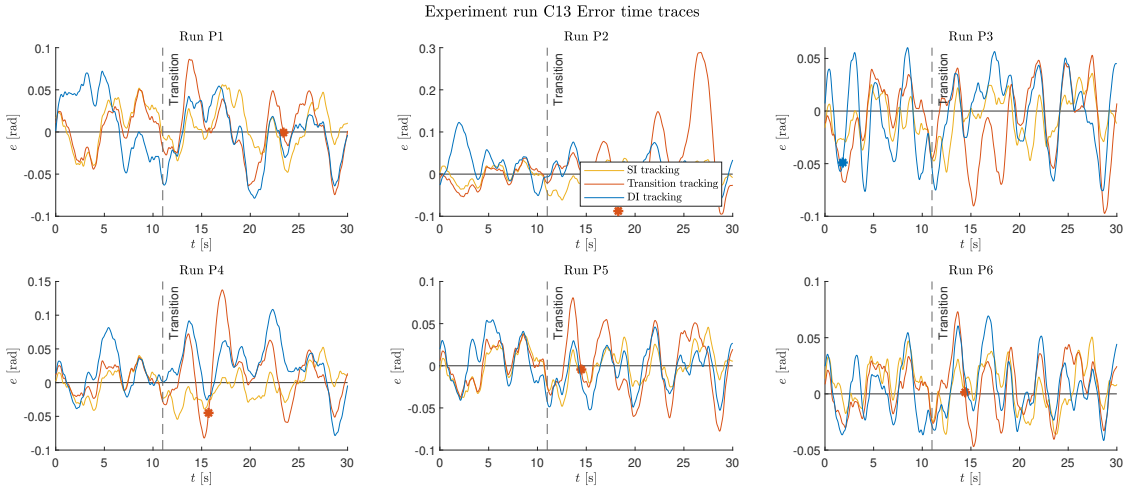
Experiment run C13 Error time traces
Run P1
Run P2
Run P3
Run P4
Run P5
Run P6
Transition
SI tracking
Transition tracking
DI tracking
e [rad]
t [s]

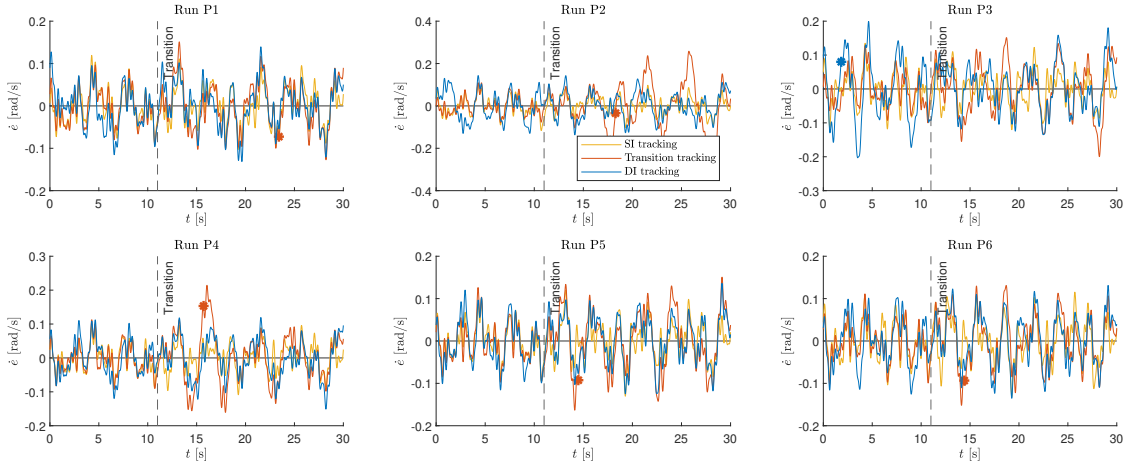
Experiment run C13 Error Rate time traces
Run P1
Run P2
Run P3
Run P4
Run P5
Run P6
Transition
SI tracking
Transition tracking
DI tracking
ė [rad/s]
t [s]

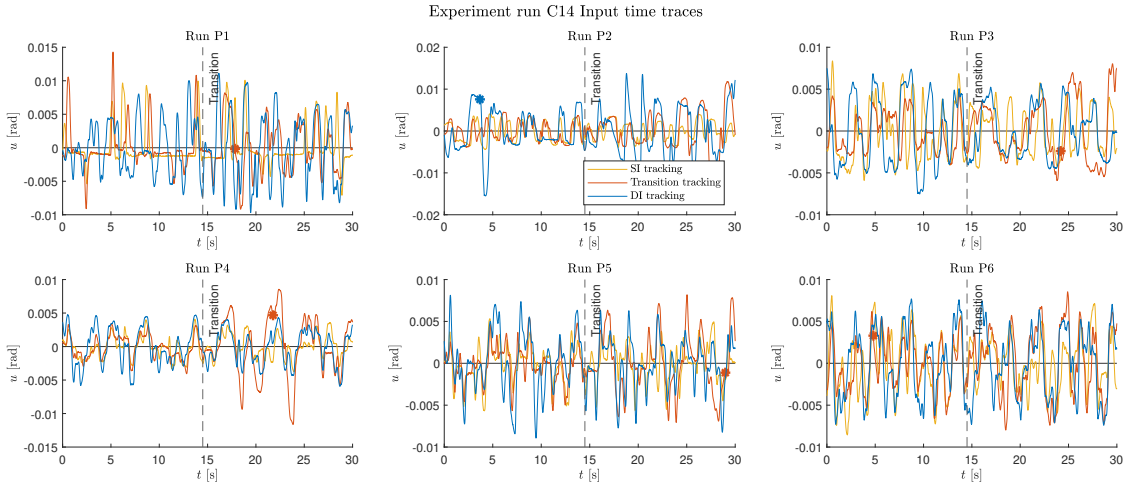
Experiment run C14 Input time traces
Run P1
Run P2
Run P3
Run P4
Run P5
Run P6
Transition
SI tracking
Transition tracking
DI tracking
u [rad]
t [s]

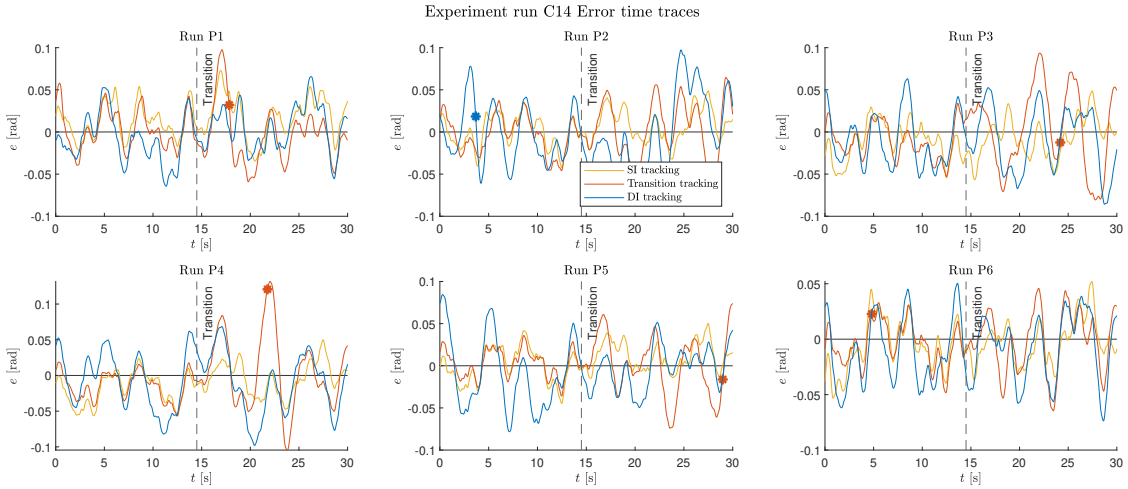
Experiment run C14 Error time traces
Run P1
Run P2
Run P3
Run P4
Run P5
Run P6
Transition
SI tracking
Transition tracking
DI tracking
e [rad]
t [s]

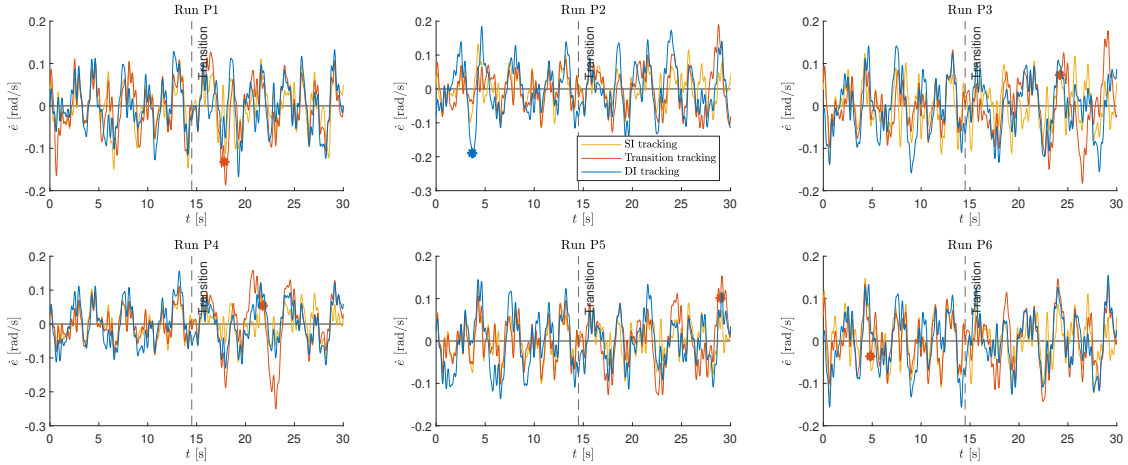
Experiment run C14 Error Rate time traces
Run P1
Run P2
Run P3
Run P4
Run P5
Run P6
Transition
SI tracking
Transition tracking
DI tracking
ė [rad/s]
t [s]

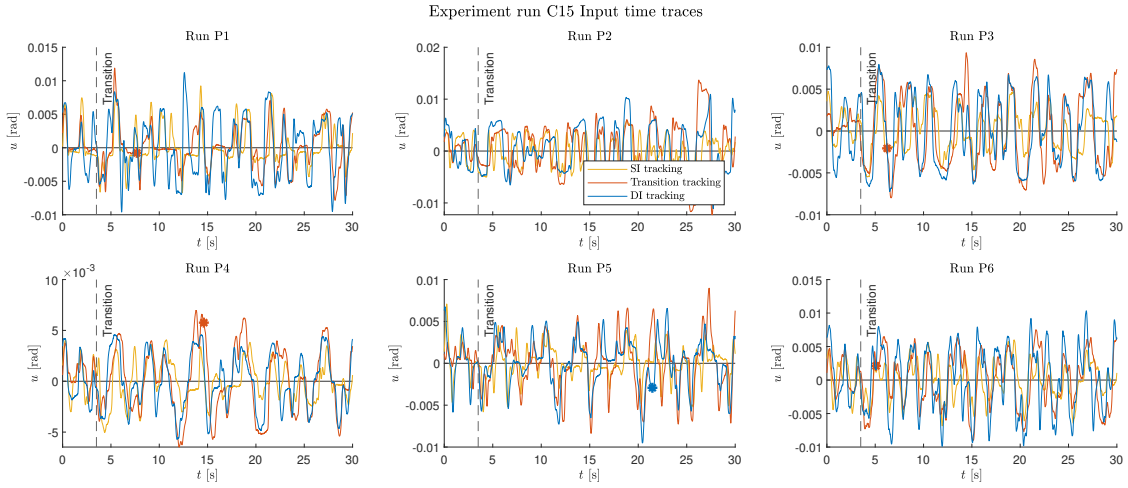
Experiment run C15 Input time traces
Run P1
Run P2
Run P3
Run P4
Run P5
Run P6
Transition
SI tracking
Transition tracking
DI tracking
u [rad]
t [s]

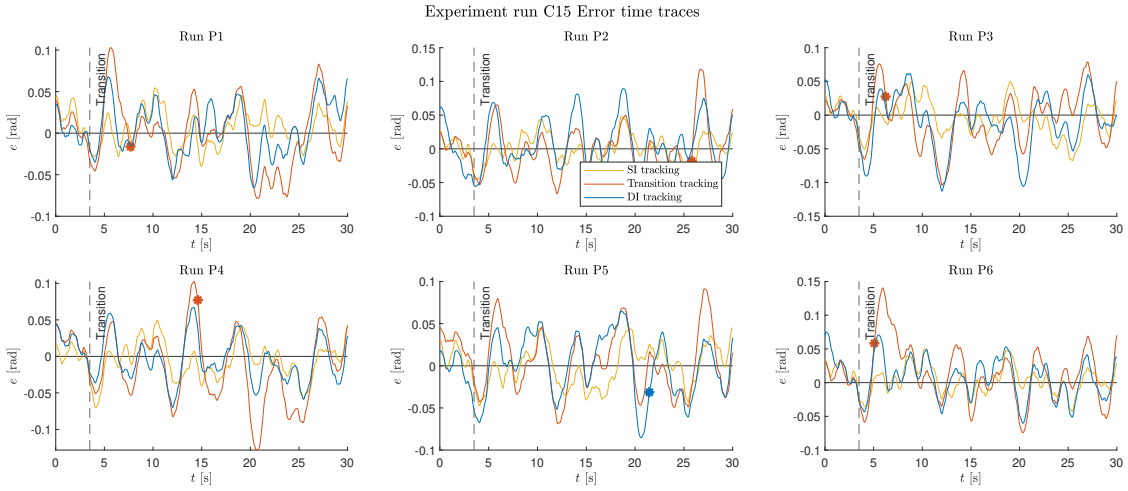
Experiment run C15 Error time traces
Run P1
Run P2
Run P3
Run P4
Run P5
Run P6
Transition
SI tracking
Transition tracking
DI tracking
e [rad]
t [s]

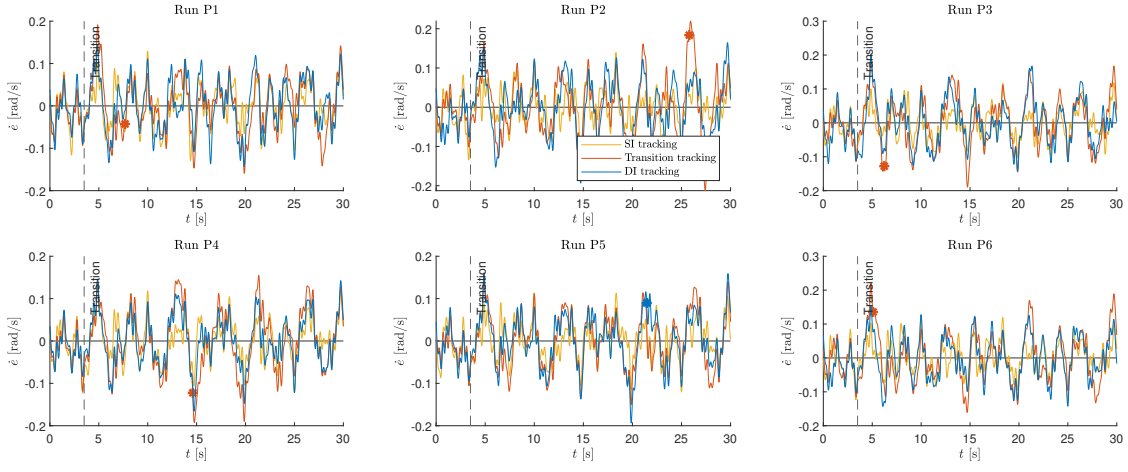
Experiment run C15 Error Rate time traces
Run P1
Run P2
Run P3
Run P4
Run P5
Run P6
Transition
SI tracking
Transition tracking
DI tracking
ė [rad/s]
t [s]

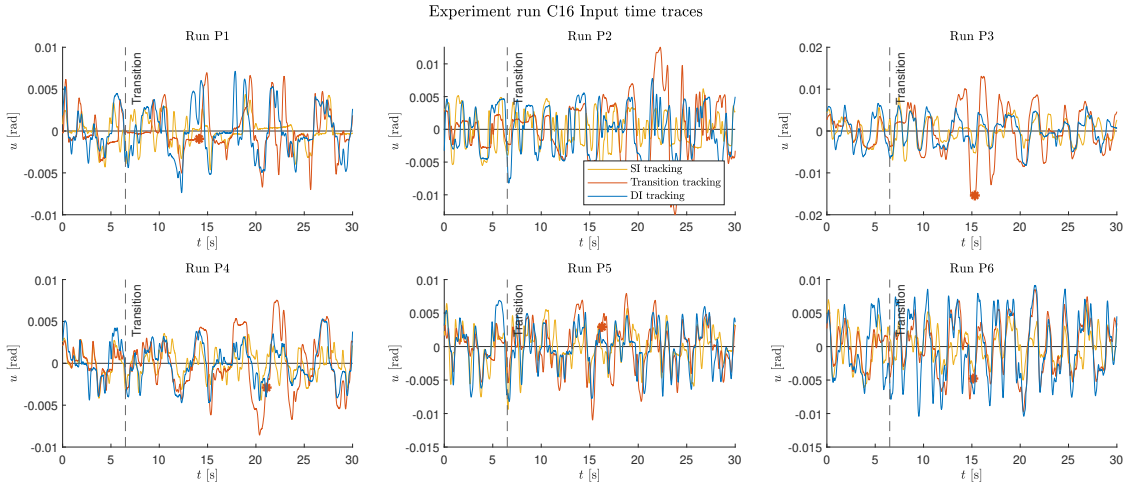
Experiment run C16 Input time traces
Run P1
Run P2
Run P3
Run P4
Run P5
Run P6
Transition
SI tracking
Transition tracking
DI tracking
u [rad]
t [s]

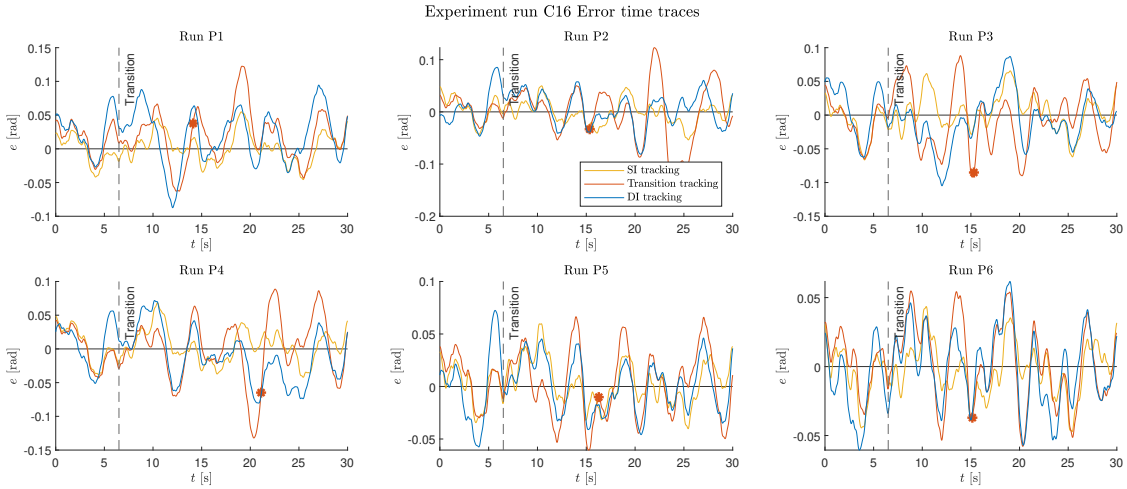
Experiment run C16 Error time traces
Run P1
Run P2
Run P3
Run P4
Run P5
Run P6
Transition
SI tracking
Transition tracking
DI tracking
e [rad]
t [s]

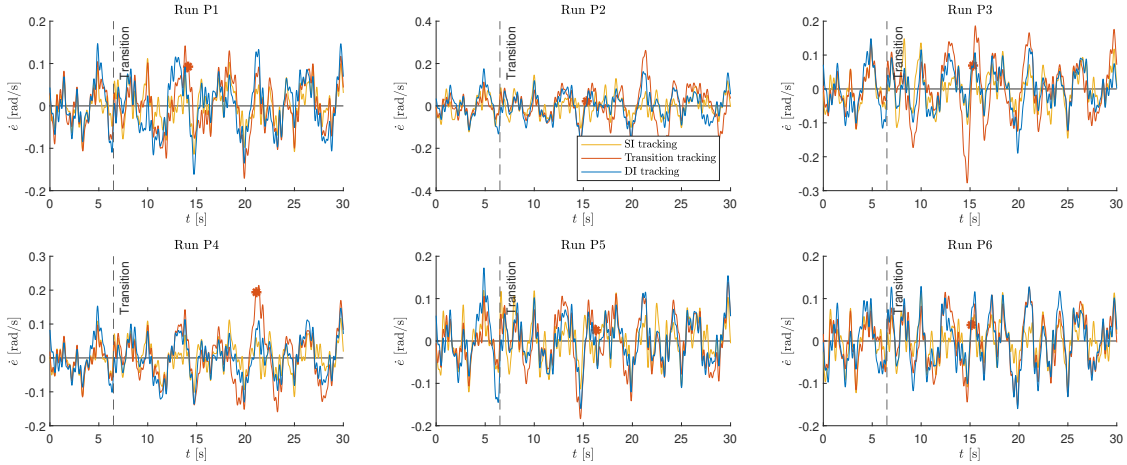
Experiment run C16 Error Rate time traces
Run P1
Run P2
Run P3
Run P4
Run P5
Run P6
Transition
SI tracking
Transition tracking
DI tracking
ė [rad/s]
t [s]

C-3 Classification of simulated detections per participant

The following two figures show the classified simulated detections per participant. The first figure, Figure C-4, shows the results based on individual standard deviation values. The second figure, Figure C-5, shows the results based on the average standard deviation values of all participants.

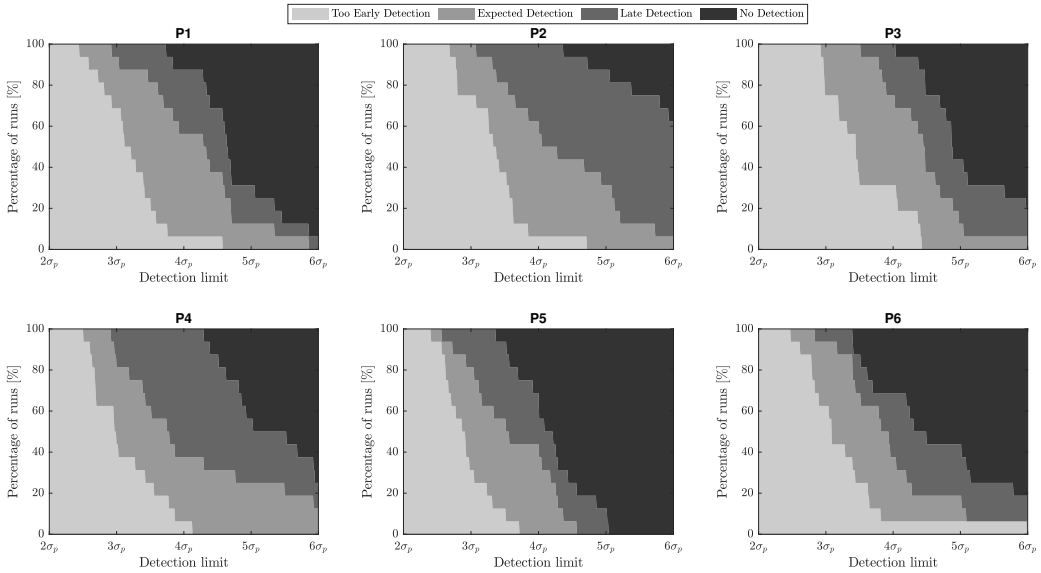

Figure C-4: Classified simulated detections per participant with individual detection boundaries

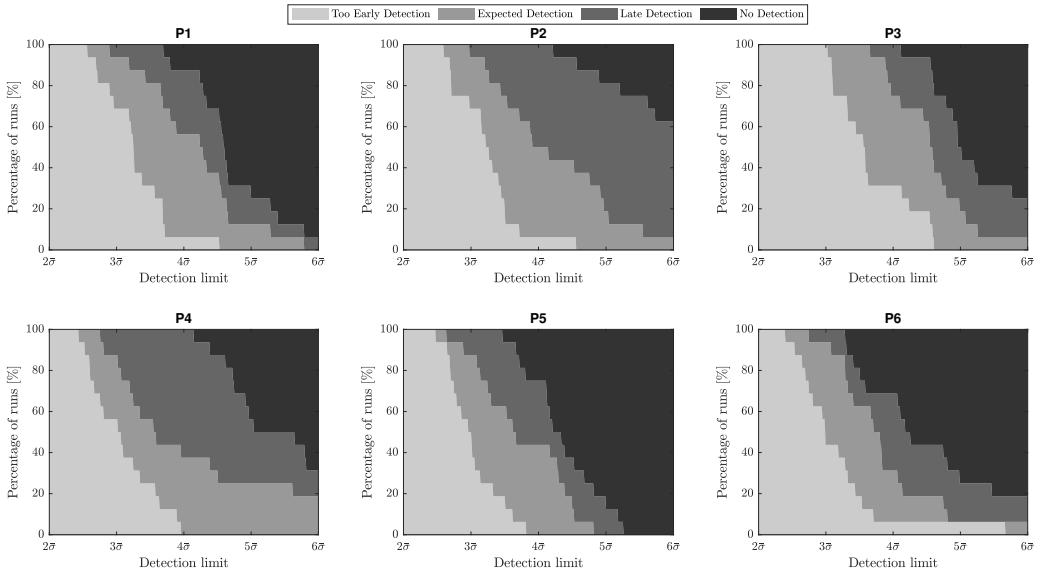

Figure C-5: Classified simulated detections per participant with average detection boundaries

C-4 Varying Reaction Time Windows

Figure C-6 shows the distribution of error and error rate values of the (predicted) detections for varying reaction time window sizes. When the button press data is directly applied (no prediction of detection), as shown in Figure C-6a, the detections are spread over the whole blue area. The results with the reaction time window applied in this research are shown in Figure C-6b. Figure C-6c presents the distribution of predicted error and error rate values when a slightly bigger reaction time window is applied: the maximum reaction time is increased with 1 second. The last figure, Figure C-6d shows the distribution of the predicted detections based on the maximum error or error rate values of the whole period before the button press.

Figure C-6a and C-6d are considered unrealistic, i.e., a participant has a minimum reaction time and reacts on a situation a limited amount of time before pressing the button. Figure C-6c shows a more concentrated distribution of detections, as it will find more actual local maximums with a bigger reaction time window. However, the magnitude of the error and error rate values for this bigger reaction time window is similar to the distribution of values in Figure C-6b.

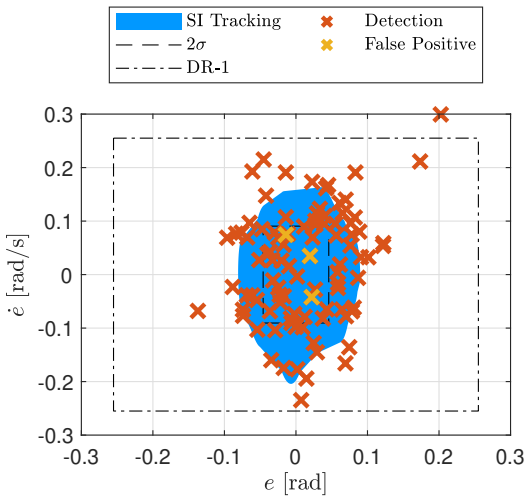

(a) Spread of detections at moment of button press

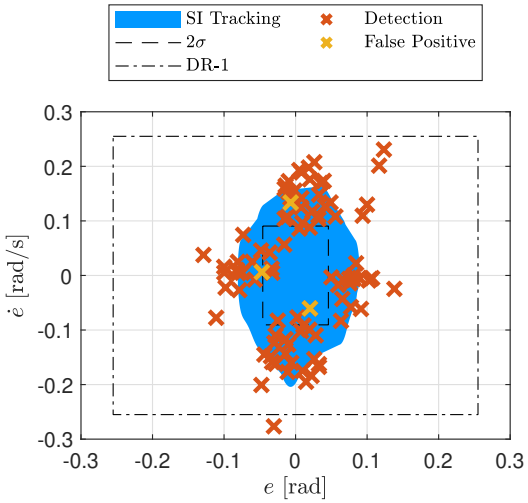

(b) Spread of detections with the reaction time window of 0.3-0.6 s before button press

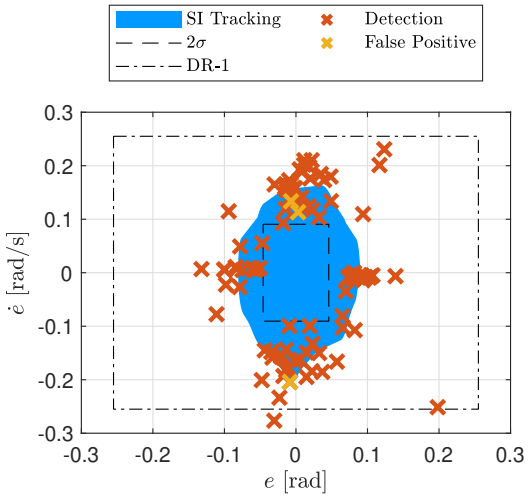

(c) Spread of detections with the reaction time window of 0.3-1.6 s before button press

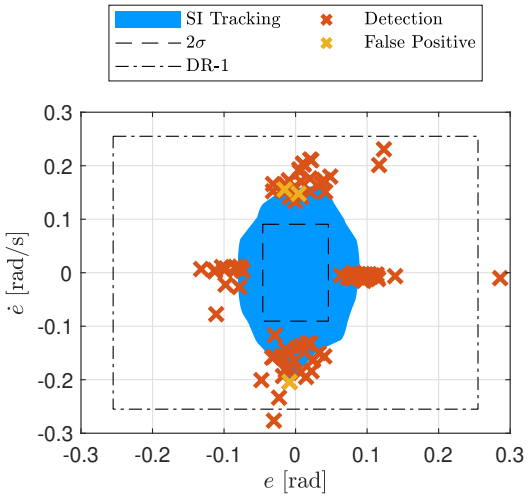

(d) Spread of detections with the reaction time window of all data before button press

Figure C-6: Spread of detections on the pre-failure tracking area for varying reaction time window sizes

Appendix D

Test Experiment Results

A small test experiment was executed with the controlled element dynamics from Phatak and Bekey [5]. The experiment was conducted with one forcing function and with one transition moment (at t=33.5 s). The two CE dynamics options used were A and B from [5] and were as follows:

$$\text{A: } H_C(s) = \frac{1.72}{s^2 + 2(0.6)(5.1)s + 5.1^2} \tag{D-1}$$

$$\text{B: } H_C(s) = \frac{320}{s(s+18.6)(s^2 + 2(0.66)(10.4)s + 10.4^2)} \approx \frac{320/10.4^2}{s(s+18.6)} \tag{D-2}$$

CE dynamics B was simplified, but yielded the same dynamics in the human crossover region as would have been achieved with the full transfer function.

After some initial testing, it was discovered that with these transfer functions it was not possible for the human operator to follow the target signal. Too large control inputs were required, which would still yield small outputs even when controlling CE dynamics B. It was decided to multiply both CE dynamics options with a gain to amplify output with the same control input.

Figure D-1 presents a run in which a gain factor of 50 was applied to both CE dynamics. It can be observed that the signal before and after transition shows similar error magnitudes. In the phase plane (left plot in Figure D-1) the first decision region from Phatak and Bekey [5] is displayed. According to Phatak and Bekey [5] a human operator detects a transition when the error or error rate passes this boundary. The phase plane is plotted from the moment of the transition ('Start'). The plot does not pass DR-1.

In another run the gain was increased to 100. Figure D-2 presents a run with this gain factor. Again, the error magnitudes are similar pre- and post-failure and the phase plane plot does not pass DR-1.

Since this experiment was only performed to quickly check the dynamics and the way a human operator would interact with them, it is not allowed to draw conclusions from it. However, it does show that it was not possible to quickly replicate the results from [5]. A more elaborate experiment is required to find the reason of the discrepancy between the two different results.

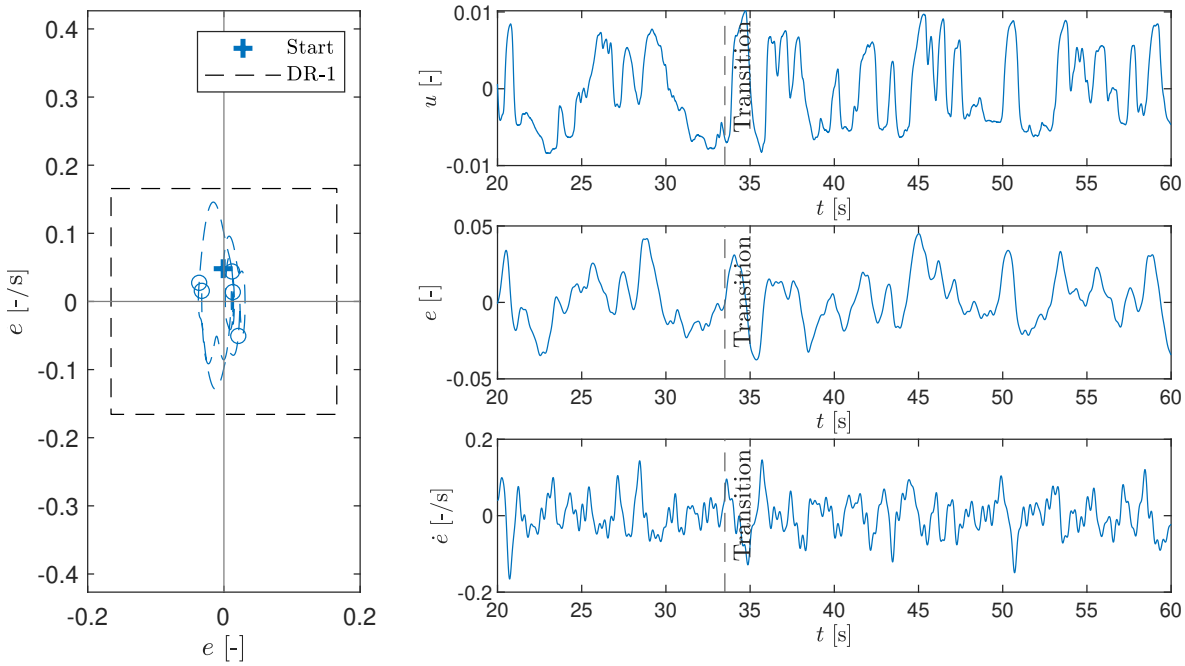

Figure D-1: Transition from CE dynamics A to B with a gain factor of 50

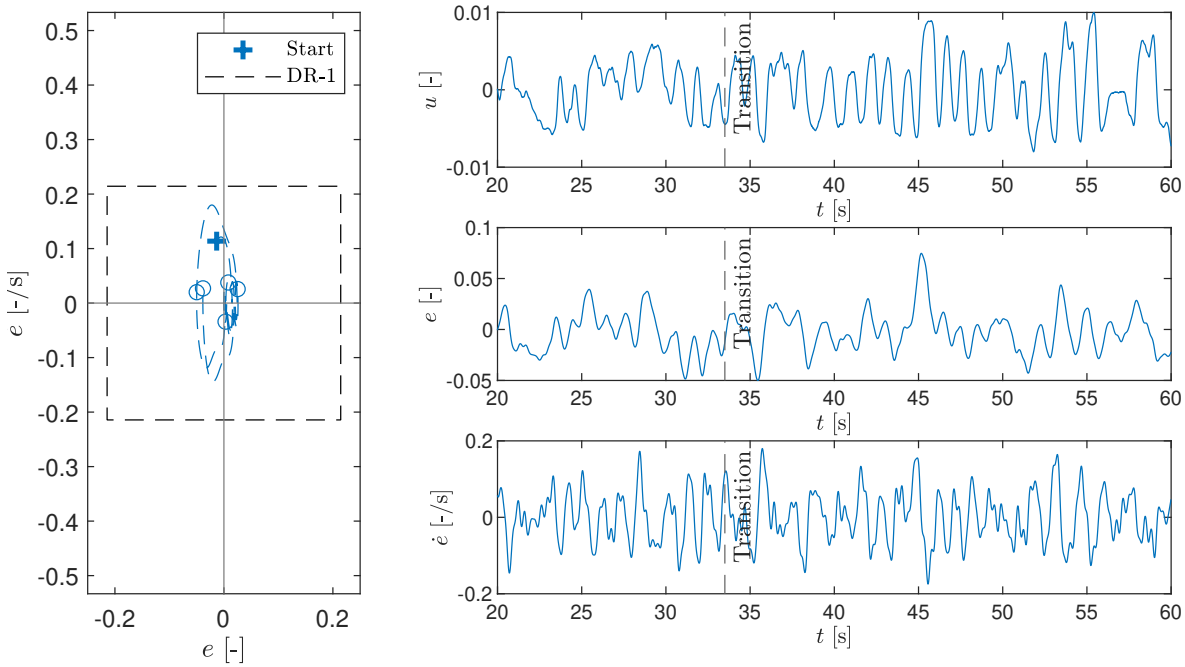

Figure D-2: Transition from CE dynamics A to B with a gain factor of 100

Appendix E

Different Computer Simulation Frameworks

Prior to the experiment, computer simulations were performed to get a better understanding of the supervisory control algorithm [5] and to test the conditions for the experiment. Unfortunately, simulating time-varying dynamics with instant changes produced certain artefacts in the output signals. This appendix presents the different model implementations and their outputs.

In the simulation program the time-varying transfer functions of the human operator model dynamics and the controlled element dynamics were combined and afterwards converted to a state-space representation. This representation was then used to calculate the output and new states each time step. A more elaborate explanation of the simulation program is given in [36].

The initial conversion from transfer function to state-space representation was into the controllable canonical form. This transfer is represented by the following example transfer function and state-space representation:

$$H(s) = \frac{Y(s)}{U(s)} = \frac{b_0 s^2 + b_1 s + b_2}{s^3 + a_1 s^2 + a_2 s + a_3} \tag{E-1}$$

$$\begin{aligned} \dot{\mathbf{q}} &= \mathbf{A}\mathbf{q} + \mathbf{B}u = \begin{bmatrix} 0 & 1 & 0 \\ 0 & 0 & 1 \\ -a_3 & -a_2 & -a_1 \end{bmatrix} \mathbf{q} + \begin{bmatrix} 0 \\ 0 \\ 1 \end{bmatrix} u \\ y &= \mathbf{C}\mathbf{q} + Du = \begin{bmatrix} b_2 & b_1 & b_0 \end{bmatrix} \mathbf{q} + 0 * u \end{aligned} \tag{E-2}$$

The output produced with this representation is shown in yellow in Figure E-1, which shows the simulation output of a run in which the CE dynamics instantly transitioned from single integrator to double integrator dynamics at t = 10 s. The human operator in this simulation adapts in two seconds after the transition, according to the parameter values previously given in Table 3-1.

The yellow line in Figure E-1 shows a steep decrease of the output directly after the transition. This is not a realistic reaction of such a transition, but an artefact due the response of the

simulation to the instant change in dynamics. It was decided to try the simulation with a different canonical form of the state-space representation, the observable canonical form.

The observable canonical form is constructed as follows:

$$\begin{aligned} \dot{\mathbf{q}} &= \mathbf{A}\mathbf{q} + \mathbf{B}u = \begin{bmatrix} -a_1 & 1 & 0 \\ -a_2 & 0 & 1 \\ -a_3 & 0 & 0 \end{bmatrix} \mathbf{q} + \begin{bmatrix} b_0 \\ b_1 \\ b_2 \end{bmatrix} u \\ y &= \mathbf{C}\mathbf{q} + Du = \begin{bmatrix} 1 & 0 & 0 \end{bmatrix} \mathbf{q} + 0 * u \end{aligned} \tag{E-3}$$

The advantage of this form with respect to the controllable canonical form is that all the parameters are located in the state equation. Since the output and the new states are determined in different time steps, it is desirable to put all the time-varying parameters in one equation. The simulation results with the observable canonical form are represented by the red line in Figure E-1.

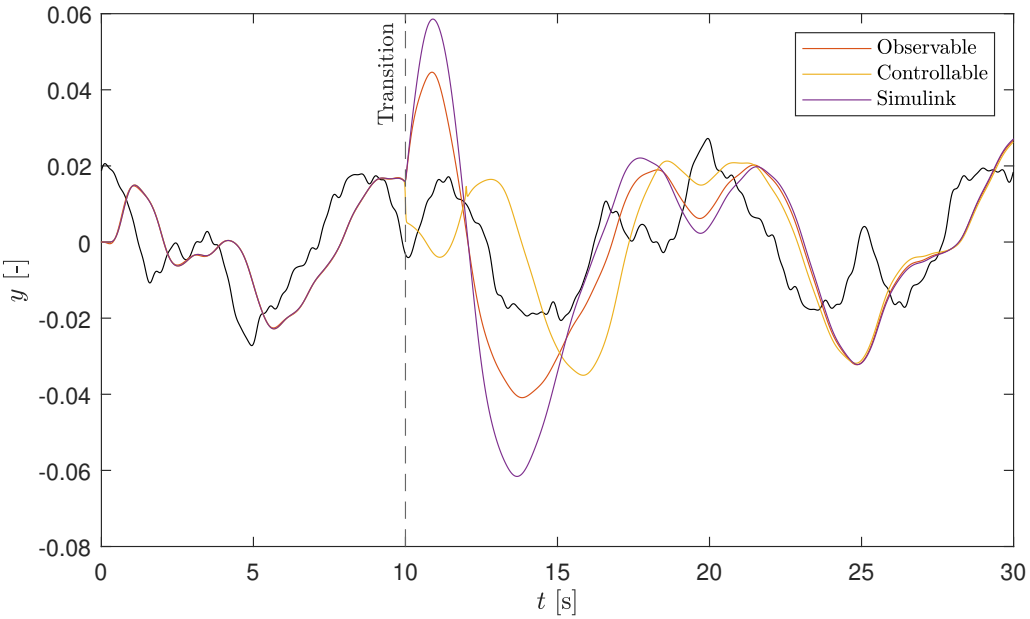

Figure E-1: Simulation run of the same system using different methods

A final time-varying simulation has been performed with Simulink [37]. The block diagram used to perform the simulation is illustrated in Figure E-2. The human operator is simulated with a time-varying function block in combination with a variable transport delay block. The controlled element dynamics only consist of a time-varying function block. It is unclear what the exact mathematics behind these blocks is. The output of the Simulink simulation is shown by the purple line in Figure E-1.

All three simulation frameworks give different results in the 15 seconds after the transition. The Observable canonical form and Simulink simulations do not show the artefact from the controllable canonical form. It is, however, not known what the correct output should look like. It will be difficult to validate this with experimental data, since it concerns such a short time span and a minimal difference between simulations.

What was outside the scope of this thesis, but what might still me interesting to investigate is looking at different discretization and integration methods. Only a zero-order hold discretization was applied, but this might not be suited for such time-varying simulations.

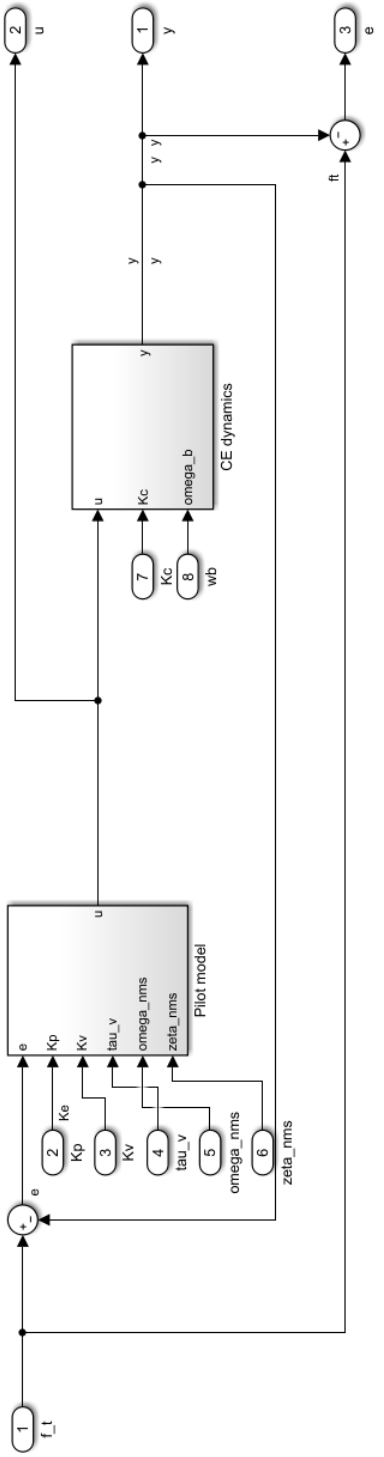

Figure E-2: Simulink block diagram of system